1-1-2013

# Predicting the Crack Response for a Pipe with a Complex Crack

Robert George Lukess
*University of South Carolina*

# PREDICTING THE CRACK RESPONSE FOR A PIPE WITH A COMPLEX CRACK

By

Robert G. Lukes

Bachelor of Science
University of Wisconsin – Madison, 2003

Master of Engineering
Johns Hopkins University, 2006

---

Submitted in Partial Fulfillment of the Requirements

For the Degree of Doctor of Philosophy in

Nuclear Engineering

College of Engineering and Computing

University of South Carolina

2013

Accepted by:

Travis W. Knight, Major Professor

Sarah Baxter, Committee Member

Michael Sutton, Committee Member

Elwyn Roberts, Committee Member

David Rudland, Committee Member

Lacy Ford, Vice Provost and Dean of Graduate Studies

## DEDICATION

This work is dedicated to my family and all the people who assisted in the completion of this research.

## ACKNOWLEDGMENT

I would like to acknowledge the tremendous support provided by the NRC in the completion of this research. I would also like personally thank NRC staff members Dr. Dave Rudland, Dr. Aladar Csontos, Jim Beardsley, Joelle Starefos, John Lubinski, Dr. David Esh, Dr. Timothy McCartin, and Christopher Hunter. All of whom contributed directly to the completion of my educational goals at one point in time.

Thanks to Battelle for providing a significant amount of information used as the basis for this research. In addition, I would like to thank the Battelle staff for providing me support when analyzing the data and performing the analysis. This project would not have been possible without their support.

I would also like to thank Dr. Knight and the rest of the engineering faculty at University of South Carolina for the time and effort they spend educating the next generation of engineers and researchers. During my time at the university I was continually amazed by the intelligence and creativity of the faculty.

Finally I would like thank my family for their support and motivation. Their tireless work maintaining our household allowed me the freedom to pursue my personal education goals. Thank you Kim, Reagan, Zoe, Agi, Tammie, and Mom for everything you have done.

## ABSTRACT

Traditional flaw evaluation in the nuclear field uses conservative methods to predict maximum load carrying capacity for flaws in a given pipe. There is a need in the nuclear industry for more accurate estimates of the load carrying capacity of nuclear piping such that probabilistic tools can be used to predict the time to failure for various types of cracks. These more accurate estimates will allow the nuclear industry to repair flaws at a more appropriate time considering external factors such as costs and man-rem planning along with the flaw repair. Analysis of the maximum load carrying capacity of a pipe with a complex crack (CC) has gained increased importance due to the recent identification of long CC's that have appeared in dissimilar metal (DM) welds thought to be caused by primary water stress corrosion cracking (PWSCC).

A numerical solution for a single material with a weld was developed that gives an accurate maximum load and crack driving force prediction for a pipe with a through wall crack (TWC), called LBBEng. To support the analysis of a CC, traditionally, an assumption is used that the CC performs similar to that of a TWC of a reduced thickness (TWCr). This modification gives a conservative prediction of the maximum load carrying capacity for a CC in a single material but was never verified for a CC in a DM weld. The research performed in this work demonstrates that the crack response of a CC can be predicted by a TWC model when modifications are made to the reduced thickness method.

## TABLE OF CONTENTS

## LIST OF TABLES

## LIST OF FIGURES

## LIST OF SYMBOLS

| | |
|---|---|
| a | Crack Length |
| $\alpha$ | Ramberg-Osgood parameter |
| $\Delta a$ | Increment of Crack Growth |
| $E$ | Elastic modulus |
| $\varepsilon_o$ | Ramberg-Osgood reference strain |
| $\varepsilon$ | Engineering strain |
| J | Measure of Elastic-Plastic Energy |
| $J_{CC}$ | J of the complex crack |
| $J_{TWC}$ | J of the through wall crack |
| $J_i$ | Elastic-Plastic Energy at Crack Initiation |
| $J_{ic}$ | Fracture toughness |
| $J_e$ | Elastic component of J |
| $J_P$ | Plastic component of J |
| $J_R$ | Crack growth resistance |
| J-R | J-resistance curve |
| $J_D$-R | J-resistance curve based on deformation theory |
| $J_M$-R | J-resistance curve based on Modified J |
| $K_{Ic}$ | Plane strain fracture toughness |
| $L_B$ | Function in the LBB.ENG2 J-estimation scheme |

| | |
|---|---|
| $M$ | Moment |
| $M_O$ | The limit moment of a through wall cracked pipe under pure bending |
| $n$ | Ramberg-Osgood strain hardening exponent |
| $\eta - factor$ | Method for estimating the fracture toughness of a pipe experiment from experimental moment rotation relationship |
| $\sigma$ | Stress |
| $\sigma_f$ | Flow stress |
| $\sigma_O$ | Ramberg-Osgood reference stress |
| $\sigma_y$ | Yield stress |
| $R_m$ | Mean radius |
| $t$ | Wall thickness |
| $\theta$ | Half crack angle |

## LIST OF ABBREVIATIONS

ABAQUS ..... Finite element analysis computer software

ASME ..... American Society of Mechanical Engineers

ASTM ..... American Society for Testing and Materials

AXIALCK ..... Axial crack database

BINP ..... Battelle integrity of nuclear piping program

BWR ..... Boiling water reactor

CC ..... Complex Crack

CGR ..... Crack growth rate

CIRCUMCK ..... Circumferential crack database

COD ..... Crack opening displacement

CRDM ..... Control rod drive mechanism

DM ..... Dissimilar metal

DMW ..... Dissimilar metal weld

EMC$^2$ ..... Engineering Mechanics Corporation of Columbus, Columbus, Ohio,

EPFM ..... Elastic-plastic fracture mechanics

EPRI ..... Electric Power Research Institute

FE ..... Finite element

FEA ..... Finite element analysis

FT ..... Full thickness

GE ..... General Electric

IPIRG ..... International Piping Integrity Research Group

IPIRG 2 ..... International Piping Integrity Research Group

IGSCC ..... Intergranular Stress Corrosion Cracking

LBB ..... Leak-before-break

LEFM ..... Linear elastic fracture mechanics

MRP ..... EPRI materials reliability program

MRT ..... Modified reduced thickness

MRTF ..... Modified reduced thickness factor

NIST ..... National Institute of Standards and Technology

NRC ..... Nuclear Regulatory Commission

NRCpipe ..... NRC sponsored fracture computer software

NSC ..... Net section collapse

PICEP ..... Pipe Crack Evaluation Program

PIFRAC ..... NRC/Battelle pipe fracture database

PWR ..... Pressurized water reactor

PWSCC ..... Primary Water Stress Corrosion Cracking

PVP ..... Pressure vessel piping

RT ..... Reduced thickness

SAW ..... Submerged arc weld

SC ..... Surface crack

SMAW ..... Shielded metal arc weld

SQUIRT ..... Seepage Quantification of Upsets in Reactor Tubes

TWC..... Through wall crack

TWCr ..... Through wall crack of reduced thickness

VHP..... Vessel head penetration

xLPR .....Extremely low probability of rupture computer code

# CHAPTER 1

# INTRODUCTION

## 1.1 HISTORY OF DISSIMILAR METAL WELD CRACKING

Primary Water Stress Corrosion Cracking (PWSCC) has been a known problem in the nuclear industry since the early 1980s. PWSCC is known to occur in susceptible materials that are in a challenging environment, both temperature and chemically, and are under high residual stresses. These conditions exist in pressurized water reactors (PWR) for welds that join ferritic and stainless steels, referred to as dissimilar metal (DM) welds, specifically welds that use nickel-chromium-iron Alloy 600/82/182. As an example, DM welds were used for control rod drive mechanism (CRDM) to vessel welds, pressurizer nozzles, and reactor coolant loop piping to branch piping and other locations where carbon steel and stainless steel are required to be joined. Figure 1.1 illustrates the typical material order for a DM weld.

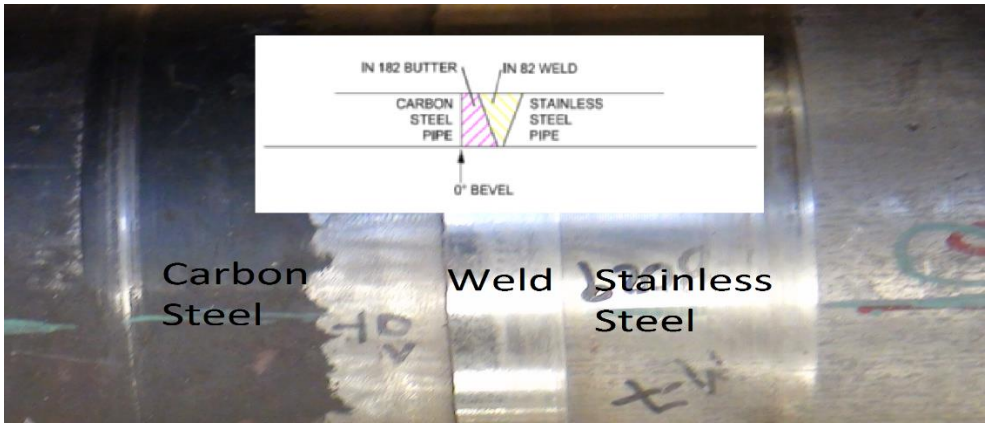


Figure 1.1. Illustrated example DM weld showing the different material regions. [5]

For currently operating nuclear power plants, DM welds in vessel head penetrations (VHP) are of the most concern because of the potential for a VHP ejection. This would result in a small-to-medium loss of coolant accident which could affect the safe shutdown of the reactor. A typical weld of a VHP is illustrated in Figure 1.2. Beginning in 1986, leaks in DM welds have been identified in VHP's of operating nuclear power plants. However, these leaks were not viewed as having high safety significance because examinations concluded that the cracks were axial and had low growth rates.

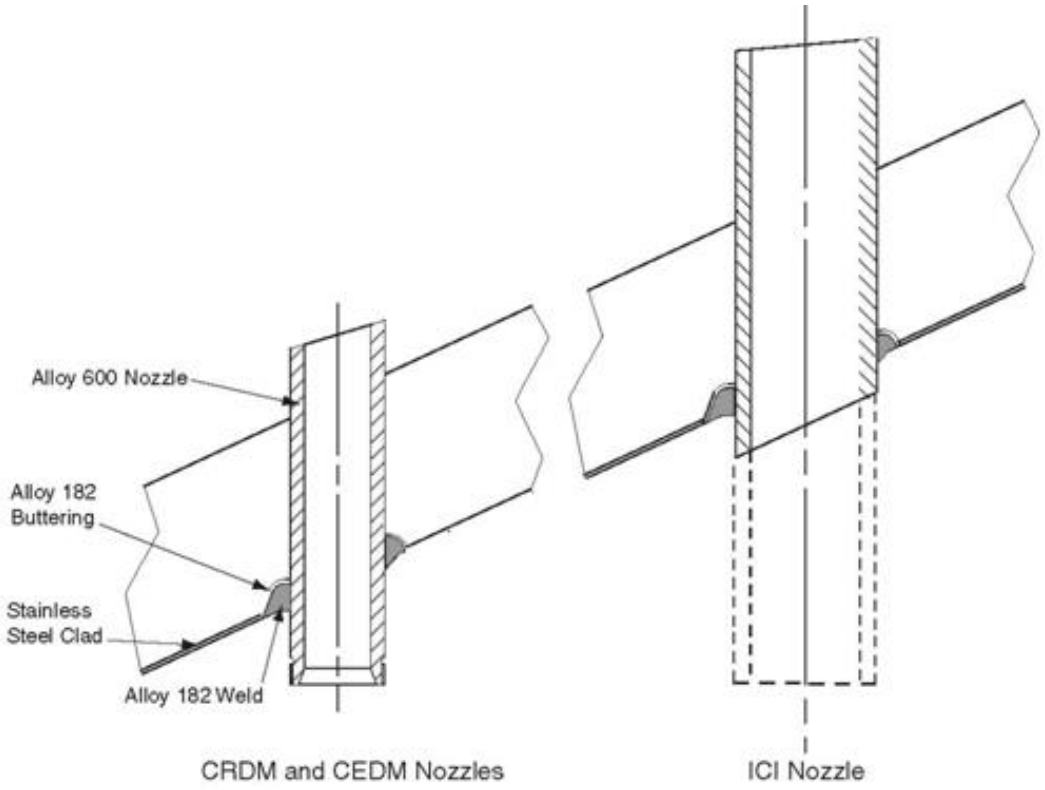


Figure 1.2. A typical weld for a VHP. [37]

In 1991 DM weld cracks were also found in VHP at the French PWR, Bugey 3. Several other examinations were performed at plants in France, Belgium, Sweden, Switzerland, Spain, and Japan. Additional cracks in VHP's were detected during these inspections. In 1991, two percent of the VHP's contained short axial cracks [1]. After these findings were discovered, plans were developed by the Nuclear Regulatory Commission (NRC) and Electric Power Research Institute (EPRI) to further assess the possibility of DMW cracking in VHP's. Safety assessments were completed by each of the PWR owners groups in 1993. The NRC reviewed those assessments and concluded that PWSCC cracking was not an immediate safety concern. The basis was that the cracks were axial in direction, would result in detectable leakage before failure, and the leakage would be detectable during normal visual examinations. In addition, the cost of the additional exposure to personnel during examination and repair was not justified by the currently viewed risk.

The first U.S. inspection of VHP's occurred in 1994 at Point Beach Nuclear Generating Station. No cracks were detected in its 49 CRDM penetrations. Later in 1994 an inspection was done at Oconee Nuclear Generating Station and revealed 20 shallow cracks in one penetration. D.C. Cook Nuclear Generating Station was also inspected that year and was found to have three clusters of cracks in one VHP. Several utilities developed susceptibility models in an attempt to predict crack growth in VHP's and use it as a basis for inspection. There was disagreement between NRC and the industry on the validity of these models [1], however, at the time the NRC agreed with the industry that DM weld cracking in VHP's did not pose an immediate safety concern.

During 2000, cracks were discovered in Alloy 182 welds joining low-alloy steel reactor vessel hot leg nozzles to stainless steel pipes at Ringhals 4 (Sweden) and VC Summer (United States). At VC Summer, a through wall crack (TWC) was found in the Alloy 82/182 weld between the low-alloy steel reactor vessel outlet nozzle and the stainless steel primary coolant pipe. Although cracking was primarily axially oriented, at VC Summer a short and shallow circumferential crack also was discovered in the inside diameter (ID) region of the Alloy 182 weld clad beneath the low-alloy steel nozzle material. This circumferential crack arrested when it reached the low-alloy steel base material. The VC Summer circumferential flaw contradicted one of the initial assumptions that flaws were primarily axial, thus elevating the concern regarding DM welds due to the presence of the circumferential flaws.

Several other PWSCC cracks were identified after 2000, as a result of increased inspections. VHP cracking at Oconee Nuclear Station Unit 1 (ONS1) in November 2000 and Arkansas Nuclear One Unit 1 (ANO1) in February 2001 was limited to axial cracking. Discovery of large circumferential cracking identified in two VHP's, one of which was a leaking complex crack, at Oconee Nuclear Station Unit 3 (ONS3) and Oconee Nuclear Station Unit 2 (ONS2) in 2001 raised concerns about the potential safety implications and prevalence of cracking in VHP nozzles in PWRs. Again, these observations contradicted the assumption that the PWSCC flaws are predominantly axial [2]. In 2002 Davis-Besse Nuclear Power Station identified a football-sized cavity in the unit's reactor vessel head. The cavity was next to a leaking nozzle with a TWC and was in an area of the vessel head that had been covered with boric acid deposits. In 2003, a small leak was discovered from a DM weld on a pressurizer relief nozzle at Tsuruga 2

(Japan). This leak was from an axial crack in the butt weld between the low-alloy steel nozzle and the stainless steel relief valve line. In 2005, Calvert Cliffs Nuclear Power Plant identified indications in a hot leg drain nozzle dissimilar metal weld. There were two axial indications contained entirely within the weld and butter closely associated with the ID and there also was one circumferential indication extending approximately 100° in circumference, with one end oriented near one of the axial indications.

The most significant occurrence of DM weld cracking occurred in 2006. Several circumferential cracks were identified by ultrasonic testing in three of the pressurizer nozzle DM welds at the Wolf Creek nuclear power plant. The discovered cracks were relatively long circumferential defects in Alloy 82/182 DM welds and were attributed to PWSCC. In one case, the flaw was sized at 43% of the pipe circumference in length and 26% of the wall thickness in depth [3]. A flaw evaluation was performed assuming idealized flaw shapes which demonstrated that these flaws could potentially cause rupture before leakage [3].

As a result of the Wolf Creek finding, the NRC and the industry has implemented an initiative to develop a more robust probabilistic analysis to evaluate identified DM weld flaws. The results from this research will feed into model validation for the NRC/EPRI ongoing cooperative effort on developing a modular-based probabilistic fracture mechanics code for determining the probability of rupture entitled Extremely Low Probability of Rupture (xLPR) [4].

## 1.2 LBB AND PWSCC

The industry has a major financial interest in the approval of the LBB methodology. LBB [41] allows for the removal of protective hardware, such as pipe-whip restraints and jet impingement shield barriers, the redesign of pipe connected components, their supports, and their internals, and other related changes in operating plants. The governing section of the regulations related to LBB is General Design Criterion 4 in Appendix A of Part 50 of Title 10 of the Code of Federal Regulations, Ref. 2.1. GDC-4 states that [23]:

"Structures, systems, and components important to safety shall be designed to accommodate the effects of and to be compatible with the environmental conditions associated with normal operation, maintenance, testing, and postulated accidents, including loss-of-coolant accidents. These structures, systems, and components shall be appropriately protected against dynamic effects, including the effects of missiles, pipe whipping, and discharging fluids, that may result from equipment failures and from events and conditions outside the nuclear power unit. However, dynamic effects associated with postulated pipe ruptures in nuclear power units may be excluded from the design basis when analyses reviewed and approved by the Commission demonstrate that the probability of fluid system piping rupture is extremely low under conditions consistent with the design basis for the piping."

Of particular interest to the subject of LBB, is the stipulation in GDC-4 that allows the use of "analyses reviewed and approved by the Commission" to eliminate from the design basis the dynamic effects of pipe ruptures. Crack growth and maximum

load prediction are critical to the implementation of LBB. LBB is generally applicable with the following exceptions:

- LBB cannot be applied to individual welded joints or other discrete locations.
- LBB is applicable only to an entire piping system.
- LBB is typically not applicable to piping susceptible to intergrannular stress corrosion cracking (IGSCC) or primary water stress corrosion cracking (PWSCC). However, if the applicant can demonstrate to the NRC through analysis that effective mitigation measures are in place to counteract these mechanisms.

Thus, there is an industry need for a predictive tool that can accurately evaluate complex cracks, such as those associated with PWSCC.

### 1.3 STATEMENT OF THE PROBLEM

Throughout the 1980's and 1990's, extensive research was conducted on the stability of flaws in nuclear piping. All of these experiments and the developed methodologies focused on idealized flaws in similar metals welds and their base metals. However, with the occurrence of PWSCC in DM welds, i.e., a nickel based weld between carbon steel and stainless steel base metals, the flaw stability characteristics are unknown. In addition, PWSCC flaws shapes are irregular and may be complex in shape, i.e., a combination of a surface breaking and through-wall defect. The differences between the materials tested and the type of the flaw relative to the past experiments lead to uncertainty in load carry capacity and crack response predictions. The stability of such

flaws may not be accurately predicted using the currently accepted methodologies and procedures developed for similar metal welds.

### 1.4 Research Hypothesis

Traditional flaw evaluation uses conservative methods to predict maximum load carrying capacity for flaws in a pipe. There is a need in the nuclear industry for a more accurate estimate of the load carrying capacity of nuclear piping such that probabilistic tools can be used to predict the time to failure for various types of cracks. These more accurate estimates will allow the nuclear industry to repair flaws at a more appropriate time considering external factors such as costs and man-rem planning along with the flaw repair. Analysis of the maximum load carrying capacity of a pipe with a complex crack (CC) has gained increased importance due to the recent identification of long CC's that have appeared in DM welds thought to be caused by PWSCC.

A numerical solution for a single material with a weld was developed that gives an accurate maximum load and crack driving force prediction for a pipe with a through wall crack (TWC), called LBBEng. To support the analysis of a CC, traditionally, an assumption is used that the CC performs similar to that of a TWC of a reduced thickness (TWCr). This modification gives a conservative prediction of the maximum load carrying capacity for a CC in a single material but was never verified for a CC in a DM weld. The research performed in this work demonstrates that the crack response of a CC can be predicted by a TWC model when modifications are made to the reduced thickness method.

## 1.5 Significance of Research

Currently, a deterministic assessment is made for LBB methodologies. The existing process and procedures do not assess piping systems with active degradation mechanisms. PWSCC is an active degradation method that is known to be occurring in systems that have been granted LBB exemptions to remove pipe whip restraints and jet impingement shields.

New methodologies or solutions are needed to accurately predict the crack response to an applied load and the driving forces required to grow cracks [35]. A new simplified methodology that can accurately predict the crack response can save significant resources by not having to develop complex finite element models.

In addition, not only the nuclear industry, but also other industries using DM welds will benefit from this research and the analysis of these experiments. The industry may, using this new technique, be able to lengthen inspection frequencies or delay repairs to a more financially suitable time, such as an outage. The industry may also be able to perform analysis to demonstrate that certain flaws will not grow under certain plant conditions, such as a reduced power operating condition. Many other international researchers have also demonstrated the need for the data from this experiment but were limited due to the cost of performing large scale pipe tests. Thus, it is likely that this data, and this new modeling technique, will benefit these researchers when the research is published.

# CHAPTER 2

# REVIEW OF LITERATURE

## 2.1 INTRODUCTION

This review of literature covers the area of fracture mechanics as it pertains to the nuclear industry. Specific issues concerning analysis of DM weld fracture are examined in detail. Large scale pipe tests require significant resources to perform, therefore, where possible correlations are made to related experiments in lieu of performing actual fracture experiments. The field of fracture mechanics relies heavily on finite element analysis (FEA) to create solutions for fracture problems. Thus, the small amount of data available from large scale pipe experiments, although not directly related to DM weld, is important to the analysis of DM welds.

## 2.2 FRACTURES IN NUCLEAR PIPING

The nuclear industry has invested a significant amount of resources in the experimental research of nuclear piping fracture starting in the 1980s. The need for fracture experiments was largely driven by intergranular stress corrosion cracking (IGSCC) found at several BWR's during the sixties and seventies. The first NRC pipe crack study group went on to publish its concern of IGSCC in 1979. The concern over a double ended guillotine break (DEGB) led to the development of the LBB concept. If the industry could demonstrate that a leak in the piping would be discovered, costly

shield and whip restraints wouldn't be required. This led to a few key milestones for the nuclear industry; the development of the American Society of Mechanical Engineers (ASME) flaw evaluation code, and the LBB criterion. In addition, many standards that are important to fracture mechanics were developed at this time such as; an American Society for Testing and Materials (ASTM) standard fracture toughness ($J_{IC}$), and an ASTM standard for J resistance (J-R) curves.

### 2.2.1 First Issues in Nuclear Piping

In 1965, cracks were discovered in stainless steel recirculation loop bypass lines of the Dresden I BWR. Additional cracks were found in six more BWRs from 1965 to 1974 [6]. The causes of all the cracks were attributed to IGSCC. During the 1970s, IGSCC became a major concern to the industry, mainly because cracks caused by IGSCC were being discovered in large diameter pipes such as; a crack in a 26 inch pipe weld at a German BWR, a crack in a 12 inch line in a Japanese plant, and a crack in a 28 inch line at the U.S. plant Nine Mile point [6]. The common factor in all the cracks was the use of austenitic stainless steel which was found to be susceptible to stress corrosion cracking.

The next major concern for cracking in nuclear piping was the discovery of cracking in the feed water piping system in the U.S. PWR plant, San Onofre. After this finding, examinations were performed and cracks were found in the feed water piping in 15 of the 32 PWRS inspected [7]. At that time, thermal fatigue was thought to be the cause of the cracks.

The result of the discovery of the cracks in both PWR and BWR plants led to an important development, the formation of the ASME Section XI committee. This

committee was tasked with developing inspection and flaw evaluation standards for the ASME Code.

### 2.2.2 ASME FLAW EVALUATION CODE

The standard for flaw evaluation in the nuclear industry is ASME Section XI [8]. The main failure mechanism in deriving the code was the net-section-collapse analysis (NSC) [9, 38] or limit load solution. This method is used when the material toughness is high enough so that the failure is controlled by the material's strength and there is little crack growth prior to reaching maximum load. This analysis assumes that fully plastic conditions exist and collapse occurs at a unique flow stress. A key assumption for the use of the NSC methodology is that the material reaches the flow stress. Most analysts term the flow stress to be the average of the yield and ultimate stresses, although some different definitions have been proposed (ex. Flow stress = $2.4S_m$, $10ksi+\sigma_y$).

Additionally, the crack geometry is idealized as either constant depth, elliptical, or parabolic. In reality, actual flaws do not form in an idealized way. But, if the assumption is that the crack is idealized to the maximum possible depth of the actual flaw, it is considered sufficiently conservative for this approach.

The problem with any such limit-load analyses is that they have limited applicability. One of the basic assumptions embodied in such analyses is that the cracked pipe section reaches fully plastic conditions. This is only the case for smaller diameter pipes and/or higher toughness materials. Another major limitation of the ASME NSC equations is that they can over predict the failure load for deep cracks, a/t >0.75 [42].

### 2.2.3 Early Fracture Mechanics in the Nuclear Industry

Prior to 1970, early fracture mechanics primarily utilized concepts from linear elastic fracture mechanics (LEFM). In 1968, Rice introduced the J-integral as an elastic-plastic fracture mechanics (EPFM) methodology [10]. Since then, this parameter has become the main method in characterizing elastic-plastic fracture in the nuclear industry.

In the late sixties, the U.S. Atomic Energy Commission, General Electric, and Battelle funded several efforts to expand the knowledge base relating to fracture mechanics. Some of the research included initiation, propagation, and arrest of axial cracks in nuclear piping at light water reactors. About 100 pipe test experiments were conducted with machined defects on pipes to validate the axially surface-cracked-pipe limit-load criterion [37].

## 2.3 Past Research in Nuclear Piping Fracture Mechanics

A significant amount of research has been performed for pipe fracture and crack propagation. The oil and gas industry along with the nuclear industry have demonstrated the most need in the past and are expected to have the most need in the future for research associated with fracture mechanics. The expense incurred in repairing large diameter piping associated with the monetary losses due to taking systems out of commission are the primary driving force to develop realistic crack stability prediction techniques.

### 2.3.1 Degraded Piping Program

Prior to 1980, fracture mechanics data and methodology for nuclear piping was very limited. As a result, the NRC sponsored a research program with the primary

objective being to verify and improve fracture mechanics analysis methods for nuclear power plant piping [11]. Results of this program were the basis for the regulatory decisions related to the application to LBB. The program was conducted in two phases, with the first phase being completed in 1983. The second phase, termed Degraded Piping Program Part II, was completed in 1989. The major difference between this program and the others performed prior to this was that the experiments in this program were performed at operating temperatures and pressures.

In total, 61 experiments were conducted with pipe sizes ranging from 4 to 42 inches. The material used for the experiments was surplus material obtained from canceled nuclear power plants. Figures 2.1, 2.2, and 2.3 illustrate the different combinations of material, type of crack, and loading conditions that were used for the experiments.

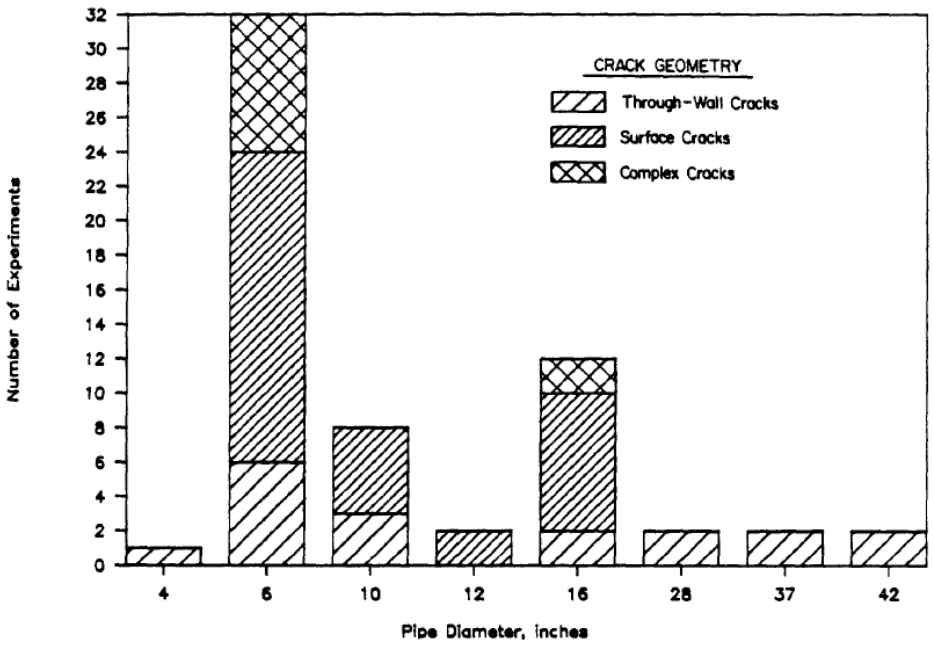


Figure 2.1. Test matrix from full scale pipe fracture experiments showing the number of experiments by diameter and crack geometry. [11]

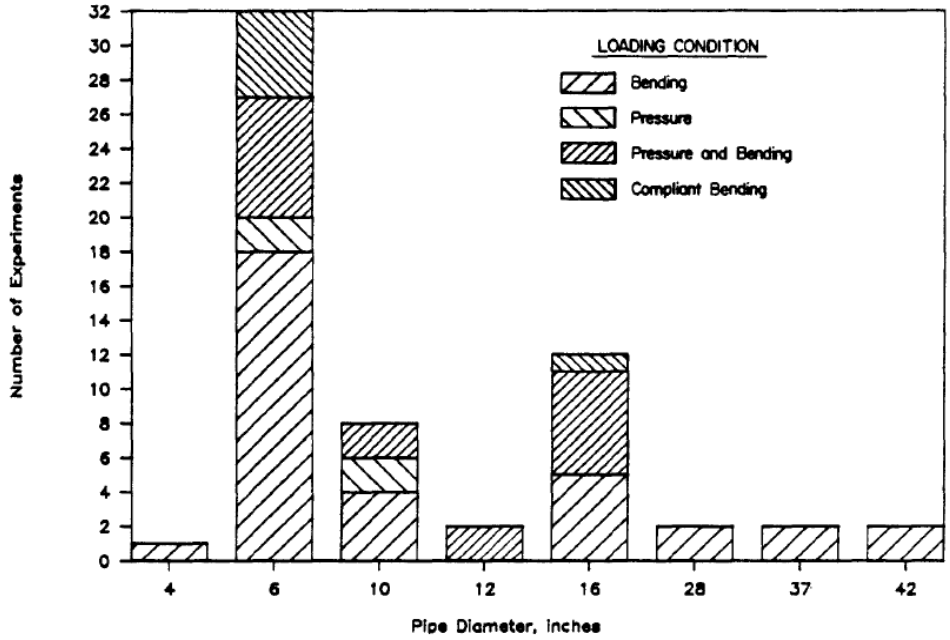


Figure 2.2. Test matrix from the full scale pipe fracture experiments showing the number of experiments by diameter and loading type. [11]

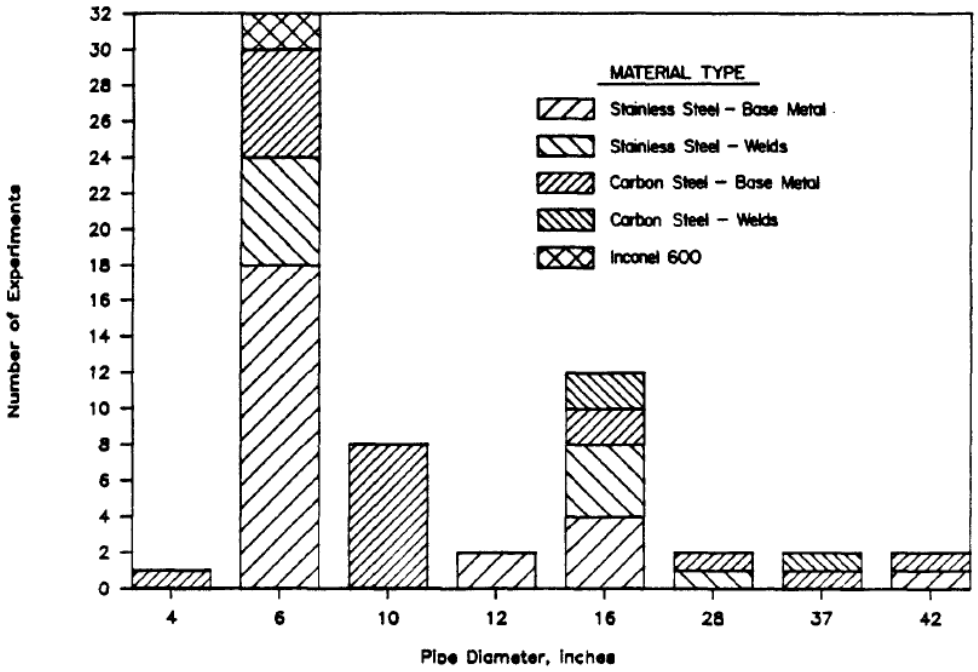


Figure 2.3. Test matrix from the full scale pipe fracture experiments showing the number of experiments by diameter and material type. [11]

The Degraded Piping Program laid the foundation for the research in fracture mechanics for nuclear piping. In addition to greatly expanding the available material property data, our understanding of complex crack behavior was improved. As seen in Figure 2.4, experiment results suggest that the apparent toughness in the complex cracked pipe will be significantly lower than that of an idealized TWC pipe. In this Figure, the y-axis is the ratio of the J-R curve calculated for a pipe tests with a complex crack ($J_{cc}$) divided by the J-R curve for a pipe test with a TWC ($J_{TWC}$). The x-axis is the ratio of the depth of the surface flaw to the pipe wall thickness (d/t) in the complex crack ligament. The significance of this finding is that the failure loads may be below that calculated using net-section collapse for a complex cracked pipe and would require an EPFM analysis. This implies that NSC is not appropriate for CC's.

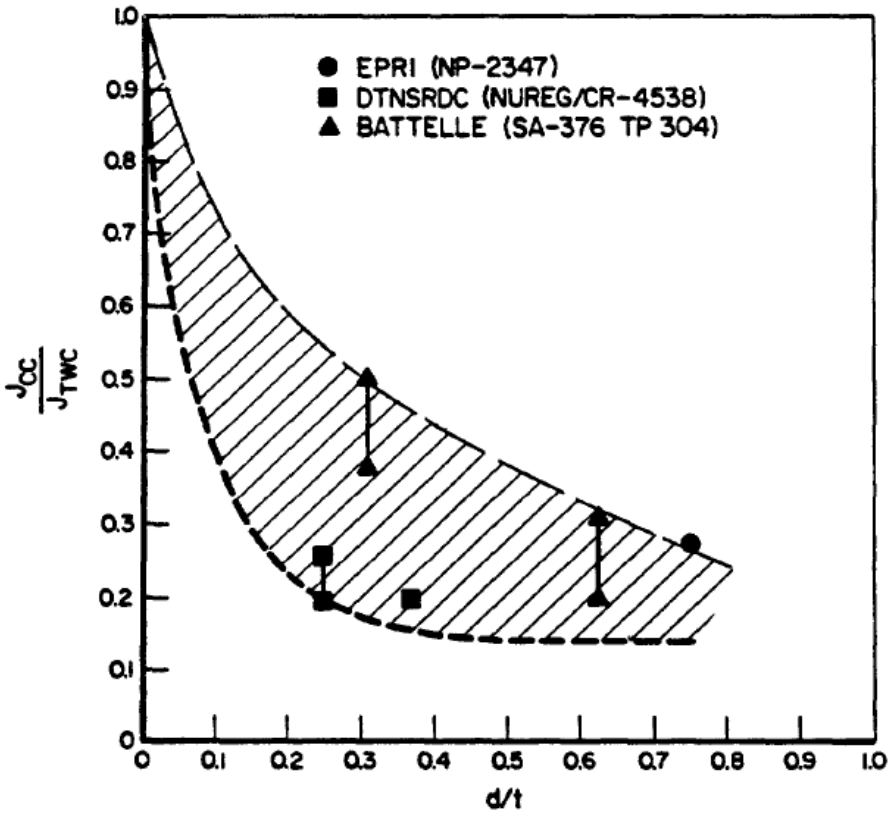


Figure 2.4. Ratio of J from complex crack experiments to J of the TWC experiments as a function of d/t. [11]

In addition to the significant findings related to complex cracks, there were several other beneficial outcomes that are directly relevant to the DM weld cracking issue that exists today. Some of those outcomes are:

- For welds, it is generally more conservative to use the base metal stress-strain curve in the load predictions rather than the weld metal strength. Some improvements could be made in developing an effective stress-strain curve, perhaps using a rule-of-mixtures, for consistency in the fracture analyses.

- Results from complex-cracked pipe experiments show that even a shallow surface crack adjacent to a TWC can significantly lower the apparent fracture resistance of the pipe.
- The program results showed that high toughness is not enough to guarantee that limit load will be reached.
- EPFM is generally needed for large diameter pipes in lieu of limit load analysis.
- Of the codes tested, LBB.ENG2 was found to be a reasonably accurate method of predicting the maximum load. LBB.ENG2 is discussed in detail in section 2.5.2.
- Using a power-law extrapolation of the $J_D$-R curve, gave reasonable and slightly conservative results when used with most pipe fracture estimation schemes.
- Over 150 tensile tests and 175 fracture toughness tests (J-R curves) were conducted in the program and were incorporated into the NRC piping material property data base (PIFRAC) [11].

The program also outlined future needs, many of which still exist today and will be accomplished through this research. Those needs include:

- Generation of additional ferritic steel weld, bimetallic welds and fusion-line toughness data, etc.,
- Refinement of the complex crack analysis and assessment of the complex crack effects on LBB predictions

### 2.3.2 INTERNATIONAL PIPING INTEGRITY RESEARCH GROUP (IPIRG-1)

IPIRG-1 [12] was a NRC led large scale fracture program that was conducted from 1986 to 1991 and was meant as a follow up to the Degraded Piping Program. The

"1" was later added to denote it was the first of two programs, but at the time it was just known as IPIRG. The revolutionary aspect of this program is that it was a joint program between the regulatory agency and the industry that involved members from nine different countries. The objective of the program was to evaluate the mechanical behavior of nuclear piping flaws. Both small (6 inch) and large (16 inch) diameter pipes were evaluated under high rate cyclic loading under PWR conditions, 550F and 2250psi.

The program provided a significant amount of information to the field of fracture mechanics for large scale pipe experiments. The program also verified the predictive capability of several analytical codes. One conclusion of the program stated, "DEGB is not likely to occur during a single loading cycle during a seismic event unless a very long surface crack exists" [12]. This statement is the major driving concern for PWSCC research due to the fact that PWSCC can result in long cracks in a relatively short period of time.

### 2.3.3 SHORT CRACKS PROGRAM

The Short Cracks in Piping and Piping Welds Program was initiated to continue the work done in the Degraded Piping Program [13]. The program was conducted from 1990 to 1995 with the main objective being to further expand the fracture mechanics knowledge base for use in the nuclear arena. Some of the key advancements include:

- Two computer codes were developed, NRCpipe and NRCpipes, which are still used for flaw evaluation by the NRC as of 2012. The codes integrated several of the J-estimation schemes, discussed in section 2.5, behind a graphical user

interface which allowed users to analyze flaws without having to have knowledge of a programming language.

- Demonstration that the fusion line of bimetallic welds between Inconel 182 weld metal and carbon steel piping has toughness comparable to the carbon steel base metal.
- The PIFRAC database was expanded to contain material property on over 800 tensile specimens and over 800 fracture toughness specimens. Pipe fracture databases for circumferentially cracked straight pipe (CIRCUMCK) and axially cracked pipe (AXIALCK) were also created. The databases contain results from 800 and 300 experiments respectively.

Another interesting outcome from the short cracks programs was the examination of why cracks would turn and move along the weld fusion line. It was found that the fusion line J-R curve reached a steady state value and the weld metal had a continually increasing J-R curve. It was postulated, that to properly model the resistance one could use the weld metal J-R curve up until the point that the fusion line J-R curve was reached then use that curve to model the rest of the behavior, as shown in Figure 2.5.

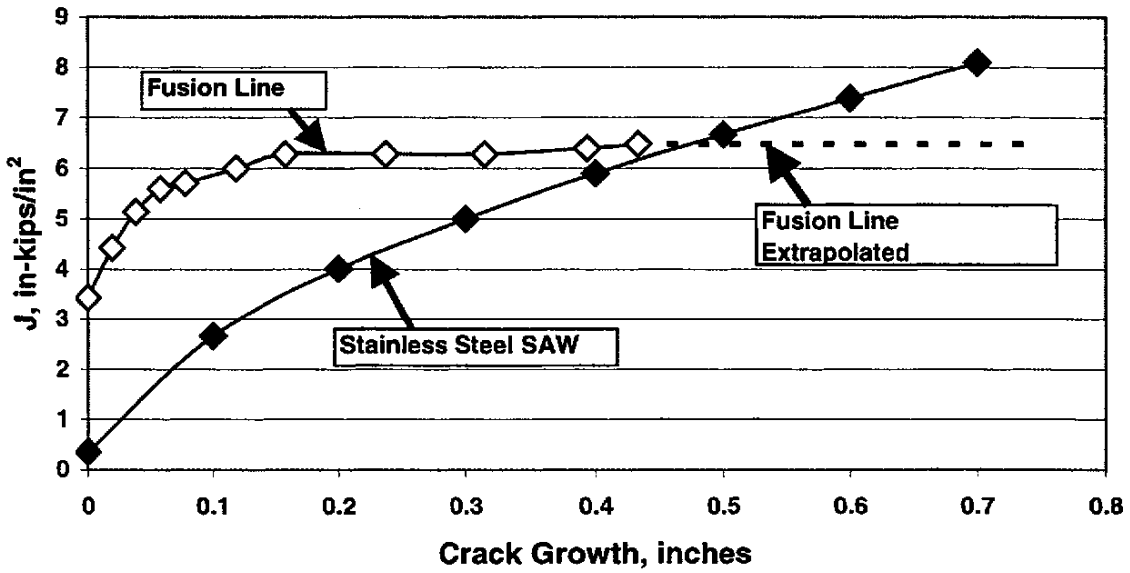


Figure 2.5. Weld metal and fusion line J-R curve data. [14]

### 2.3.4 INTERNATIONAL PIPING INTEGRITY RESEARCH GROUP (IPIRG-2)

IPIRG-2 was the second international piping research group and was primarily focused on cracked pipe under seismic loading [15]. This research program was expanded to include the NRC, EPRI, as well as 15 other countries. The experiments included carbon and stainless steel pipe with and without welds. Data from this program was used to further develop J-estimation schemes and expand the piping databases. Some of the key conclusions from the program were [15]:

- A relationship was developed between yield/ultimate strength ratio versus toughness under dynamic and cyclic loading relative to the toughness under quasi-static monotonic loading. This type of relationship is important since most of the typical pipe material fracture toughness data in the world are developed under quasi-static loading.

- It was shown that cyclic plastic loading prior to crack initiation and during ductile crack growth causes a toughness degradation effect which is a function of a number of complicated parameters, but could be simplified for bounding cases.
- A simplified methodology was developed to predict axial and circumferential surface-cracked elbow fracture loads that looks promising as a modifiable method. This uses a simple geometric multiplier times the straight pipe solutions to predict the cracked elbow loads at the start of ductile tearing and at maximum load.
- It was demonstrated that the existing circumferential through-wall-cracked pipe analyses for short cracks, as used in LBB analyses for large diameter pipe, was valid in a pipe-system experiment.
- It was shown that for a girth weld surface crack at a pipe-to-elbow weld, that the elbow ovalization did not affect the fracture loads.
- For LBB analyses, factors that affect the COD for normal operating stresses were found to be more important for the conditional failure probabilities than the magnitude of the seismic loads, i.e., weld residual stresses, pipe-system boundary conditions that restrain the COD from pressure stresses, problems with the friction factor equations with tight cracks in the leak-rate codes, etc. are most important.

### 2.3.5 International and Miscellaneous Programs

Many other programs that were not of the same magnitude as those discussed, both in the U.S. and internationally, were performed over the past few decades that

contributed to the fracture mechanics knowledge base. Some of the most significant programs and their associated outcomes are listed below.

#### 2.3.5.1 BATTELLE INTEGRITY OF NUCLEAR PIPING (BINP)

At the end of the Second IPIRG program, Battelle was charged with the responsibility of identifying any holes remaining in the technology that may still need to be addressed in the area of pipe fracture technology. The BINP program was developed to address the most pressing of those topics. The BINP program [16] had several outcomes that are important to fracture mechanics. One outcome, task 8b of the program, was focused on PWSCC. Some of the conclusions of this task were that are applicable to this research are:

- Circumferential PWSCC is dominated by service loads
- Axial crack growth is dominated by residual stresses
- Circumferential PWSCC cracks tend to grow very long prior to breaking through wall. This could lead to very long complex cracks that could go undetected for a long period of time.

#### 2.3.5.2 JAPANESE CARBON STEEL PIPING PROGRAM

In the 1990s, the Japanese completed a program on carbon steel pipe fracture [17, 18]. These tests were quasi-statically loaded pipe tests on 6, 16, and 30 inch diameter pipe. Experiments were conducted on Japanese carbon steel pipe under pressure and bending at 300 C Battelle and in Japan. The tests provided some results that showed high

toughness pipes tend to fail at limit load conditions and added to the material property databases.

#### 2.3.5.3 NRC/HDR/BATTELLE DYNAMIC PIPE ANALYSIS

The objective of this program was to have Battelle independently analyze the results from a pipe test performed at the HDR facility in Germany [19]. Battelle used the methodologies developed from IPIRG-1 to analyze a water hammer induced dynamic load and its effects on fracture. The major outcomes of this program were improvements to the Battelle crack pipe element methodology. Improvements from this program were later incorporated into the NRCpipe Code. Additionally, data from two more large scale pipe tests were incorporated into the material databases.

#### 2.3.5.4 MRP 115 AND 216

In response to the concern of PWSCC by federal regulators, EPRI commissioned research projects called Materials Reliability Program Crack Growth Rates for Evaluating PWSCC of Alloy 82, 182, and 132 welds (MRP 115) and Materials Reliability Program Advanced FEA Evaluation of Growth of Postulated Circumferential PWSCC Flaws in Pressurizer Nozzle DMWs (MRP 216) published in 2002 and 2007 respectively [20, 21]. MRP 115 had a primary objective to develop a crack growth rate (CGR) model for alloys 82/182/132, the materials of concern for PWSCC. An expert panel was formed to lead this task and collected CGR laboratory test data from all known sources and subsequently developed a deterministic CGR model. Additionally, the study focused on the parameters that cause PWSCC such as chromium content, chemical environments, effects of

hydrogen, effects of welding conditions, and the effects of other impurities in the materials. MRP 115 extends the work previously completed under MRP 55 [36].

After the large surface crack was found at Wolf Creek nuclear power plant, the NRC with its contractors Battelle and EMC$^2$, completed a technical review [22] that analyzed the CC to determine if it was plausible that the crack could have ruptured before evidence of leak occurred. The conclusion of the extensive technical review was that rupture was possible. The financial implications of that conclusion, if found to be a basis for changing the regulations, could have been significant to licensees by requiring fuel outage times to be shortened, have mid-cycle outages, increase inspection frequency, or eliminate the LBB relief for PWSCC vulnerable systems. Upon publishing the findings, EPRI commenced an independent study of the issue, MRP 216.

The stated objective of MRP 216 was "to evaluate the viability of detection of leakage from a through-wall flaw in an operating plant to preclude the potential for rupture of pressurizer nozzle DM weld, given the potential concern about growing circumferential stress corrosion cracks" [21] As part of this evaluation, EPRI staff utilized a newly revised computer package FEAcrack. FEAcrack is specifically designed for fracture analysis of pipes and plates utilizing either WARP3D or ABAQUS for FEA. The code was improved to allow for growth of cracks having a custom profile. This was an important advancement, because nuclear industry staff made the claim that idealized crack shapes resulted in a large overestimation of the crack area and thus a large underestimation in the crack stability which led to accelerated crack growth which was believed to be overly conservative. The NRC performed a confirmatory analysis with similar results to that of the industry analysis.

In all, the study included 119 cases to address the weld-specific geometry and load input parameters. 109 of the cases in the main study showed either stable crack arrest or leakage. In most cases, there was a large amount of time for either the crack to become stable or for leakage to occur. Ten cases were added with multiple flaws which also resulted in stable crack arrest or leakage. An additional finding of the study was that a number of cases showed that stable crack arrest occurred prior to through-wall penetration. The deterministic crack growth model generated in MRP 115 was used for crack growth in the FEA model. Additionally, a comparison was made between the EPRI code Pipe Crack Evaluation Program (PICEP) and the NRC code Seepage Quantification of Upsets in Reactor Tubes (SQUIRT). From the study, it was found that SQUIRT had a slightly higher leak rate in most cases but generally both codes were in good agreement [21] as shown in Figure 2.6.

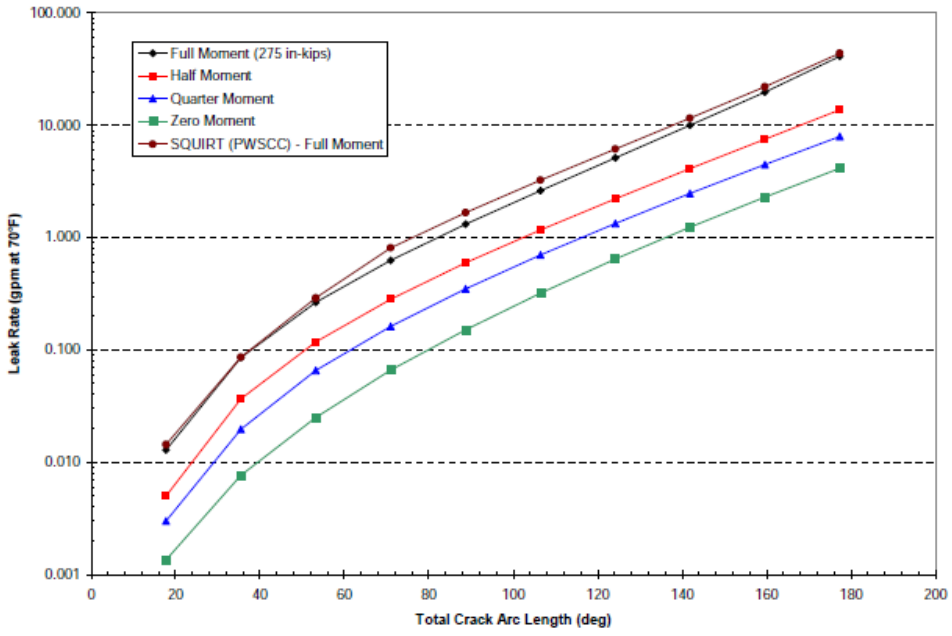


Figure 2.6. Comparison of leak rates for PICEP and SQUIRT for the Wolf Creek Flaw. [21]

## 2.4 FRACTURE ANALYSIS METHODS

There are two principal methods that are commonly used fracture analysis for predicting failure for circumferentially cracked pipe. These two methods are finite element analyses and J-estimation schemes. The finite element analyses of a circumferentially cracked pipe, although in principle quite simple, involves a great deal of computational effort to model the 3-dimensional geometry of the crack under load and also requires a model to be created for each specific case. In contrast, the J estimation schemes make various simplifying assumptions and often rely upon curve fitting of previously developed finite element solutions to generate approximate solutions for critical fracture parameters. The level of effort associated with conducting a J-estimation analysis is significantly less than that for conducting the finite element analyses and J-estimation solution are more readily incorporated as modules into other codes, as will be done for xLPR.

Estimation methods are used to predict crack initiation loads, maximum loads, and load line displacement from a J-R curve. In a typical J-estimation analysis the load point rotation due to the presence of a crack, $\Phi^c$, and the relevant driving force admit additive decomposition of elastic and plastic components given by:

$$J = J_e + J_p$$

$$\phi^c = \phi_e^c + \phi_p^c$$

The symbol $\phi^c$ is the load-point rotation and $J$ is the crack driving force. The subscripts "e" and "p" refer to the elastic and plastic contributions. In the following, some general information on common estimation methods is listed.

These J-estimation schemes were validated by experiments conducted at Battelle [37]. These experiments were of pipes with TWCs in base metals and similar metal welds. The data illustrates that the GE/EPRI method is conservative and the LBB.ENG2 method resulted in the closest estimation of the load carrying capacity from the experiments. In addition, the validation suggests that for similar metal welds with circumferential cracks, the weld metal toughness and the base metal strength properties should be used for accurate load-carrying capacity predictions.

### 2.4.1 ORIGINAL GE/EPRI METHOD

This method is based on a compilation of finite element solutions for TWC pipes using deformation theory of plasticity. J is calculated as:

$$J_e = f_1\left(\frac{\theta}{\pi}, \frac{R_m}{t}\right)\frac{M^2}{E}$$

$$J_p = \alpha\sigma_O\epsilon_O R_m\theta\left(1-\frac{\theta}{\pi}\right)h_1\left(\frac{\theta}{\pi}, \frac{R_m}{t}, n\right)\left(\frac{M}{M_O}\right)^{n+1}$$

Where

$\alpha$ is the Ramberg-Osgood parameter

$\sigma_O$ is the Ramberg-Osgood reference stress

$\epsilon_O$ is the Ramberg-Osgood reference strain

$R_m$is the mean radius

$\theta$ is the half crack angle

$n$ is the Ramberg-Osgood strain hardening exponent

$t$ is the wall thickness

$M$ is the moment

$E$ is the elastic modulus

$M_O$ is the limit moment of a through wall cracked pipe under pure bending

The expressions $f_1$ and $h_1$ are influence functions calculated from finite element results that are tabulated in reference 24 and 25.

### 2.4.2 LBB.ENG2 METHOD

The LBB.ENG2 method involves an equivalence criterion incorporating a reduced thickness analogy for simulating system compliance due to the presence of a crack in pipe. The elastic component, $J_e$, is the Sanders solutions. The plastic component, $J_p$, is:

$$J_p = \frac{\alpha}{E\sigma_0^{n-1}} \frac{\pi R_m}{2(n+1)} H_B(n,\theta) L_B(n,\theta) I_B \left(\frac{M}{\pi R_m^2 t}\right)^{n+1}$$

$I_B$ is a compliance function and $H_B(n,\theta)$ and $L_B(n,\theta)$ are functions with explicit forms available in references 26, 27, and 28

The LBB.ENG2 method was also extended to account for a crack in a weld [29]. This method is called LBB.ENG3 and the plastic solution is given by:

$$J_p = \frac{\alpha_1}{E_1\sigma_{01}^{n_1-1}} \frac{\pi R_m}{2(n_1+1)} H_B(n_1,n_2,\theta) L_B(n_1,n_2,\theta) I_B \left(\frac{M}{\pi R_m^2 t}\right)^{n_1+1}$$

The additional subscripts on the variables E, $\sigma_0$, $\alpha$, and n represent base and weld metal properties. All other symbols not defined in this section are defined in 2.4.1.

### 2.4.3 TADA-PARIS METHOD

For this method [30] J is obtained by an η-factor method using an interpolation between the linear-elastic and full plastic limit-load solutions. Thus, J calculated by this method only depends on the pipe geometry and flow stress.

For linear elastic and fully plastic conditions in TWC pipes, the J-rotation relationship is well known. This method interpolates between these two known solutions by artificially increasing the crack size using a plastic zone correction and substituting the artificially increased crack size into the elastic solution to obtain the moment-rotation relationship in the elastic-plastic regime. From LEFM, the moment and elastic rotation due to the crack ($\phi_e^c$) are related by:

$$M = \frac{E\pi R_m^2 t}{I_B}\phi_e^c$$

Applying the correction factor to get an effective crack size ($\theta_e$) and total rotation ($\phi^c$) in place of ($\theta$) and ($\phi_e^c$), the equations for $J_e$ and $J_p$ using this method are:

$$J_e = \frac{K_I^2}{E}, K_I = \frac{M}{\pi R_m^2} F_B \sqrt{\pi R_m \theta}$$

$$J_p = \frac{\sigma_f R_m \left[\sin\left(\frac{\theta}{2}\right) + cos\theta\right]}{M_{RP}} \int_0^{\phi_p^c} M d\phi_p^c$$

In this solution, $\sigma_f$ is the flow stress and $M_{RP}$ is the rigid-plastic moment from a limit load analysis. All other symbols not defined in this section are defined in 2.4.1.

### 2.4.4 NRC.LBB

The LBB.NRC method for TWC pipes [31] is similar to that of the Paris/Tada method. The difference is that the elastic component of rotation is increased by the Irwin plastic-zone correction, written as:

$$\phi_p^c = \alpha \left( \frac{\sigma}{\sigma_f} \right)^{n-1} \phi_e^c$$

The plastic component of rotation is increased or decreased depending on the current applied stress level. Thus, the effects of strain-hardening are incorporated in the evaluation of the J-integral. All other symbols not defined in this section are defined in 2.4.1.

### 2.4.5 Limitations of Current Methods

When performing a flaw analysis, it is appropriate using the current standards to assume an idealized flaw shape [32, 33]. The current estimation schemes that are utilized by the nuclear industry require the flaw to be ideal, either constant depth or semi-elliptical as shown in Figure 2.7. However, recent analyses have shown that PWSCC cracks are not ideal, as shown in Figure 2.8. These cracks can grow as very long surface cracks before breaking through the surface and becoming complex cracks of irregular shape.

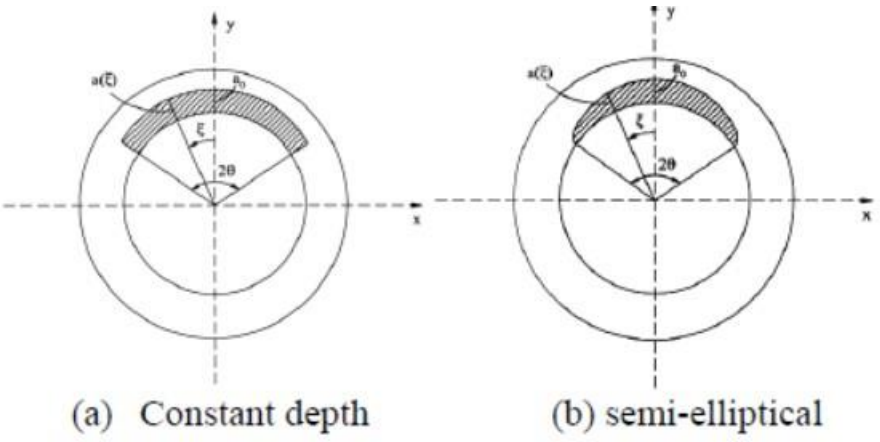


Figure 2.7. Surface crack idealized shapes. [5]

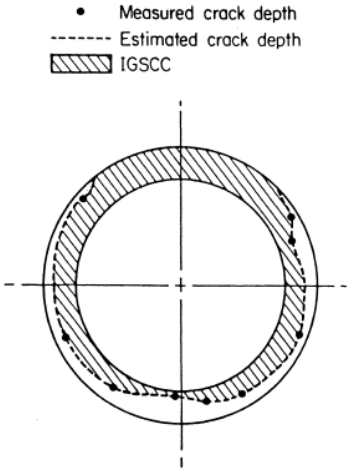


Figure 2.8. Complex crack shape from Duane Arnold nuclear plant. [5]

For high toughness base metal cracks, the data is inconclusive because historical experiments have demonstrated failure under both limit load at EPFM. For nuclear piping with a DM weld, experimental data does not exist for CC's or TWCs to make an evaluation of the failure mode. In addition, two recent independent technical reviews of the crack found in a DM weld at Wolf Creek nuclear power plant, performed by the NRC and EPRI [22], indicated different failure modes for the same crack. The NRC technical review, in particular, was significant because it showed that the crack would rupture prior to leakage as required by LBB.

Existing estimation schemes also require the modification of the input data to account for complex cracks. The method for accounting for complex cracks is to create a TWC with a reduced thickness (TWCr), as seen in Figure 2.9. This method was verified for certain base metal cracks and showed good agreement for maximum load, although slightly conservative. However, the method has not been tested for high toughness DM weld cracks. Additionally, the method does not account for the plastic deformation and additional constraint that has occurred along the surface crack portion of the complex crack.

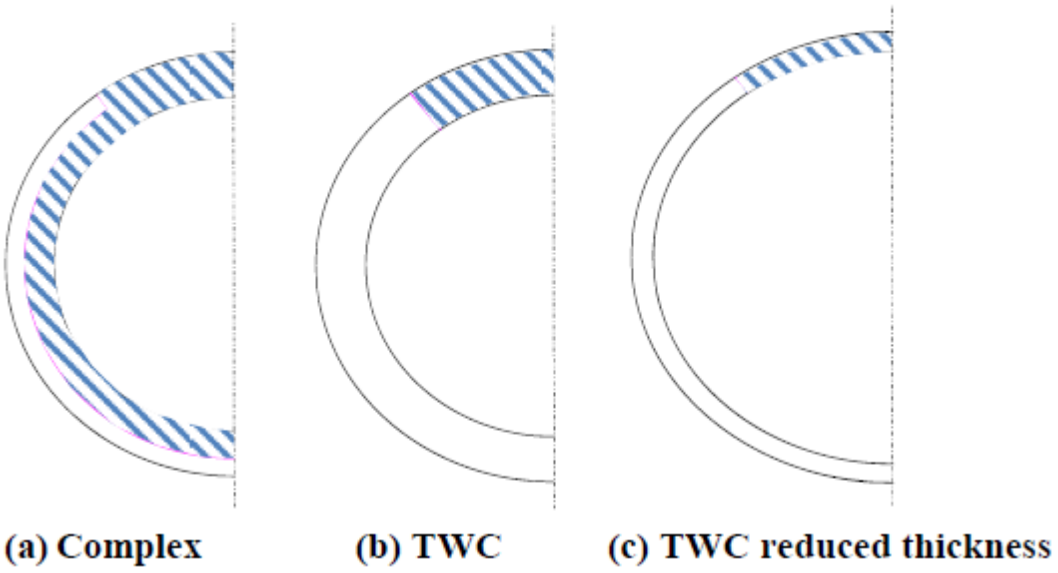


Figure 2.9. Crack shape modification for current estimation schemes. [34]

All but one of the current estimation schemes are designed for single materials. LBB.ENG3 was developed so that two materials can be evaluated, a base metal and a weld metal. A method was proposed [35] to modify the material data for the current estimations schemes to account for the three different materials. The method required

averaging the base metal properties to create an equivalent material. The method shows good accuracy for TWC but not for complex cracks when verified by FEA. The method was never verified by actual experimental data.

# CHAPTER 3

# METHODS AND PROCEDURES

## 3.1 METHODOLOGY

The method used for fracture analysis is that of generating a numerical solution that can accurately predict the experimental fracture behavior. The primary data gained from fracture experiments are load versus displacement curves and crack growth. Using this data, estimation schemes are generated to accurately predict the experimental load displacement curves, or moment-rotation, which can then be scaled to account for different geometrical configurations.

## 3.2 EXPERIMENT DESIGN

The pipe fracture experiment was conducted in a 4-point bending test without internal pipe pressure while the pipe was maintained at a temperature of 600F. Loading was at a quasi-static loading rate. The test specimen was unloaded several times after maximum load is reached which heat tinted the fracture surface for crack growth determination, as seen in Figure 3.1. The specimen was then cooled, reloaded until completely broken, and the crack length increment ws measured optically from the unload marks. The nominal dimensions of the pipes used for this experiment are a diameter of 8.5 inches and a thickness of .85 inches.

Figure 3.1. Test specimen with arrows annotating the unload marks.

### 3.2.1 TEST SET UP

The pipe tests were conducted in Battelle's Fatigue and Structures Laboratory using the 500 kip MTS fatigue machine as a load frame seen in Figure 3.2. The test was performed on an unpressurized pipe at 315C (600F). The inner span for the 4-point bend loading is 1.32 m (52 inches). The outer span is 3.15 m (124 inches). For the load frame shown in Figure 3.3, the inner two rams pulled down on the pipe, putting the bottom half of the pipe in tension. The crack is located on the bottom of the pipe centered laterally and axially.

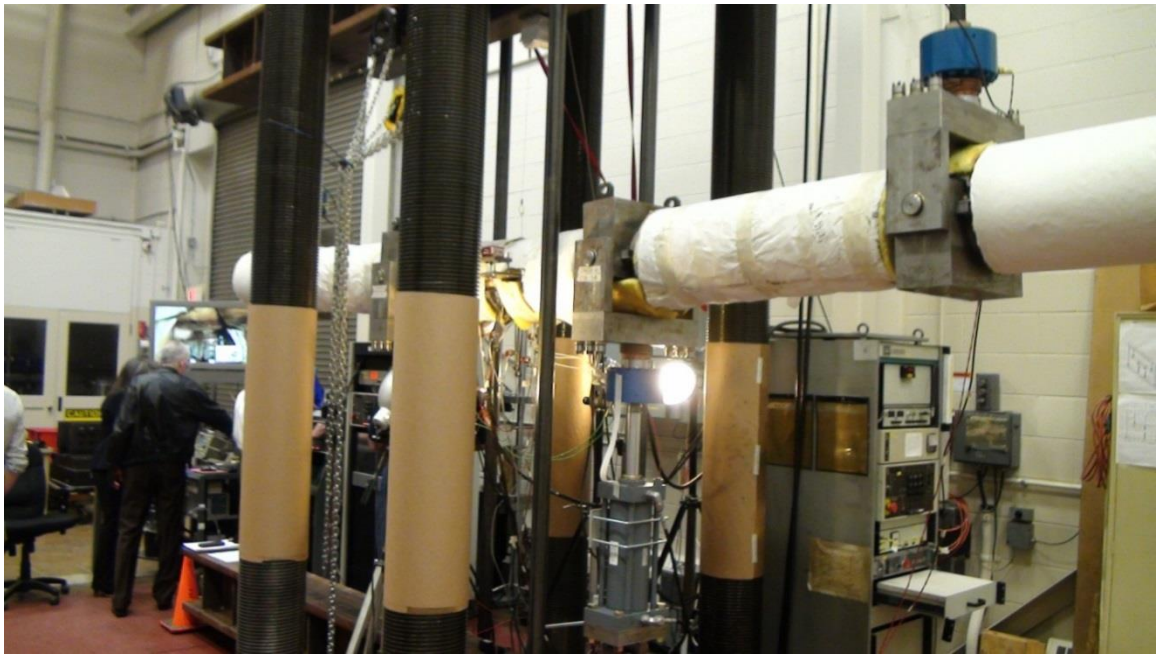

Figure 3.2. 500 kip MTS servo-hydraulically controlled test frame in Battelle's Fatigue and Structures Laboratory.

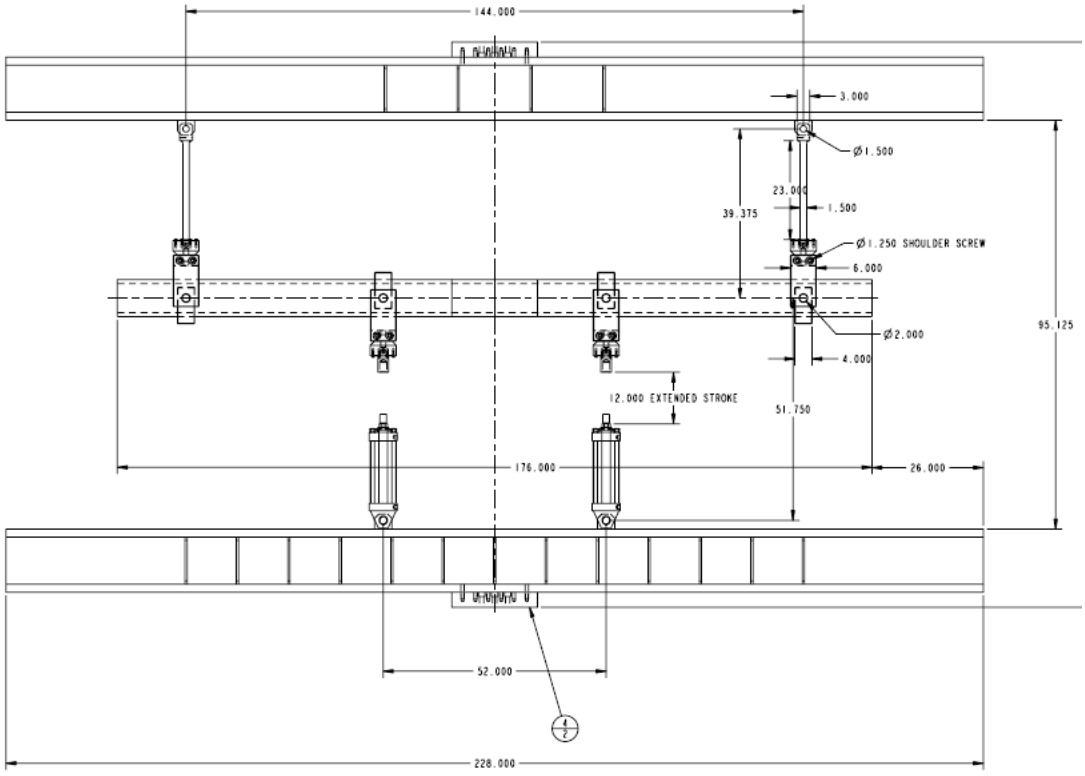


Figure 3.3. Strongback and saddle design to be used in DMW pipe fracture experiments (picture provided by Battelle). Full size photo in Appendix D.

During some initial load testing it was found that the outer saddle, Figure 3.4, could slide in some instances making the data more difficult to analyze. Thus, going forward, slide limiters were welded on to the pipe to prevent the saddles from moving while the pipe is loaded.

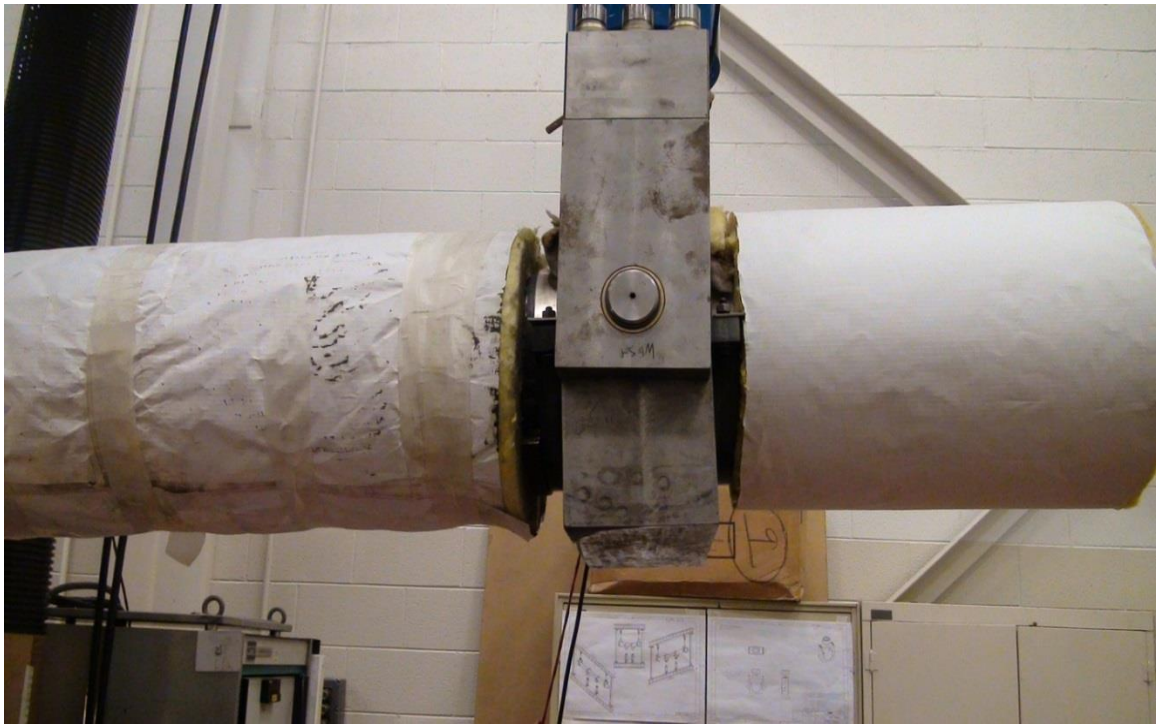

Figure 3.4. Outer saddle.

A large amount of data was collected during this test. Video data of crack growth was recorded during the entire test recording the crack growth as seen in Figure 3.5. The instrumentation plan for the complex cracks and through wall cracks are the same. The data collected during the cracked pipe experiments included the following:

- The applied load at each of the 4 load points.
- The load-line displacement at the two hydraulic actuators.

- The displacement at the crack plane with respect to the load frame, made with a string potentiometer.
- Rotations (using inclinometers) of each of the 4 load points.
- Crack mouth opening displacements (CMOD) at the crack centerline and both of the initial through-wall crack tips. Clip gages will be used to measure the CMOD data. Figure 3.6 is a photo of the clip gage that is used in this experiment.
- Crack initiation using electrical potential.
- Electric potential probes is applied across the crack at the crack centerline and both of the initial through-wall crack tip locations on the outside pipe surface. In addition, there will be a location where the base metal electric potential data will be measured.
- Pipe rotation data using inclinometers mounted on the top of the pipe on either side of the test weld will be measured.
- Pipe temperature is measured using thermocouples.

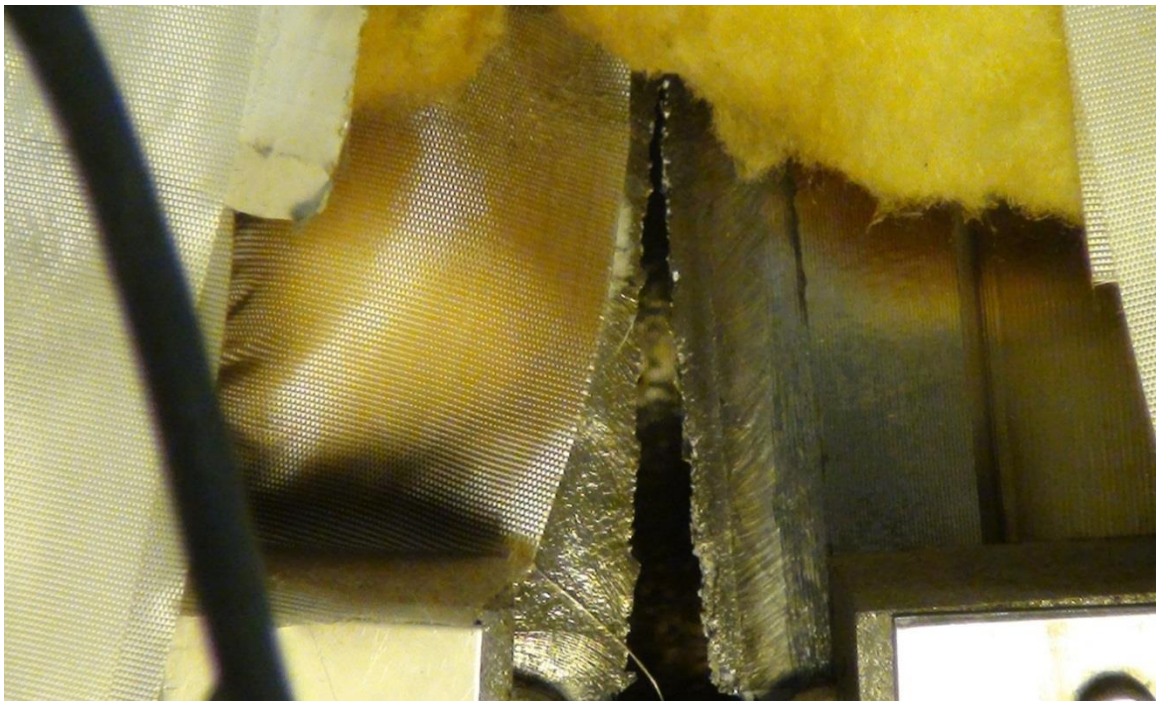

Figure 3.5. Video still from DMW 4 pipe test.

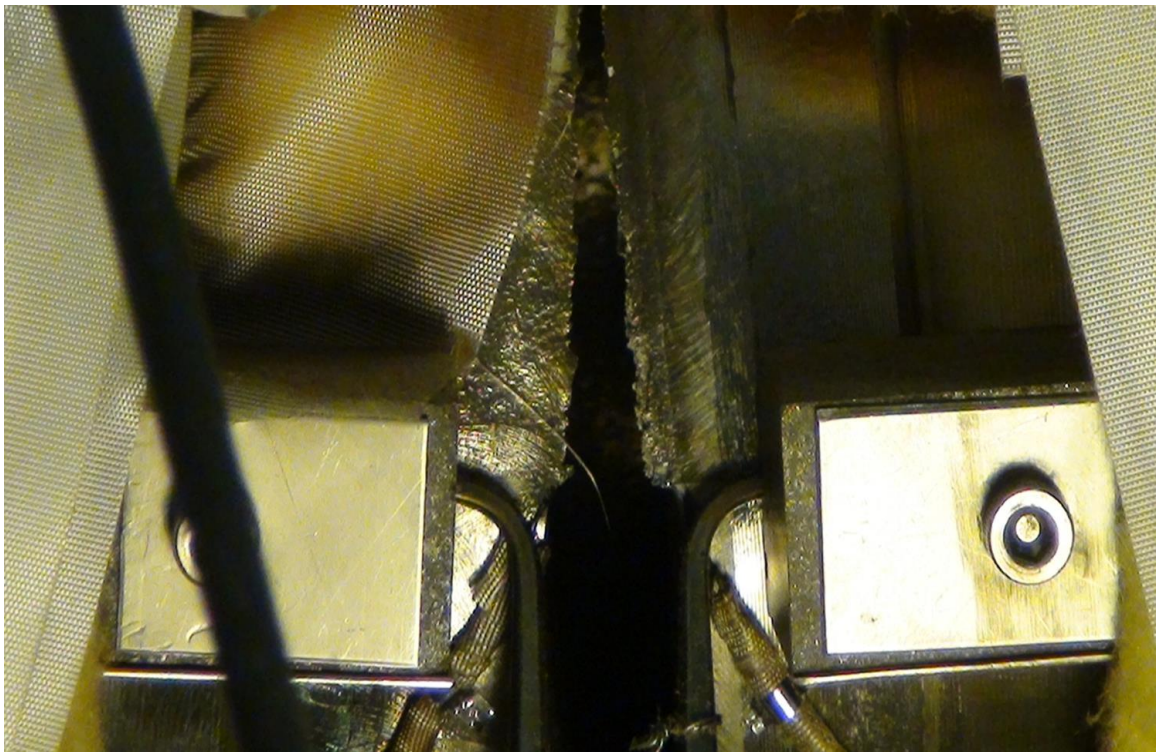

Figure 3.6. Picture of clip gage used for the CMOD measurements.

### 3.2.2 SPECIMEN PARAMETERS

The pipe specifications for this experiment are similar to that used in common reactor applications. However, some variance is expected because the pipe was not necessarily manufactured at the same facility as the pipe that is used in reactor applications. The potential slight difference in materials is believed to have minimal impact on the correlations and estimation solutions that are developed as a result of the experiment. Some of the important pipe parameters for this test are:

- 8 inch diameter Schedule 160 pipe nominally 8.625 inches OD with a wall thickness of 0.85 inches (Normally 8 inch Schedule 160 pipe is 0.906 inches thick but for this experiment the ID has been machined to yield a uniform wall thickness)
- The weld OD and ID have also been machined to remove the weld crown and any burn through on the ID
- Welds join sections of a high strength A106C carbon steel pipe to Type 316 stainless steel pipe; this particular A106C pipe has strength properties at temperature (600 F) that approach those of A508 Grade 2 material
- Butter applied using SMAW Inconel 182 stick
- Buttered carbon steel pipe post-weld heat treated
- Main weld made using GTAW Inconel 82 weld wire

Property tests were performed on the material used in this experiment to obtain material/test specific properties. Ramberg-Osgood parameters were also determined from the stress strain data. Tensile test data is listed in Table 3.1.

Table 3.1. Material properties for carbon and stainless steel.

| DMW program tensile tests | | | |
|---|---|---|---|
| | SS side of specimen | CS side of specimen | Inconnel (82, 182) |
| $\sigma_{y(psi)}$ | 22600 | 42000 | 46400 |
| $\sigma_{u(psi)}$ | 68700 | 89200 | 81300 |
| E(psi) | 2.50E+07 | 2.80E+07 | 2.95E+07 |
| $\sigma_0$ | 22600 | 42000 | 46400 |
| $\epsilon_o$ | 0.000904 | 0.0015 | 0.001573 |
| $\alpha$ | 3.35 | 4.22 | 4.45 |
| n | 10.1 | 2.16 | 6.31 |

### 3.2.3 SPECIMEN FABRICATION

This experiment required the fabrication of thirteen different pipes with DM welds. Of the 13 fabricated pipes, seven were machined with CCs, one with a pure SC, and five with TWCs. The cracks in each experiment are located either in the main weld, the butter, or along the fusion line between the carbon steel pipe material and the inconel butter. The CCs were machined with different SC depths; a shallow crack (20% of the wall thickness), an intermediate crack (40% of the wall thickness) and a deep crack (60% of the wall thickness). DMW 13 was cycled to create a sharp crack tip, while the other experiments were not and are not considered to have a sharp crack tip. For the CCs and the TWC experiments, the fraction of circumference that was machined as a TWC was 20% for one pipe and 37% for the other TWCs and CCs. The choice of a 37% TWC and the depth of SCs were selected because they are similar to many of the previous experiments that were performed by Battelle and also to limit the load application requirements for the experimental setup. Thus, this will simplify the comparison of results to previously performed single metal fracture experiments.

For the CC specimens the internal SC was machined first. This SC was machined using a vertical machining cutter using a tapered blade, see Figure 3.7.

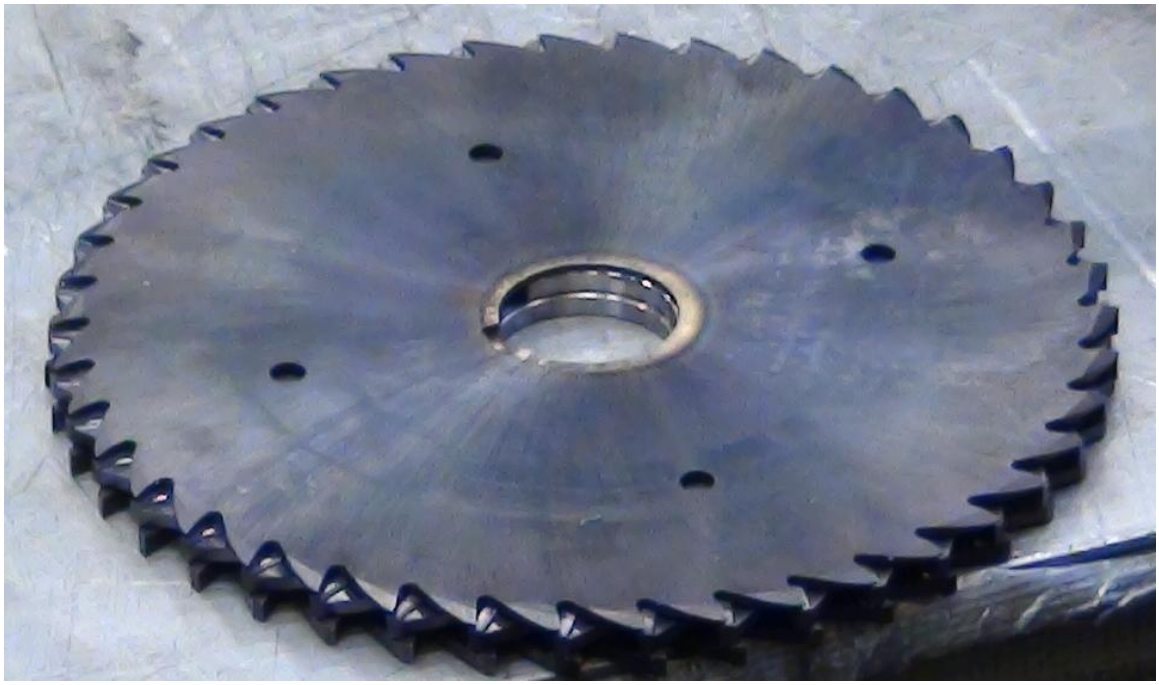

Figure 3.7. Blades used in machining the internal SC.

After the SC was machined, the bulk of the TWC was introduced using a wire cut electro-discharge-machining (EDM) process. The tips of the TWC were sharpened using a plunge EDM process with a tapered electrode as shown in Figure 3.8 and Figure 3.9. The shape of the electrode was designed to eliminate the sharp corner at the interface of the SC and the TWC.

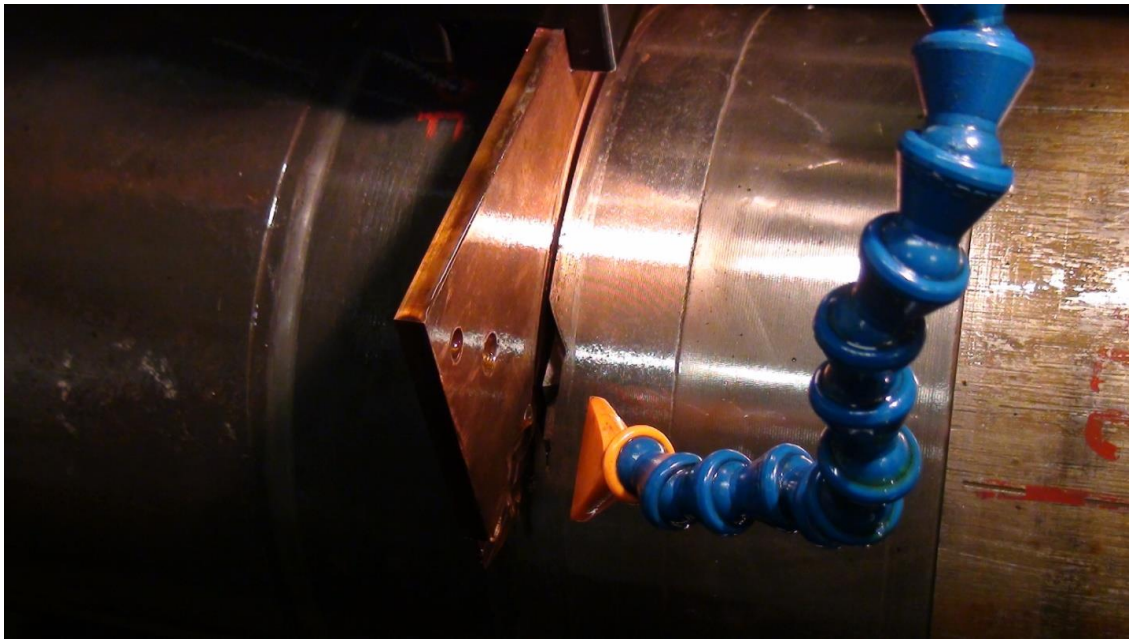

Figure 3.8. EDM cutter being used to create a TWC in the pipe.

Figure 3.9. Picture of electrode used in EDM process with electrode design feature used to reduce taper circled.

Following the completion of the machining process of the test pipe section, the inside pipe surface was instrumented with the necessary instrumentation that were

required to obtain the data listed in 3.2.1. Next, the moment arms were welded onto the test specimens then the pipe was placed into the strongback and saddles and the exterior of the pipe instrumented. Finally the instrumentation was hooked up to the data acquisition system.

### 3.3 TEST PLAN

Table 3.2 lists the number and combination of experiments that were performed based on the three key variables; type of crack, location, and size of crack. The combination of different variables were developed using the lessons learned from past base metal complex crack-shaped experiments. In addition, companion laboratory-sized fracture and tensile experiments were conducted to fully characterize each material.

Table 3.2. Test matrix of DM weld pipe experiments.

| Experiment Number | Type of Crack | Crack Location | Surface Crack a/t | Surface Crack θ/π | TWC θ/π |
|---|---|---|---|---|---|
| DMW-0 | Uncracked | N/A | N/A | N/A | N/A |
| DMW-1 | Complex Crack | Weld | 0.2 | 1.0 | 0.37 |
| DMW-2 | Complex Crack | Weld | 0.4 | 1.0 | 0.37 |
| DMW-3 | Complex Crack | Weld | 0.6 | 1.0 | 0.37 |
| DMW-4 | Complex Crack | Butter | 0.2 | 1.0 | 0.37 |
| DMW-5 | Complex Crack | Butter | 0.4 | 1.0 | 0.37 |
| DMW-6 | TWC | Weld | N/A | N/A | 0.20 |
| DMW-7 | Complex Crack | Fusion Line | 0.2 | 1.0 | 0.37 |
| DMW-8 | Complex Crack | Fusion Line | 0.4 | 1.0 | 0.37 |
| DMW-9 | TWC | Butter | N/A | N/A | 0.37 |
| DMW-10 | TWC | Weld | N/A | N/A | 0.37 |
| DMW-11 | TWC | Weld | N/A | N/A | 0.37 |
| DMW-12 | Surface Crack | Weld | 0.6 | 1.0 | N/A |
| DMW-13 | TWC (fatigue precracked) | Weld | N/A | N/A | 0.37 |

The test matrix includes 13 cracked pipe fracture experiments plus one uncracked experiment. The uncracked experiment was performed to ensure that the experimental facility functions as expected, primarily establishing that the data acquisition system is functioning properly. The calibration of all instrumentation is traceable back to the National Institute of Standards and Technology (NIST). In addition all tests were:

- Conducted without internal pressure

- Conducted at 315C(600F)
- Brought to temperature and held at temperature for an hour prior to loading
- Displacement control loaded at quasi-static loading rates

After the maximum load was achieved, the test specimen was unloaded and reloaded several times to mark the fracture surface. Post-test measurements of the marked fracture surface will be used to help calibrate the d-c EP versus crack growth curve. Digital videos and pictures of the crack tips were recorded and synchronized in time with the data acquisition system, illustrated in Figure 3.10.

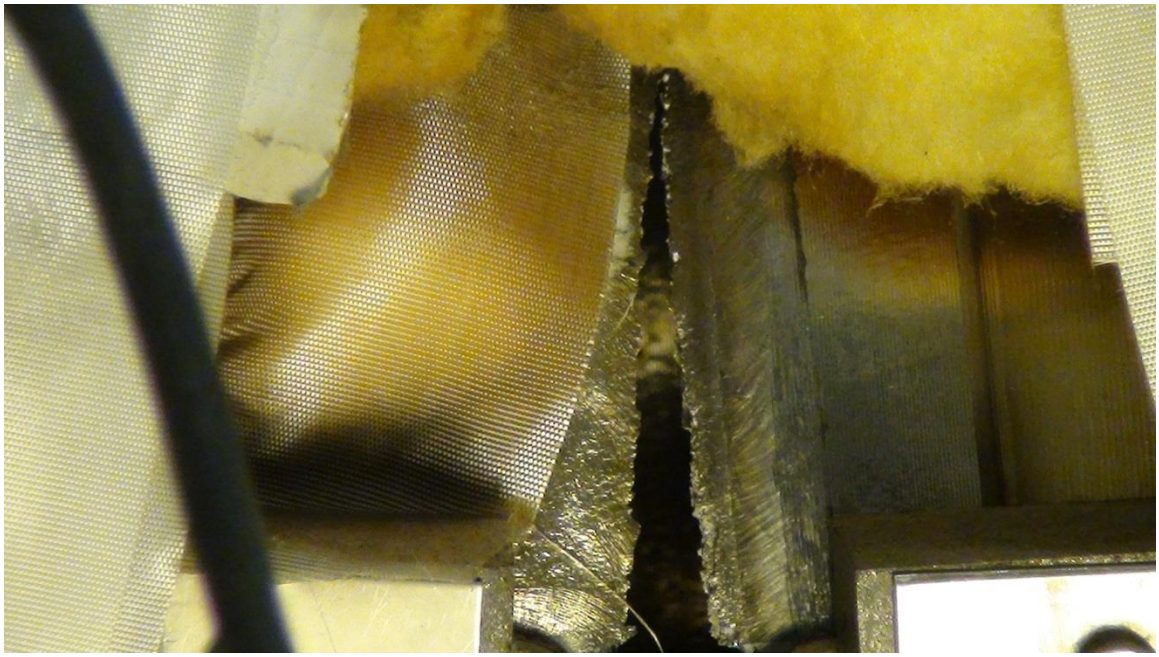

Figure 3.10. Image recorded from DMW 4 experiment illustrating crack growth and the crack tip.

When the loading was complete, the pipe was allowed to cool back to room temperature. After cooled, the pipe sample was further loaded to break open the test specimen at room temperature so that post-test measurements of the fracture surface could be made.

### 3.3.1 Data Reduction

Data reduction consists of converting measured voltages from the data acquisition system to physical values using the appropriate calibration factors. Several plots can be made directly from the data:

- Applied moment as a function of pipe rotation
- Applied moment as a function of the load-line displacement
- Applied moment as a function of the crack centerline CMOD
- CMOD at the different CMOD measurement locations as a function of the load-line displacement
- d-c electric potential at each crack tip as a function of the corresponding CMOD in order to assess the instant of crack initiation
- Crack growth as a function of load-line displacement

### 3.3.2 Quality Assurance

All of the pipe tests were conducted in accordance with the applicable ISO 9001 quality assurance procedures. As required by the ISO 9001 procedures, formal test plans, test procedures, program reviews, and reporting were strictly followed and are being maintained by the testing facility.

## 3.4 Current Solution to Complex Crack Analysis

The NRC and the nuclear industry currently use one of two techniques to evaluate CC behavior in nuclear piping. CC's are currently analyzed either using finite element (FE) analysis or by using one of the J-estimation solution discussed in section 2.4 of this

document. Due to the complexity and the significant amount of time to create a FE model, the industry and the NRC generally use a J-estimation solution.

The NRC currently uses a software package called NRCpipe, version 3.0 created in 1996, to evaluate crack initiation and maximum moments for flaws in nuclear piping. NRCpipe is the graphical user interface (GUI) for the use of several different J-estimation schemes. Figure 3.11 shows the estimation scheme selection interface and the available options. Although the option exists to select a complex crack, the functionality does not exist. The radio button for a CC was added for the intended future development that never occurred. The program as well as the underlying J-estimation solutions have remain unchanged since 1996.

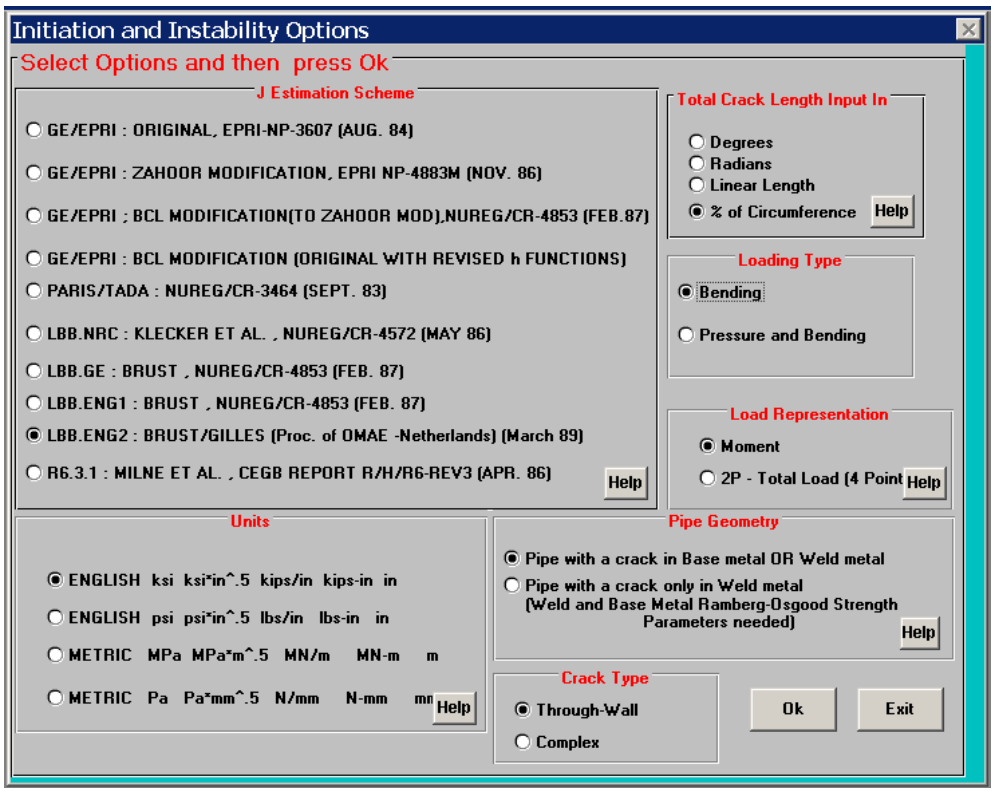


Figure 3.11. Estimation scheme selections in NRCPipe software package.

The currently established J estimation schemes don't have complex crack functionality. However, due to the extreme complexity and cost of using FE analysis, the nuclear industry has utilized an estimation method which allows them to use existing J estimation solutions to evaluate CC's. The process behind the estimation method used is to make a simplifying assumption for CC's that the circumferential crack portion is equivalent to that of a pipe with a TWC of a reduced thickness (TWCr), as illustrated in Figure 3.12. Simply, the complex crack is assumed to be a TWC with a smaller uniform thickness equal to that of the pipe thickness minus the crack depth.

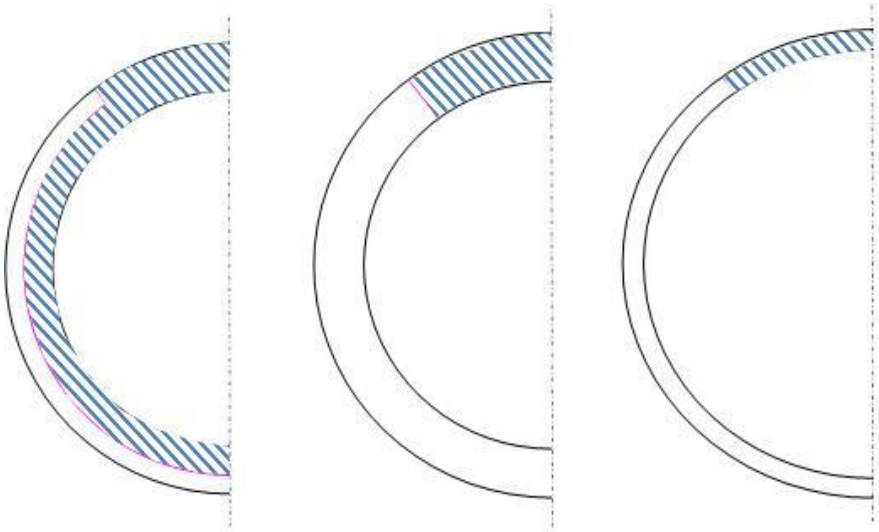

Figure 3.12. Illustration of complex crack method for use in LBB.ENG2 and other estimation solutions. The images are complex crack, TWC, and the theoretical TWC with reduced thickness respectively. [5]

This analysis methodology has been benchmarked against single material pipes. These previous analysis illustrated a conservative behavior that exists for this methodology. Using the reduced thickness method produces results that under predict

the maximum load and under predict the crack driving force. Additionally, the reduced thickness method was never evaluated for a pipe with a DM weld.

### 3.5 Development of a New Reduced Thickness Method

The completed experiments have also yielded insight other than the recorded data. One important qualitative observation was observed from the CC experiments. This observation is that in all of the CC experiments crack growth only occurred along the TWC front. As seen in Figure 3.13, the complex crack grows from the inside out in a circumferential direction. The red line in the picture indicates the unload marks on the DMW1 experiment. The red arrow indicates the direction of growth. This growth pattern occurred similarly regardless of the SC depth. This observation gives merit to the hypothesis that a CC may be modeled as a TWC since the qualitative fracture behavior is similar.

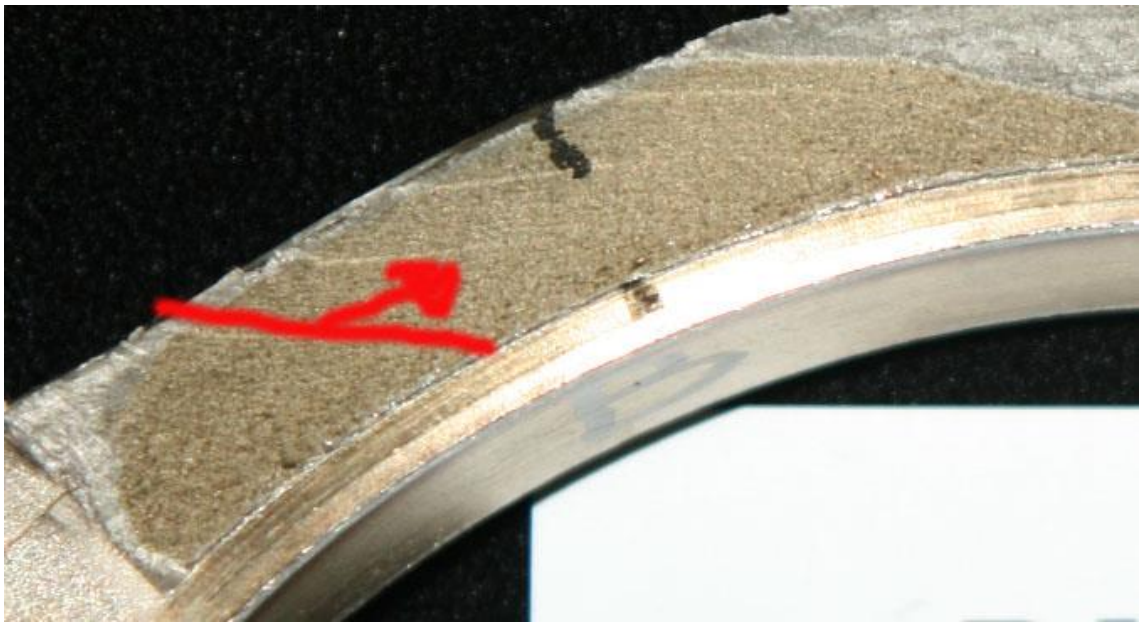

Figure 3.13. Image of DMW1 illustrating crack growth direction.

### 3.5.1 Reduced Thickness Method

The reduced thickness technique was evaluated for the complex crack experiments performed as part of this research. A model was developed using the reduced thickness method as previously described. As with the base metal experiments, the reduced thickness method yielded a conservative maximum load for a pipe with a flaw in a pipe with a DM weld. Figures 3.14, 3.15, and 3.16 illustrate the conservative behavior using the reduced thickness method. Prior to this analysis, the behavior of a DM weld with a flaw, with respect to the reduced thickness method, was never analyzed.

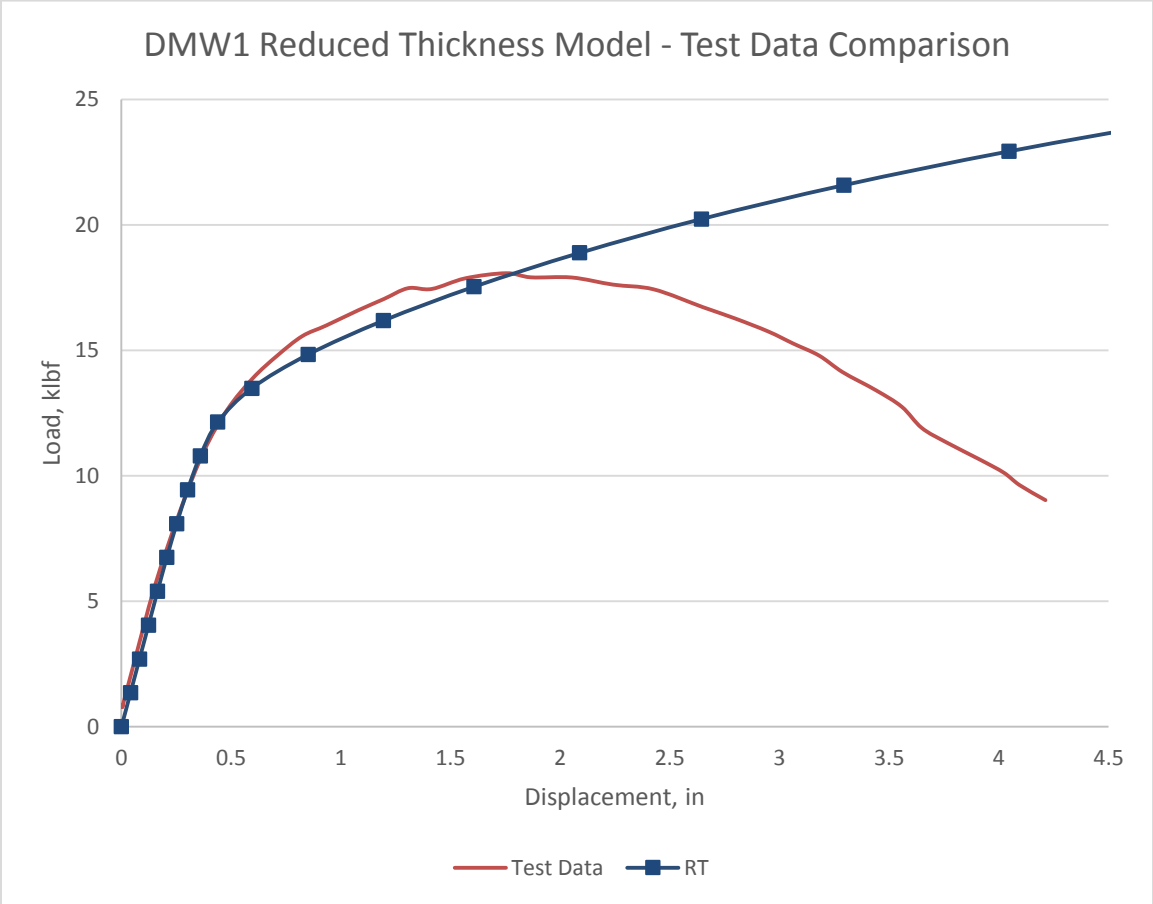


Figure 3.14. Illustration showing the conservative behavior of the reduced thickness assumption.

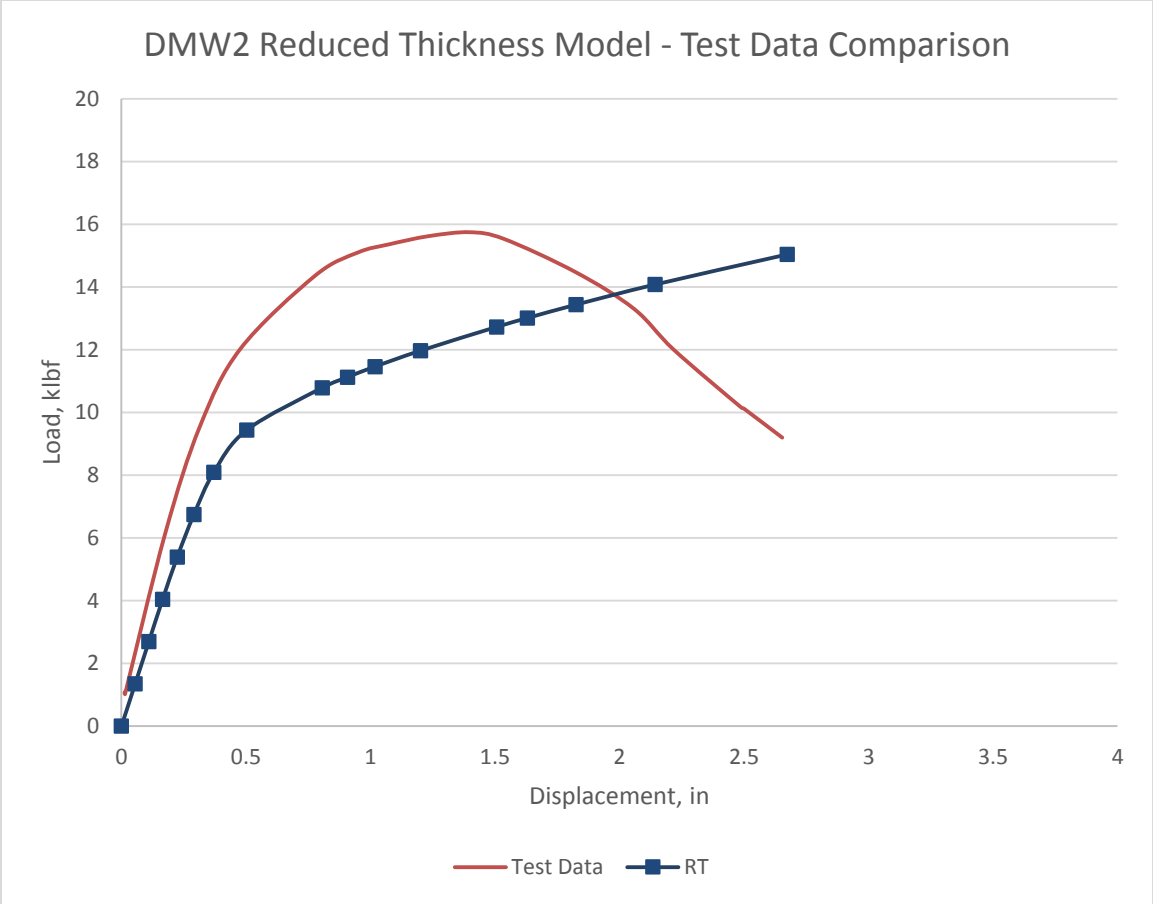


Figure 3.15. Illustration showing the conservative behavior of the reduced thickness assumption.

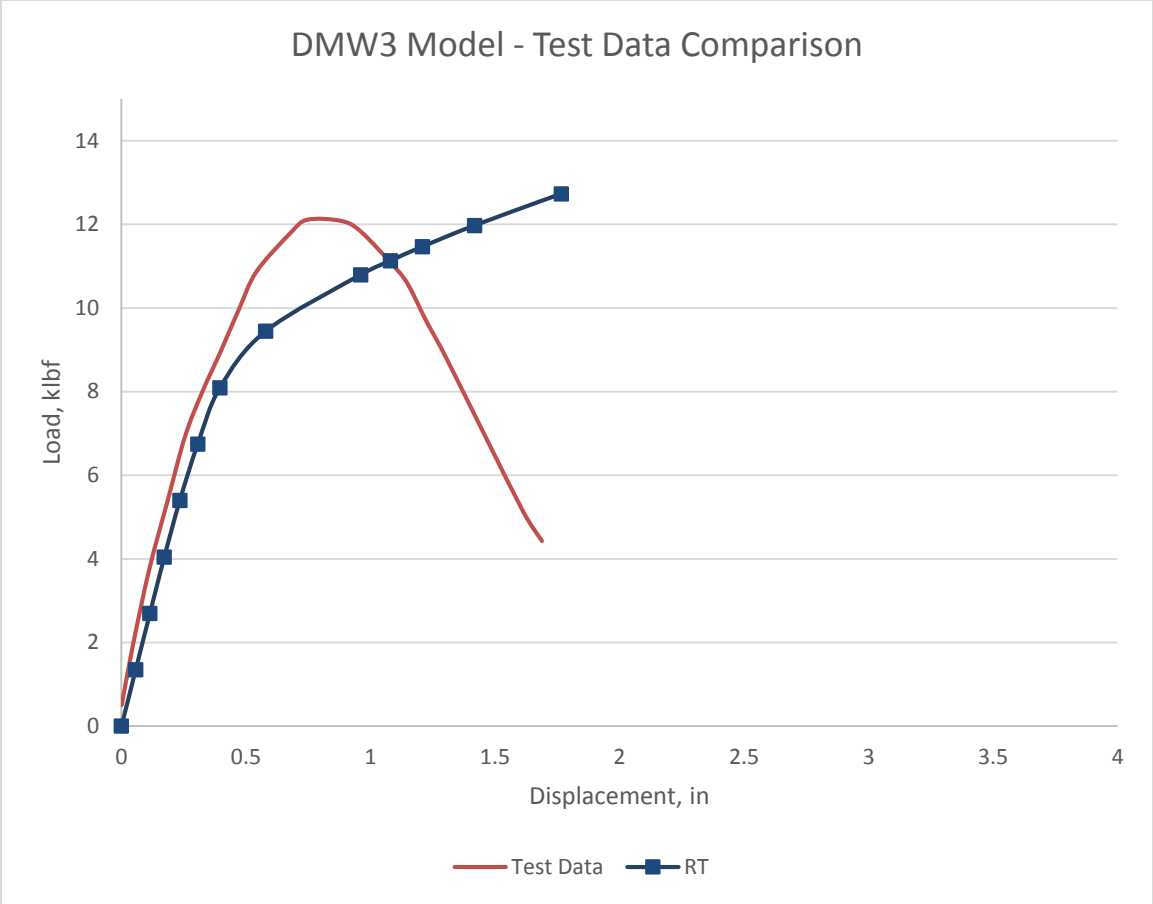


Figure 3.16. Illustration showing the conservative behavior of the reduced thickness assumption.

All of the models were created using ABAQUS FEA software and designed to mimic the 4 point bend model test setup. Figure 3.17 illustrates the model prior to bending displaying the different sections and materials. The material in red is the stainless steel and the material in silver is the Inconel, the other material sections are carbon steel. Figure 3.18 illustrates the model after applying the load to the model. All models use a mesh of type linear hexahedron with CD38R elements. The three 4-point models use around 38000 elements with 52000 nodes.

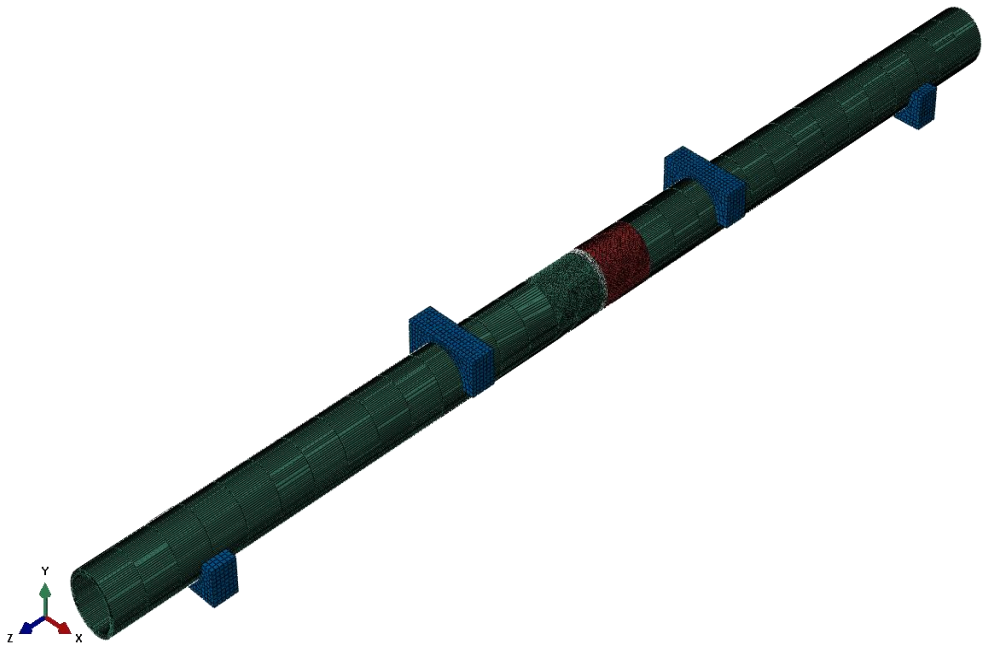


Figure 3.17. 4-point bend model illustration prior to modeling.

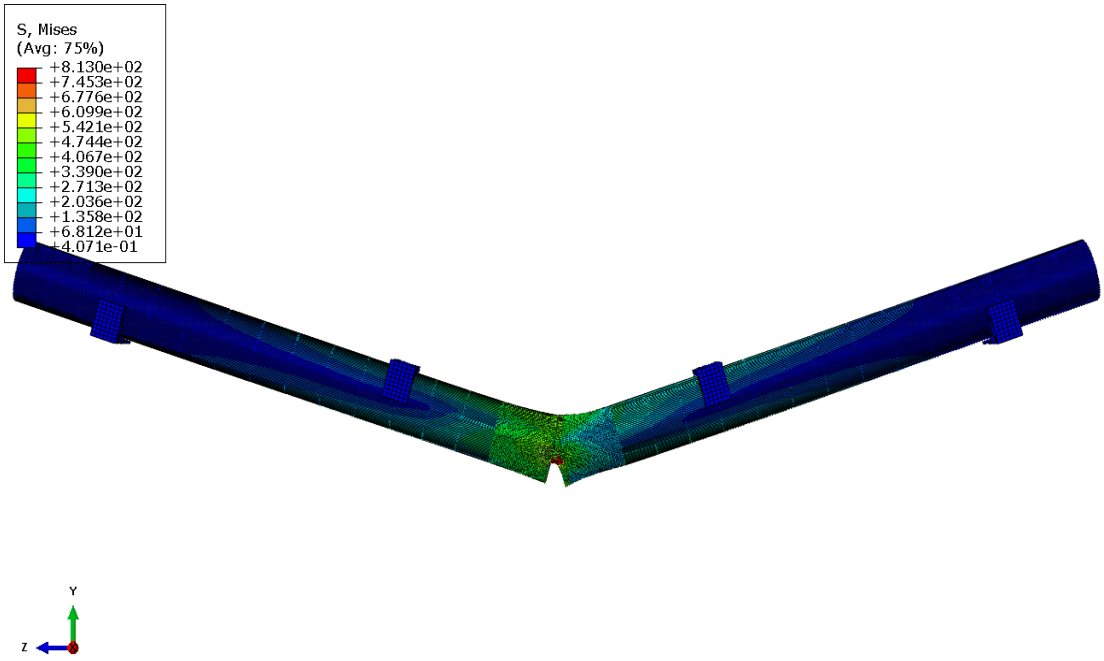


Figure 3.18. 4-point bend model after load application.

### 3.5.2 Modified Reduced Thickness Method

As illustrated in the previous section, the reduced thickness method yields a conservative prediction for maximum load. The reason for this behavior is that it doesn't account for the increased compliance along the SC portion of the CC. Thus, to account for this behavior, the TWCr model needs to be adjusted to account for this increased compliance so that an accurate prediction can be made.

To accurately modify the TWCr model, an understanding of the fracture mechanics properties at the crack front needs to be understood. To understand this behavior, and quantify it, the CC needs to be modeled using FE analysis and the driving force for crack growth (J) needs to be evaluated. Thus, J versus applied moment for the TWC portion of the crack front from the CC model is extracted from the FEA model. This will be done for three different experiments, DMW 1, 2, and 3. These three experiments represent CC's with SC depths of 16.9, 38.3 and 58.6% respectively.

Next, a TWCr model was developed and analyzed using FE analysis. Again, J versus moment was extracted. These values are compared to the values extracted from the CC model and the difference in J is analyzed. Analyzing these differences will give insight on how to modify the compliance of the TWCr model such that the driving force for both models align, thus, forcing the modified TWCr model to behave like the CC model at the crack front. Finally, the correlations developed are evaluated using the 4-point bend model and compared to the experimental data to ensure that fracture mechanics translate to aligned load displacement behavior. The ultimate output yielding a TWC 4 point bend model with the same load displacement behavior, up to crack initiation, as the CC experiment data.

# CHAPTER 4

# RESULTS

The results in this document consist of both experiment results and FE model results. The experiment results, generated from the DM weld 4 point bend experiments, are used to evaluate the results from the FE models. This evaluation will be used to verify the analysis technique developed by this research.

## 4.1 EXPERIMENT ANALYSIS

Two important observations were made from analysis of these experiments. The first observation, as previously discussed, was that crack growth only occurs along the TWC portion of the CC. The second observation was that the crack location within the weld had little effect on the maximum load.

Cracks were machined into three different areas within the weld; butter, center of the weld, and the fusion line. The differences between the locations are discussed in previous sections. The purpose of machining cracks into different locations within the weld was to study the effect of crack location on load carrying capacity. Although there were some differences in the load displacement curves, the maximum load capacity, or maximum moment, was not greatly affected by crack location. Maximum moments for DMW 1, 4, and 7 which are all CC's with a 20% SC in the weld, butter, and fusion line have maximum moments of 821.40, 834.55, and 843.55 in-kips respectively.

Since the maximum load, or moment, is not affected significantly by the crack location within the weld, selecting one flaw location to analyze is sufficient to understand what modifications need to be made to the compliance to align the fracture properties. For this analysis, 16.9, 38.3, and 58.6% CC's in the weld were chosen. Figure 4.1 illustrate the load displacement behavior for all three CC's.

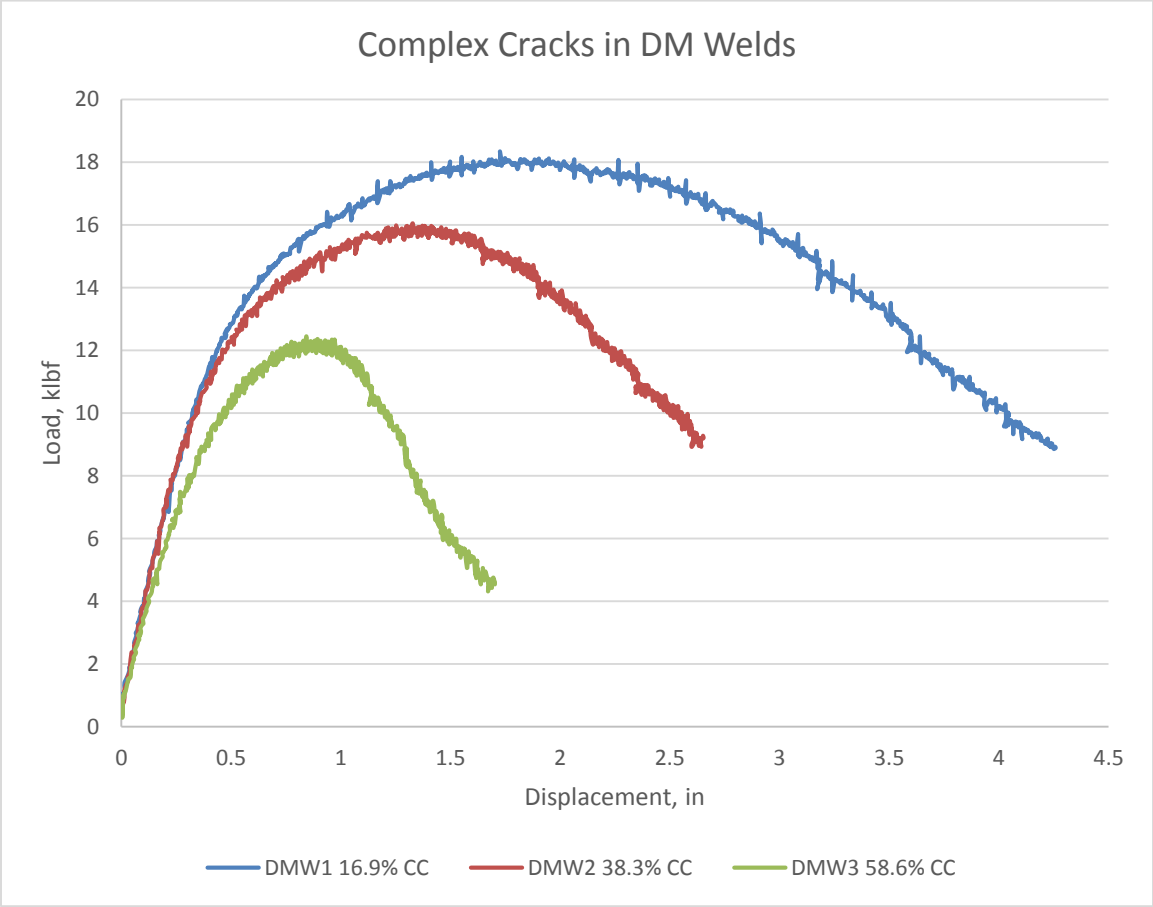


Figure 4.1. Plot of raw data from the DMW1, 2, and 3 CC experiments.

For easier manipulation, the data from Figure 4.1 was reduced such that curve structure is maintained but the data points are reduced. Figure 4.2 illustrates this result of

the data reduction which was reduced from about 40000 data points to less than 200. Additionally, the data for the reduced plots is contained in Appendix A.

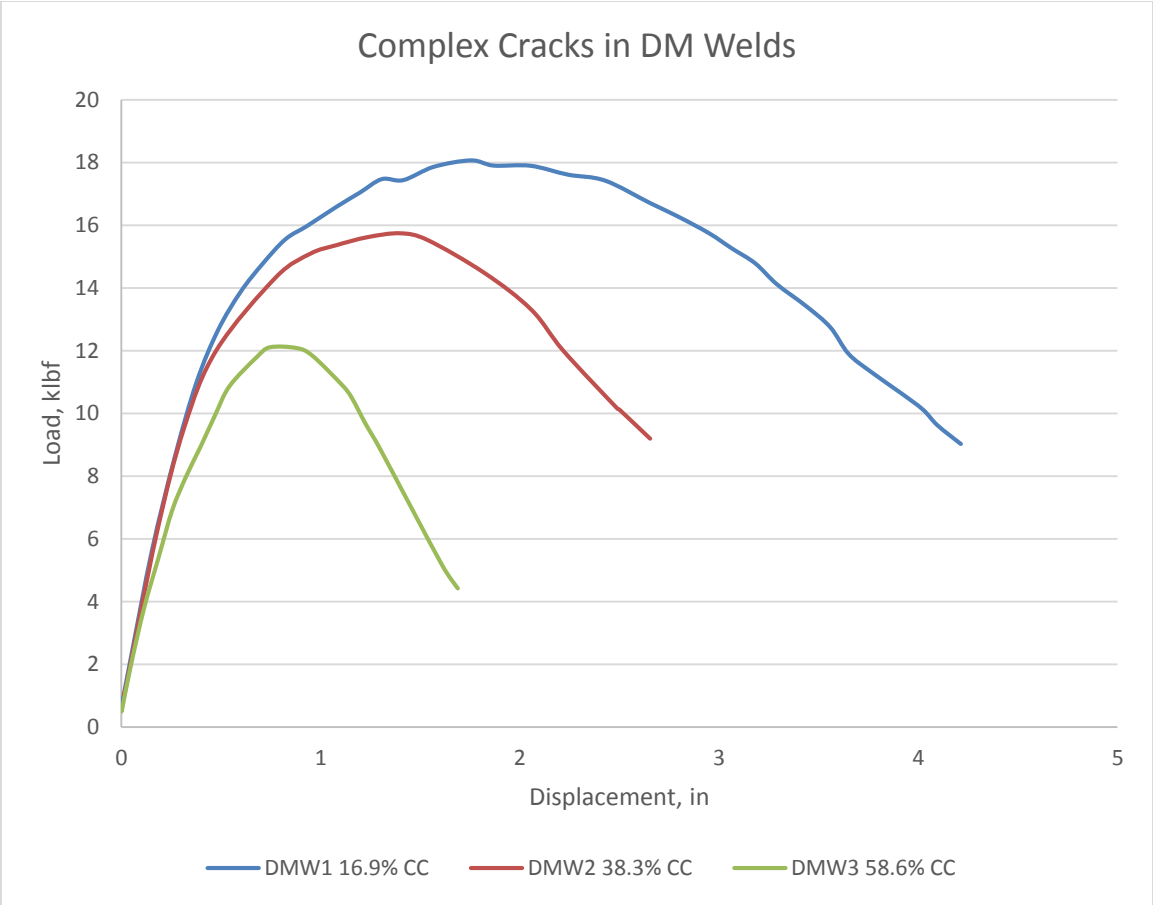


Figure 4.2. Plot of reduced data from DMW 1, 2, and 3 CC experiments.

### 4.2 General Model Parameters

The elastic-plastic FE analyses were conducted using ABAQUS6.11 to compare the crack driving force and the load-displacement between different types/sizes of cracks. For these analyses, the dimensions were taken from each experiment and used in the creation of the models. Isoparametric elements were used, with the crack tip simulated using elements collapsed into a small key-hole with a 0.13mm (0.005inch) radius. The small key hole is used to simulate the blunting that occurs at the crack front. Symmetry

boundary conditions were applied so that a half model was simulated as seen in Figure 4.3.

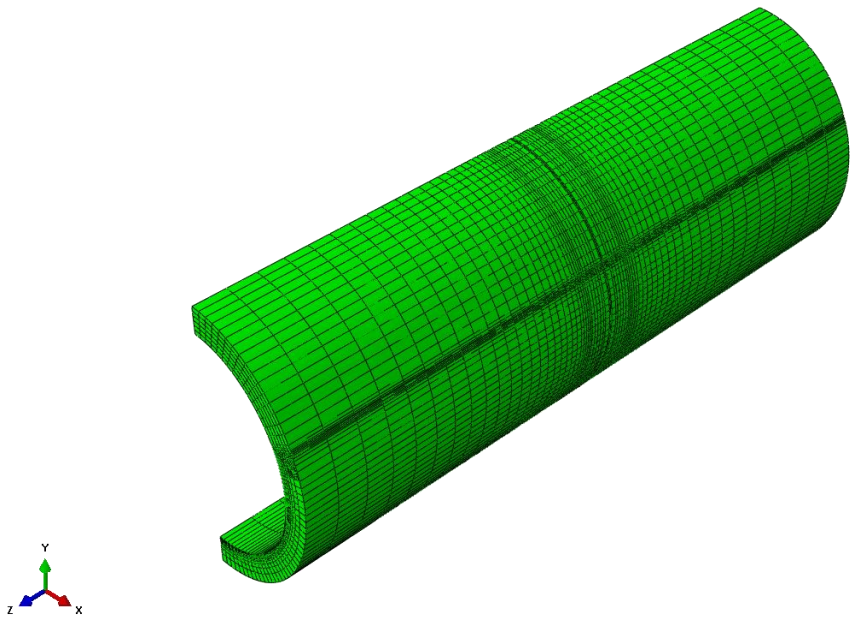


Figure 4.3. Isometric view of CC and TWC model mesh used for the analysis.

The geometry and dimensions of the models were chosen to be exactly like the conducted experiments and consist of a stainless steel pipe welded with Alloy 182 to a carbon steel pipe, as seen in Figure 4.4. Pure bending was applied to one end of the model in the form of a rotational boundary condition. The other end of the model was fixed. The material properties assumed in the analyses are given Appendix B, and the properties are listed for the materials at experiment temperature.

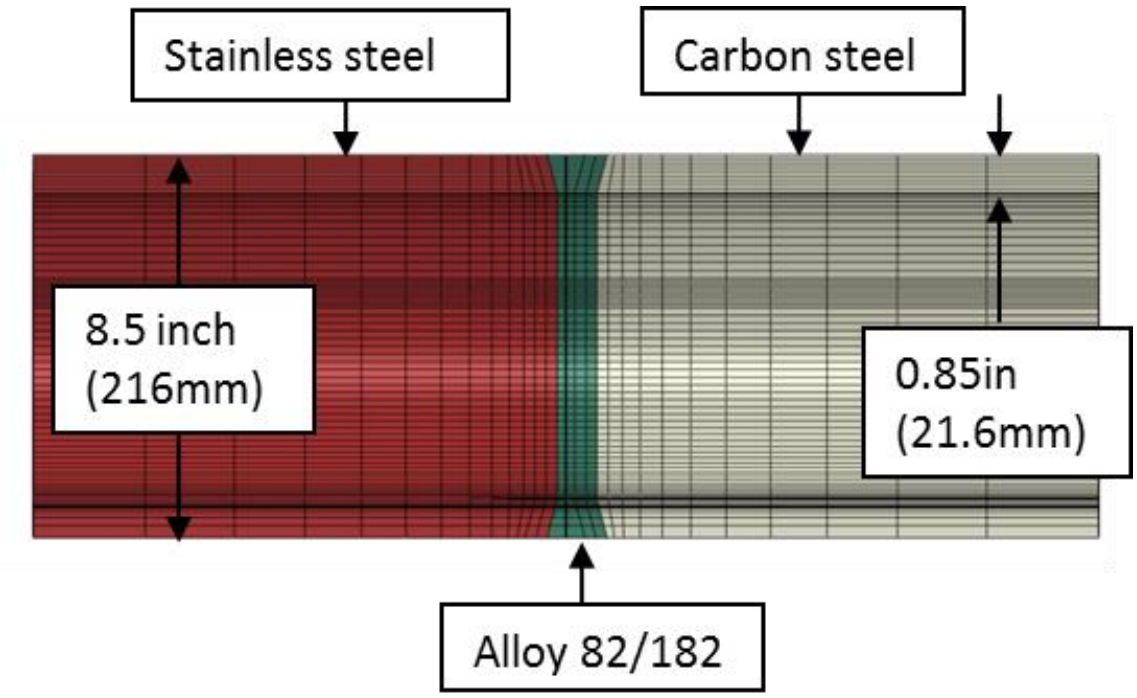


Figure 4.4. Materials and nominal dimensions used in model development.

Using this geometry, several different analyses were conducted. In all cases except DMW 2, the crack angle was held fixed at 37 percent of the pipe circumference. The DMW 2 experiment had a slightly smaller crack angle, a half crack length of 4.94 in, thus all DMW 2 models had the associating smaller angle. Models created for this analysis include:

- 1 CC model representing DMW 1
- 5 TWC models representing DMW 1 at different RT's (FT, RT, 40, 50, and 60 RT)
- 1 CC model representing DMW 2
- 9 TWC models representing DMW 2 at different RT's (FT, RT, 50, 53, 56, 58, 60, 62, 65 RT)
- 1 CC model representing DMW 3

- 7 TWC models representing DMW3 at different RT's (FT, RT, 47, 50, 51, 52, 62 RT)
- 3 TWC 4 point bend models representing each experiment

The J-integral was calculated directly by ABAQUS along four contours at each nodal location along the crack front. The J-integral values were averaged along the crack front neglecting the values calculated at the free surface. Moment and rotation are also calculated directly by ABAQUS. The thickness of the TWCr model is adjusted such that the J versus moment curves align. This new model is termed to be a modified TWCr model.

To verify that the newly developed modified TWCr model adequately predicts the load displacement behavior of a CC, the new technique needs to be verified against the experimental data. Since the experiment was conducted in a 4 point bend, it is appropriate to verify technique in a 4 point bend model. Thus, a 4 point bend model was created to verify the modified TWCr against the experimental data, as seen in Figure 4.5.

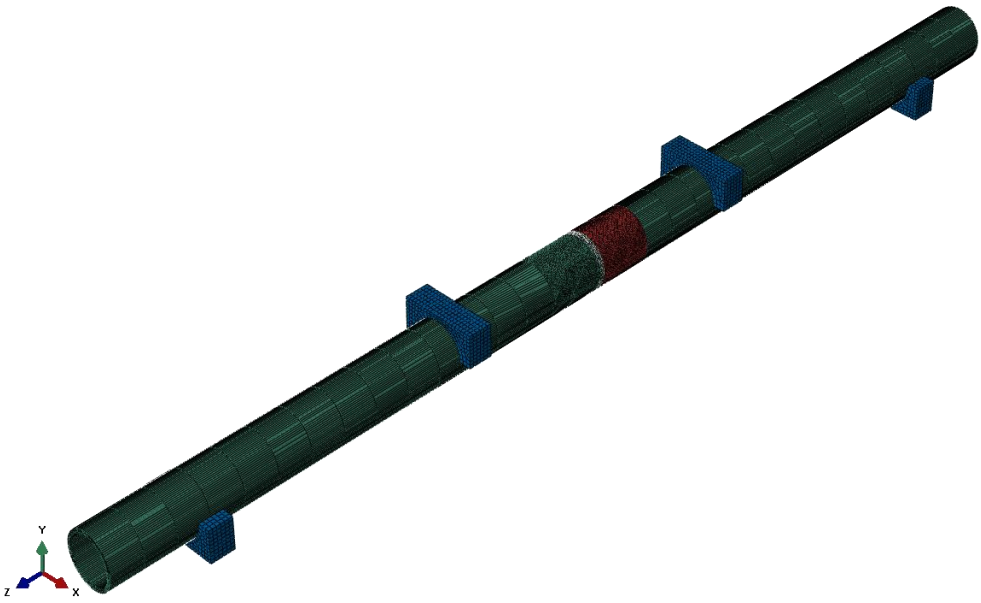


Figure 4.5. Illustration of the 4 point bend model created to verify the new model technique.

All models were created using ABAQUS 6.11 and the material data used is listed in Appendix B. The dimension used in each model, CC, TWCr, and the 4 point bend model, are taken directly from the dimensions from each experiment. Specific experiment dimensions are listed in Table 4.1.

Table 4.1. Applicable data from the DMW 1, 2, and 3 experiments

| |
|---|
| Experiment DMW1 |
| Crack location = weld |
| Type of crack = complex |
| Outside diameter = 219.7 mm (8.610 inches) |
| Wall thickness = 22.0 mm (0.866 inches) |
| Surface crack depth = 3.70 mm (0.146 inches) |
| Through-wall crack length2 = 254 mm (10.0 inches) |
| Maximum moment = 92.80 kN-m (821.4 in-kips) |
| Crack initiation moment = Not determined |
| Loading rate = 0.95 mm/minute (0.0375 inches/minute) |
| Date of experiment = 9/13/2011 |
| |
| Experiment DMW2 |
| Crack location = weld |
| Type of crack = complex |
| Outside diameter = 217.3 mm (8.555 inches) |
| Wall thickness = 21.6 mm (0.852 inches) |
| Surface crack depth = 8.28 mm (0.326 inches) |
| Through-wall crack length = 251 mm (9.875 inches) |
| Maximum moment = 82.86 kN-m (733.4 in-kips) |
| Crack initiation moment = 79.95 kN-m (707.6 in-kips) |
| Loading rate = 1.27 mm/minute (0.05 inches/minute) |
| Date of experiment = 12/19/2011 |
| |
| Experiment DMW3 |
| Crack location = weld |
| Type of crack =complex |
| Outside diameter = 217.6 mm (8.566 inches) |
| Wall thickness = 22.0 mm (0.867 inches) |
| Surface crack depth = 12.9 mm (0.508 inches) |
| Through-wall crack length = 254 mm (10 inches) |
| Maximum moment = 64.85 kN-m (574.0 in-kips) |
| Crack initiation moment = 62.15 kN-m (550.0 in-kips) |
| Loading rate = 0.95 mm/minute (0.0375 inches/minute) |
| Date of experiment = 1/23/2012 |

Additionally, other relevant dimensions common to all experiments are listed in Table 4.2. The test pipe in the model and experiment consist of three distinct sections; the north moment arm, the south moment arm, and the test specimen. The moment arms are carbon steel pipes that are welded to each side of the test section so that the pipe is long enough to allow the ram to apply sufficient load. The test specimen consists of carbon steel and stainless steel welded to an inconel section.

Table 4.2. 4 point bend model dimensions.

| DMW 1-3 | | |
|---|---|---|
| | in | mm |
| Total Length | 176.00 | 4470.40 |
| Weld section length | 19.33 | 490.98 |
| CS section length | 9.25 | 234.95 |
| SS section length | 9.25 | 234.95 |
| Length between inner saddles | 52.00 | 1320.80 |
| Length between outer saddles | 144.00 | 3657.60 |
| Length from outer edge to outer saddle | 16.00 | 406.40 |
| Length from inner to outer saddle | 46.00 | 1168.40 |

The 4 point bend model was tested versus the TWC experiment data to verify the accuracy of the model. As seen in Figure 4.6, the 4 point bend model accurately predicts the load displacement behavior for a TWC up to crack initiation. As previously described, DMW 11 is a 37% TWC model in the weld, which coincides with DMW 1, 2, and 3 experiments which have CC's that are also located in the weld.

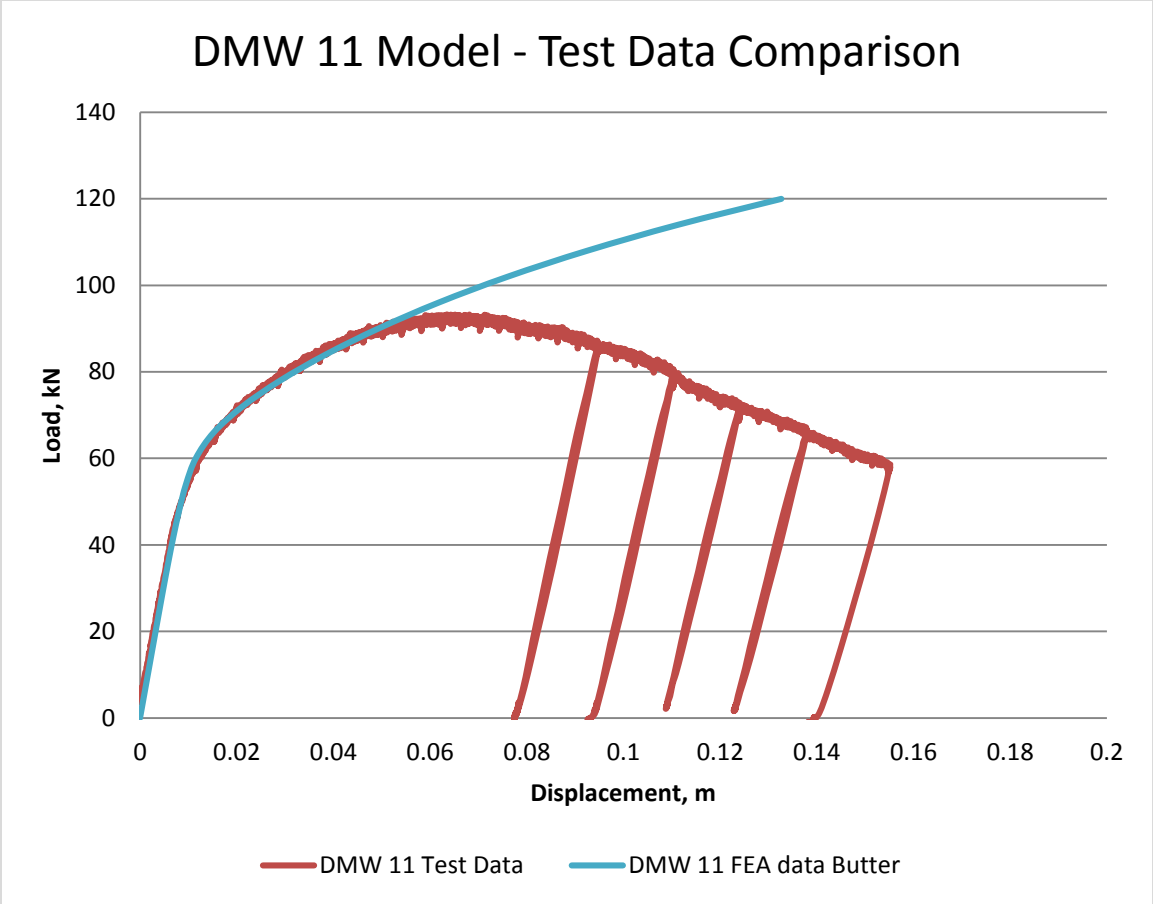


Figure 4.6. 4 point bend model validation.

### 4.3 Complex Crack Response Prediction

DMW 1, 2, and 3 are CC experiments containing a 16.9%, 38.3%, and 58.6% SC respectively each with TWC of 37% for DMW 1 and 3 and a 36.7% for DMW 2. An FEA model for a CC and a TWCr representing each of the three experiments is used to analyze the crack response up to initiation. The thickness of the TWC is then modified until the crack responses align at initiation. The new model, with a modified thickness, is verified against the experiment data.

### 4.3.1 Experiment Data

The load displacement curves for the DMW 1, 2, and 3 experiments are illustrated in Figure 4.7, 4.8 and 4.9 respectively. As previously stated, the data was extracted from a pipe containing a flaw, a CC, loaded in four point bend. The load and displacement are measured from the inner saddles, other measurements are discussed in the previous chapter. The data points have been reduced to smooth the curve, but the curve structure has not changed. This data will be used to verify the accuracy of the newly created modified TWCr model.

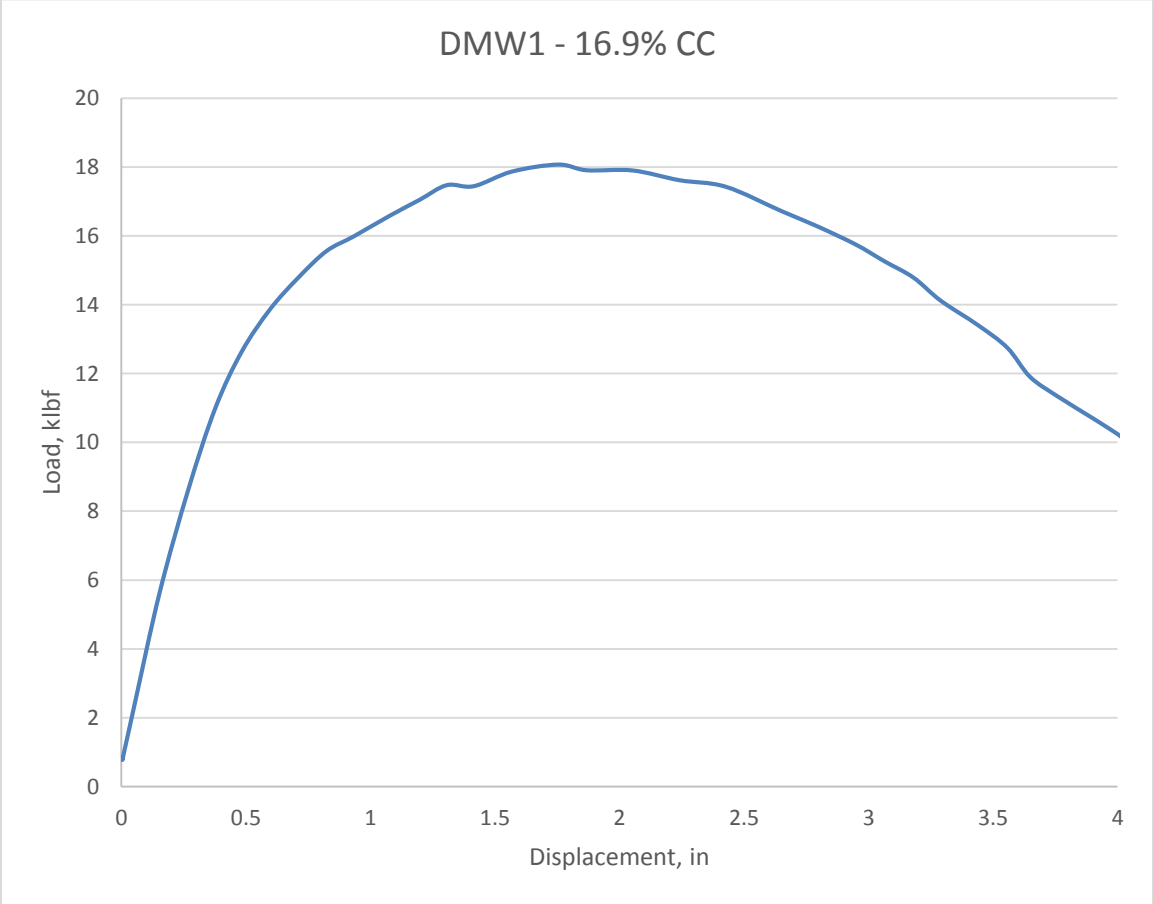


Figure 4.7. Results recorded from the DMW 1 experiment.

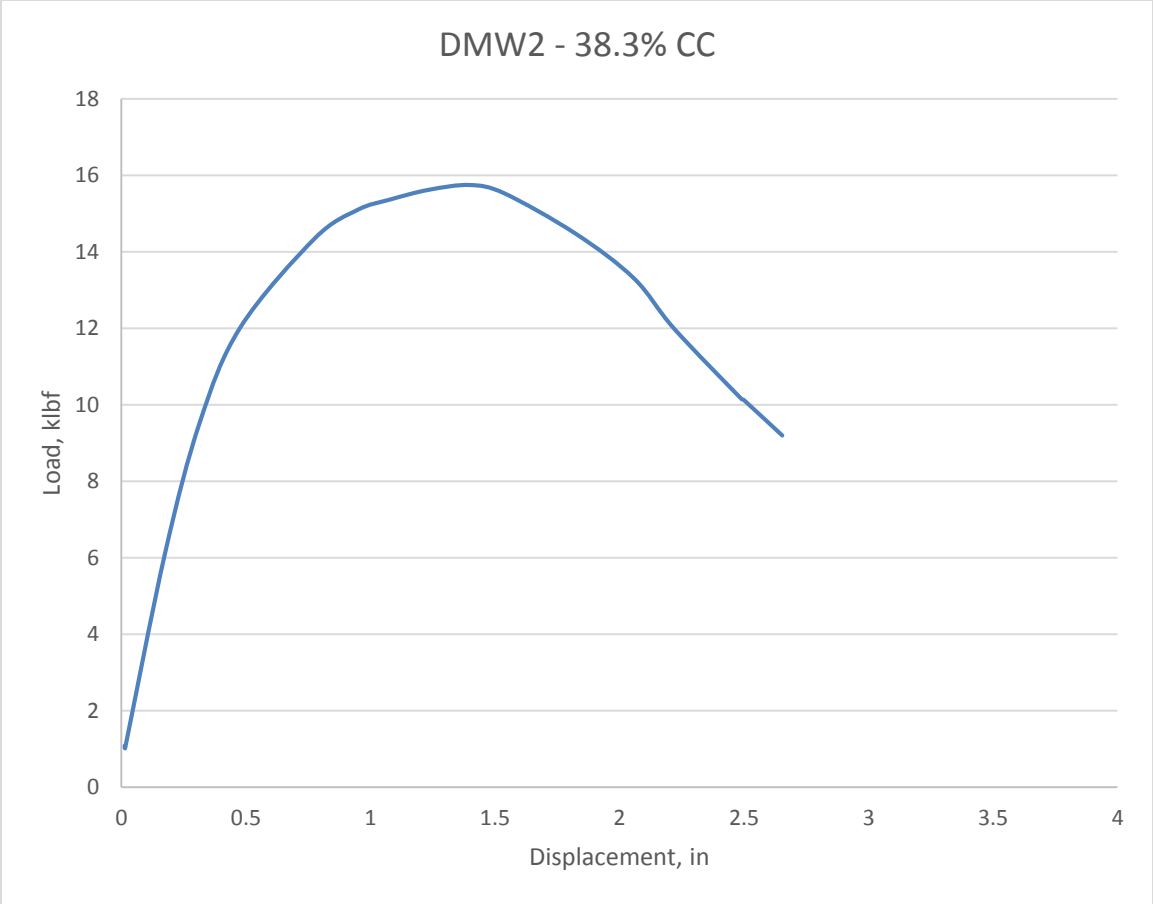


Figure 4.8. Results recorded from the DMW 2 experiment.

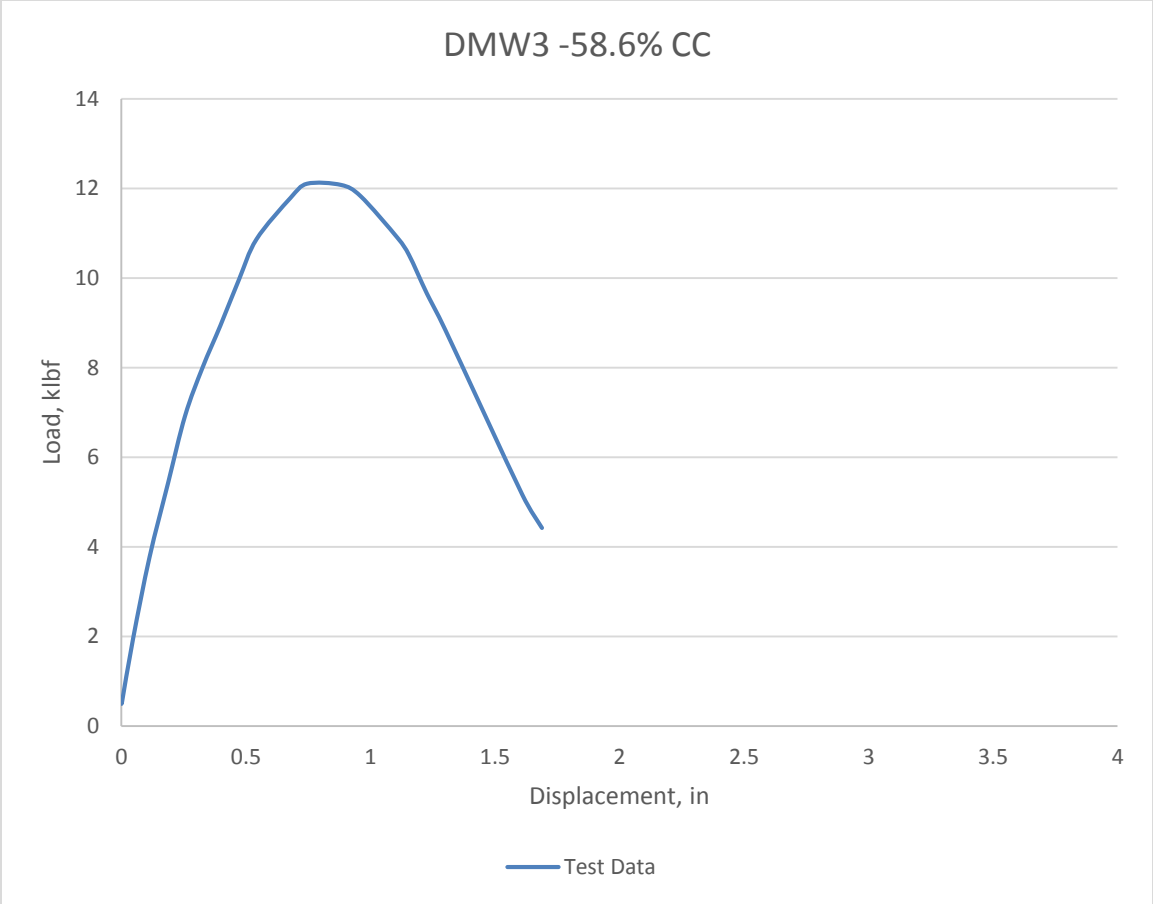


Figure 4.9. Results recorded from the DMW 3 experiment.

### 4.3.2 Modified TWCr Model Development

To identify the necessary changes to the TWCr model, the driving force versus moment curve needs to be compared between the TWCr and the CC FE models. Figure 4.10 illustrates the completed analysis for DMW 1, illustrating the final changes to the TWCr to account for the additional constraint.

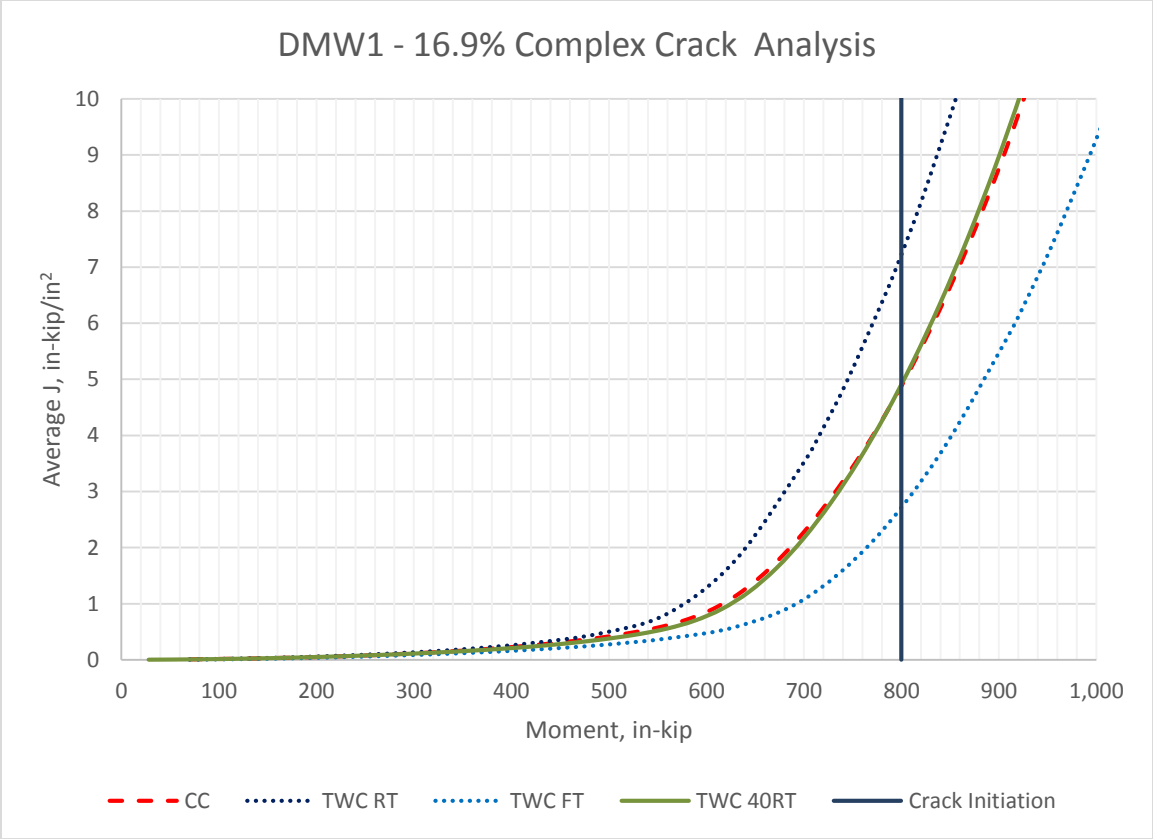


Figure 4.10. Illustration of the DMW1 FE models. Comparing the driving force for crack growth of the RT, FT, and MRT models to the CC FE model.

The J versus moment for the complex crack is extracted and plotted along with the RT and FT TWCr models. The RT and FT models set the bounds for the evaluation of the modified TWCr model. It is expected, for the depth of SC's being evaluated, that the modified TWCr model thickness will fall between these two thicknesses. As demonstrated in section 3.5.1, the TWCr is conservative for all of the experiments being evaluated. Thus, it can be stated that the RT is the minimum thickness for the new model. For the upper bound, it is intuitive that setting the thickness to the full thickness will is the maximum thickness for the new model. Thus, the thickness of the modified TWCr will fall between these two values.

Since the thickness of the modified TWCr will fall between the RT and the FT, the value of the modified TWCr is recorded as the fractional difference of the thickness between the RT and FT greater than the RT (ex. 40RT). This fraction will be between zero and one. Different thicknesses were used until the J versus moment curves were matched at initiation. If the driving force is matched at initiation, in theory, the load response behavior should also match at initiation.

In Figure 4.10 the thickness that aligns the modified TWCr model to the CC J versus moment curve is a TWC with a thickness of 40RT (t=0.778in). This new thickness is termed the modified reduced thickness (MRT). Figure 4.10 only illustrates the RT, FT, CC, and new modified TWCr J versus moment curves. All other models evaluated were removed from the plot to improve the clarity of the plot. The plots that illustrates all of the models evaluated for models DMW 1, 2, and 3 are located in Appendix C. Figure 4.11 and 4.12 illustrate the analyses performed for DMW 2 and 3. The values of the modified thicknesses for those two analyses are 62RT (t=0.728in) and 51RT (t=0.618in) for DMW 2 and 3 respectively.

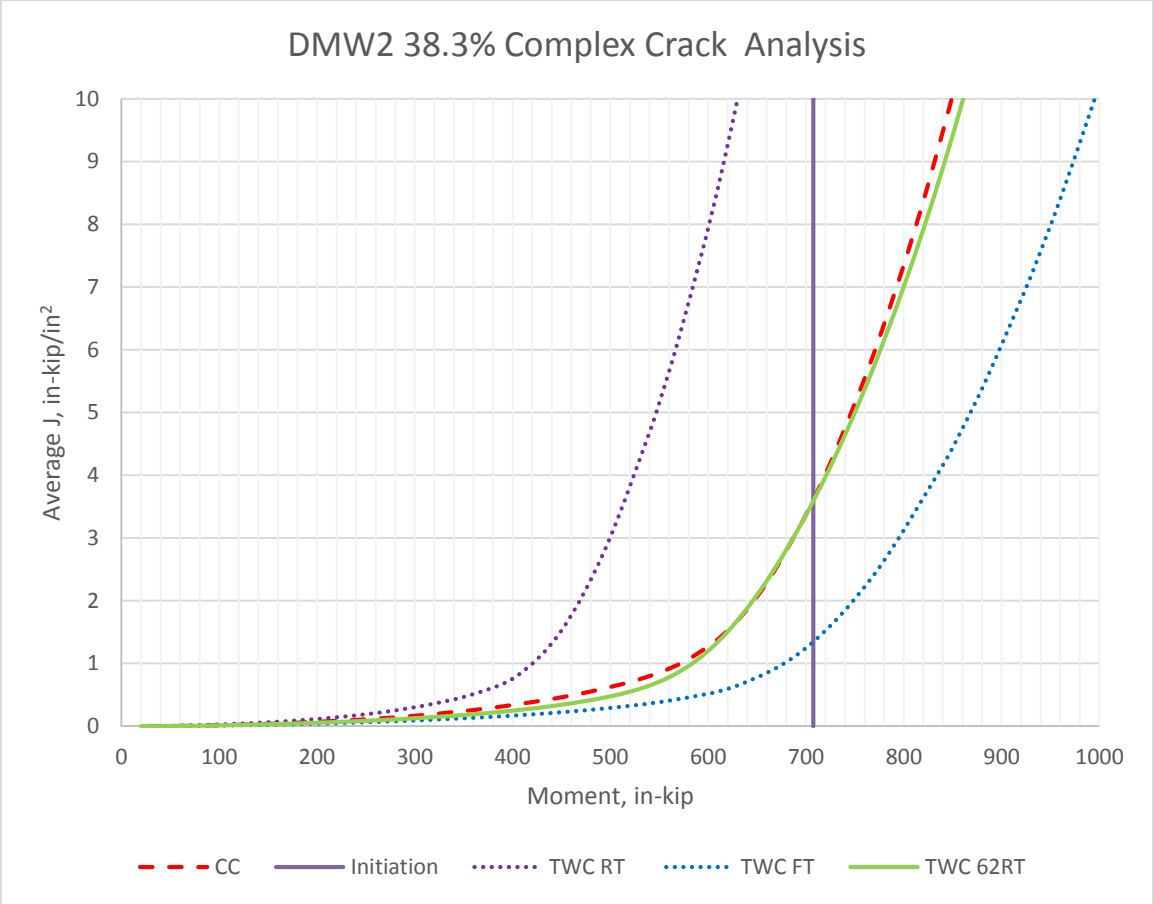


Figure 4.11. Illustration of the DMW2 FE models. Comparing the driving force for crack growth of the RT, FT, and MRT models to the CC FE model.

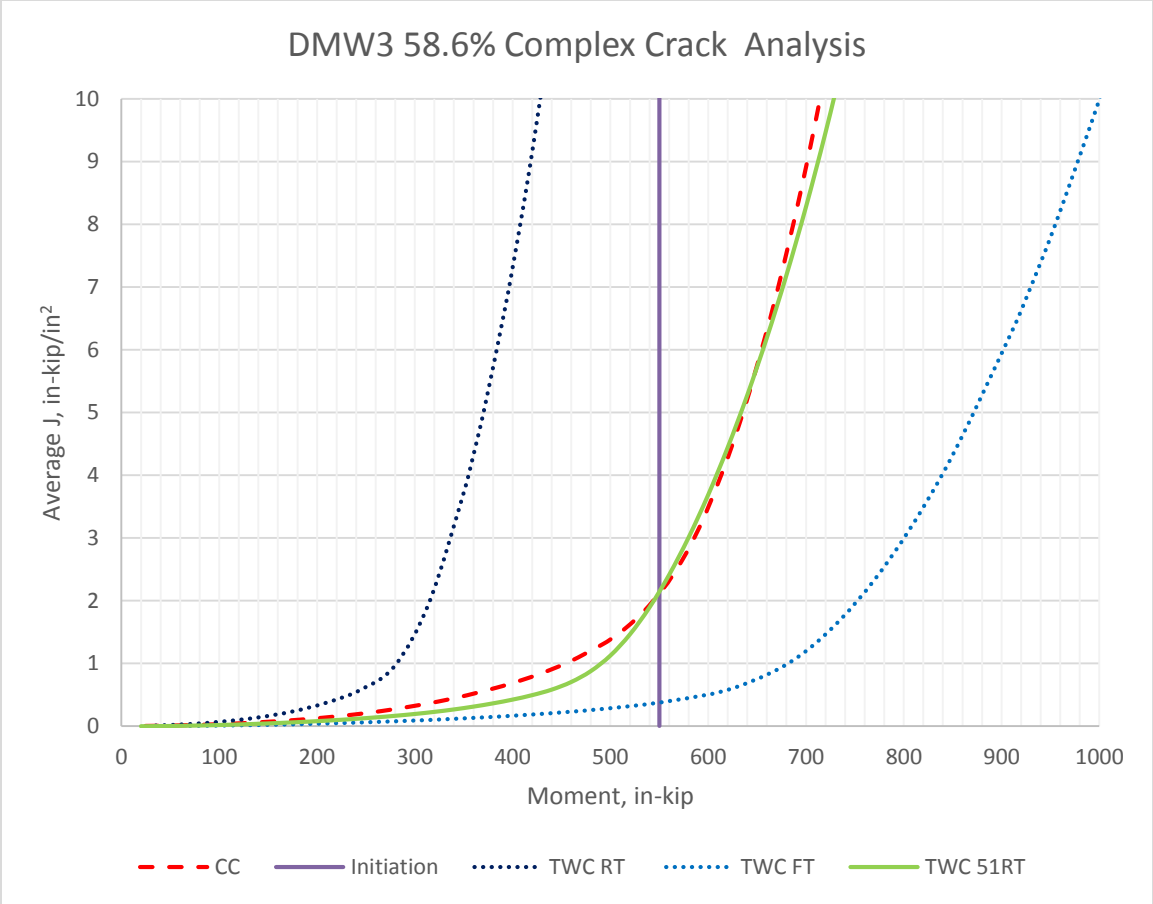


Figure 4.12. Illustration of the DMW3 FE models. Comparing the driving force for crack growth of the RT, FT, and MRT models to the CC FE model.

Figures 4.10, 4.11, and 4.12 also demonstrate the significant inaccuracy of the reduced thickness method. As the SC depth increases the reduced thickness method gets increasingly conservative. Thus, for CC's with a deep SC the reduced thickness method is very inaccurate. Conversely, the smaller the SC the more accurate the reduced thickness method is. As expected, the larger the SC, the more the constraint affects the behavior of the driving force at the crack front.

### 4.3.3 Model Verification

For industry, the load displacement behavior of a pipe with a flaw is of primary concern. To ensure that the new modified TWCr model accurately represents the load displacement behavior, the new model needs to be benchmarked against the experiment data. The experiment was done in a 4 point bend, so each experiment was modeled in a 4 point bend using a TWC with the new MRT as discussed in section 3.5.1. Figure 4.13, 4.14, and 4.15 illustrate the load displacement output for the DMW 1, 2, and 3 FE models, experiment data, and RT models. The RT models are included to illustrate the conservatism of the RT model as compared to the new modified TWCr. Crack initiation in each experiment occurs before the max load is reached but after the elastic region.

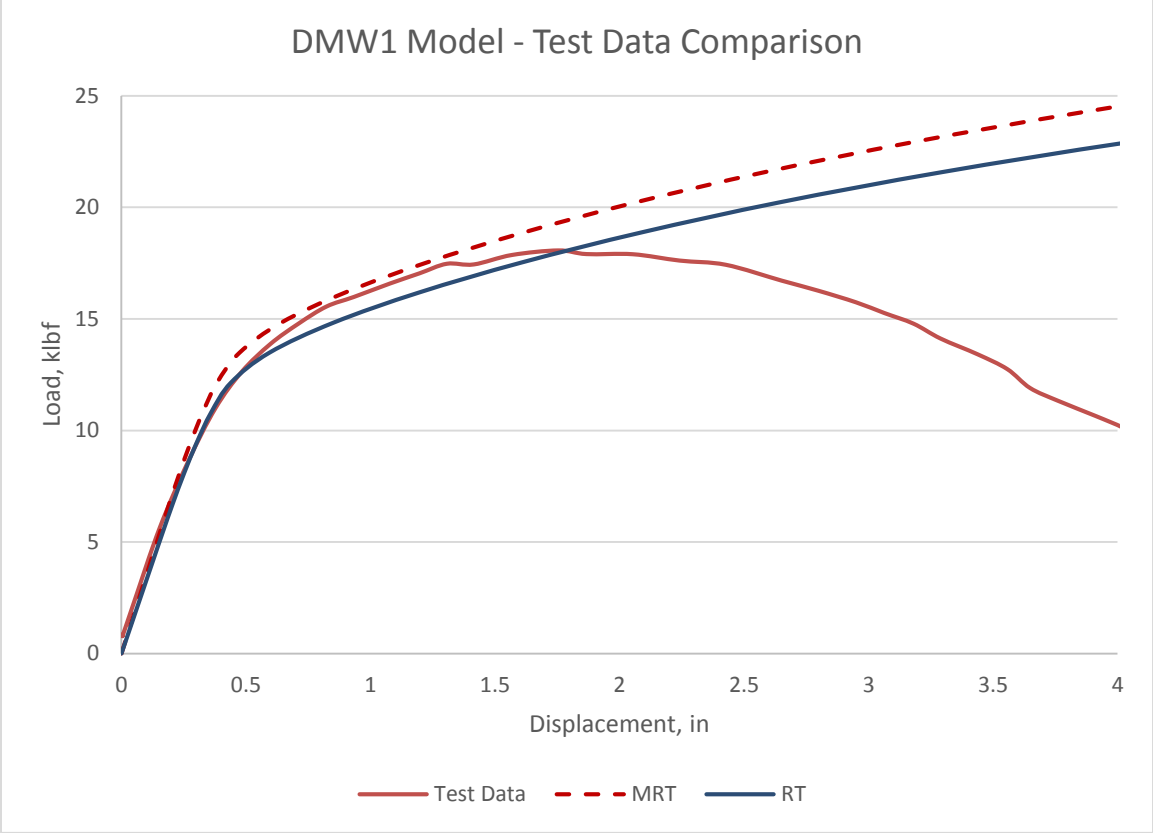


Figure 4.13. Illustration of the FE models using the MRT and RT as compared to the test data.

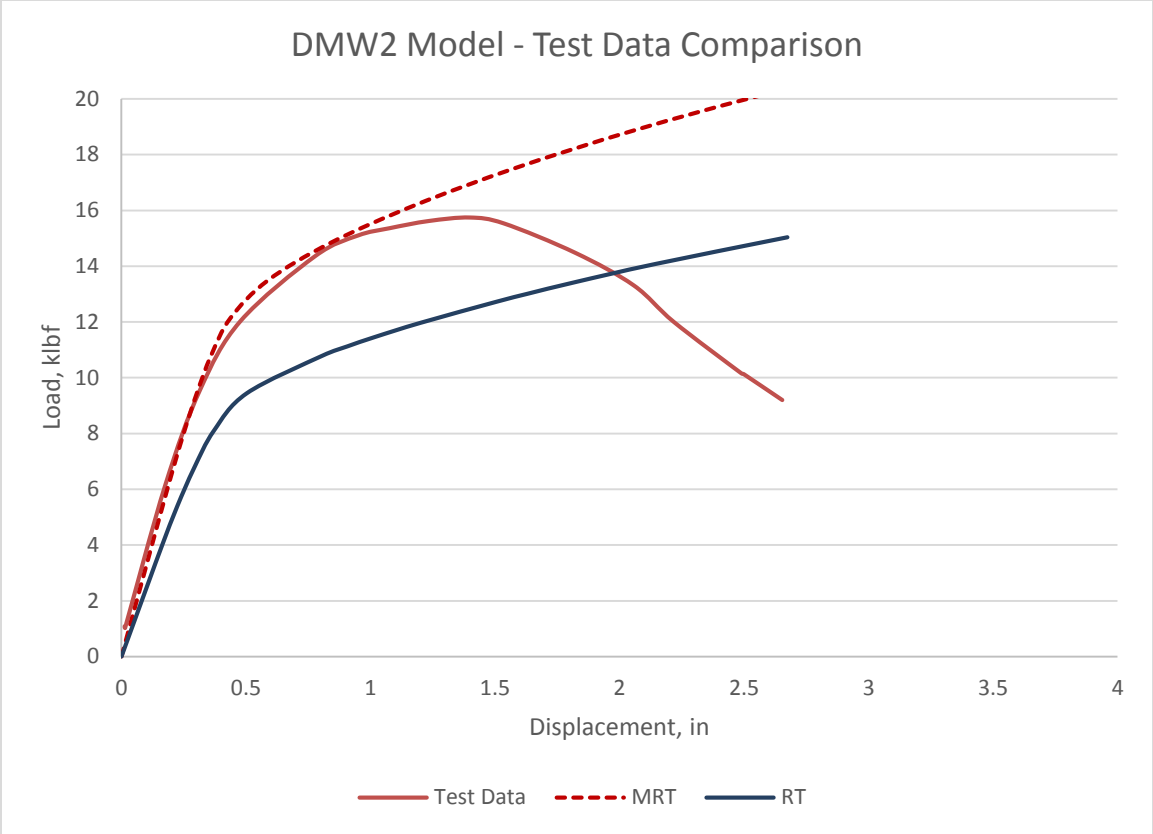


Figure 4.14. Illustration of the FE models using the MRT and RT as compared to the test data.

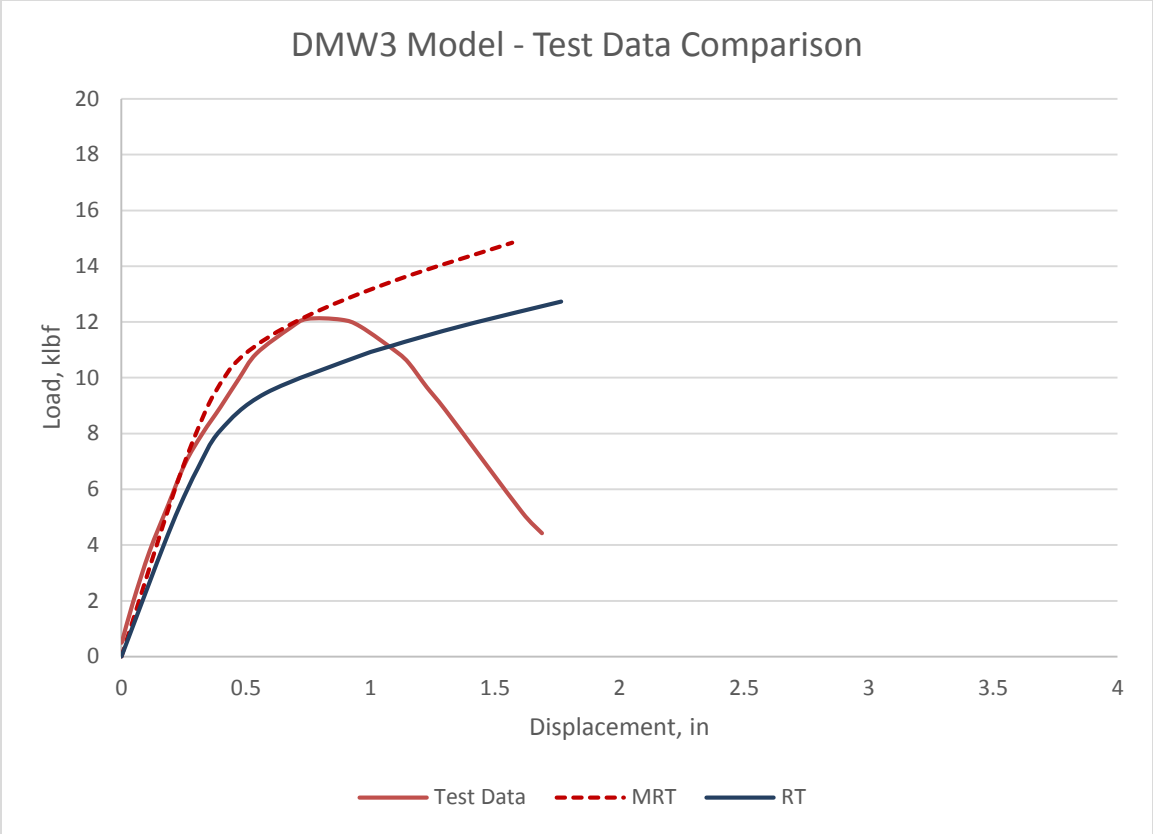


Figure 4.15. Illustration of the FE model using the MRT and RT as compared to the test data.

All of the plots indicate that the new models, using the new MRT's, accurately predict the load displacement responses to the applied load up to crack initiation, meaning, a TWCr can be used to accurately represent the behavior of a CC. This new reduced thickness method will predict the crack response up to crack initiation. Thus, combining this model along with a J-tearing model will predict the pipe response as a load is applied.

# CHAPTER 5

## DISCUSSION OF RESULTS

The purpose of this research was to answer the fundamental question about whether a CC be adequately represented by a TWCr model. As verified by the analysis performed as a part of this research, for the specific conditions analyzed, a TWCr model can accurately predict the crack response for a CC. Simply, a TWCr exists such that the driving force for the CC and the TWCr are similar enough to produce an equivalent load displacement response up to crack initiation.

To develop a TWCr that accurately represents the load displacement behavior of a CC, a modification needs to be made such that the constraint of the SC portion of the CC is accounted for. One method to account for the increased constraint, is to modify the thickness of the TWCr model. The degree to which the thickness should be modified is determined by examining the fracture mechanics at the crack front, specifically the crack driving force. Aligning the crack driving for a the CC model and the TWCr model yield a thickness where the TWCr model exhibits the load displacement behavior as recorded form the experiments. This new thickness, termed the MRT, is then divided by the full thickness of the pipe to create a unit less modified reduced thickness factor (MRTF). Several key observations were made about the MRTF;

- The deeper the SC the worse the TWCr assumption is, and the more need there is for a modified TWCr mode.

- The MRTF can't be greater than 1 and the MRTF can't be less than the RT, so those two conditions bound the MRTF.
- Finally, the MRTF is dependent on the TWC length. To analyze the variation of the MRTF as a function of SC depth, the TWC half lengths need to be the same because as the crack grows the MRTF changes.

The DMW 2 experiment had a TWC half crack length of 4.9375, whereas the other two experiments have a half crack length of 5. Since the driving force changes as the TWC length changes, to evaluate the trend of the MRTF as a function of percent SC, the TWC half length's need to be the same. Thus, another model of DMW 2 was created with a TWC half crack length of 5. Models created for the analysis of a new DMW 2 (5c) include:

- 1 CC model representing DMW 2 (5c) with a half crack length of 5c
- 8 TWC models representing DMW 2 (5c) (FT, RT, 47, 50, 56, 62, 65, 68)

Test data does not exist for model with this smaller half crack length dimension to verify the model, but the process was verified using three different experiments, documented in the chapter 4 of this research. Therefore it is reasonable to assume that the process to develop the new modified TWCr model is accurate. Figure 5.1 illustrates an isometric view the CC model created, with a moment applied, which is identical to DMW 2 with the exception of the TWC half length. Figure 5.2 illustrates the same model in a YZ view. As with the other models, Figure 5.3 illustrates the modified TWCr model after a moment is applied. Figure 5.4 illustrates the completed analysis for DMW 2 (5c), illustrating the final changes to the TWCr to account for the additional constraint.

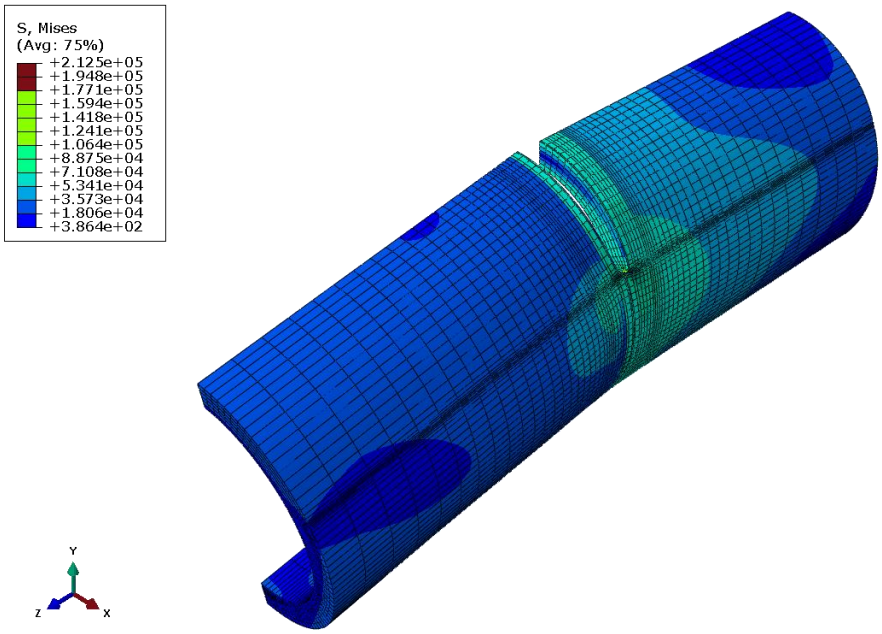


Figure 5.1. Isometric view of DMW 2 5c CC model, moment applied.

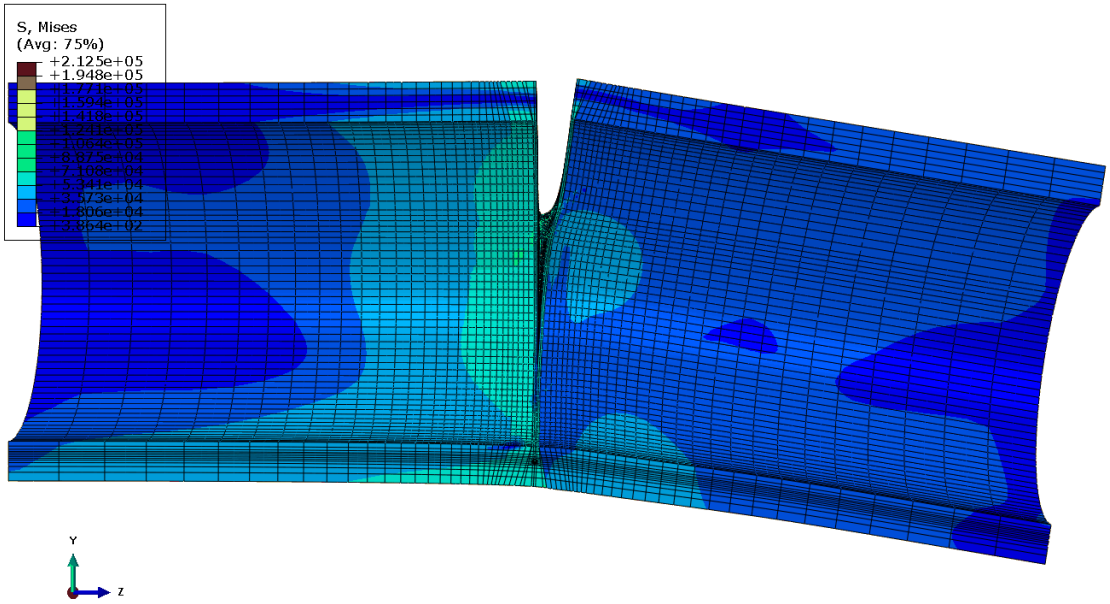


Figure 5.2. Side view (YZ) of DMW 2 5c CC model, moment applied.

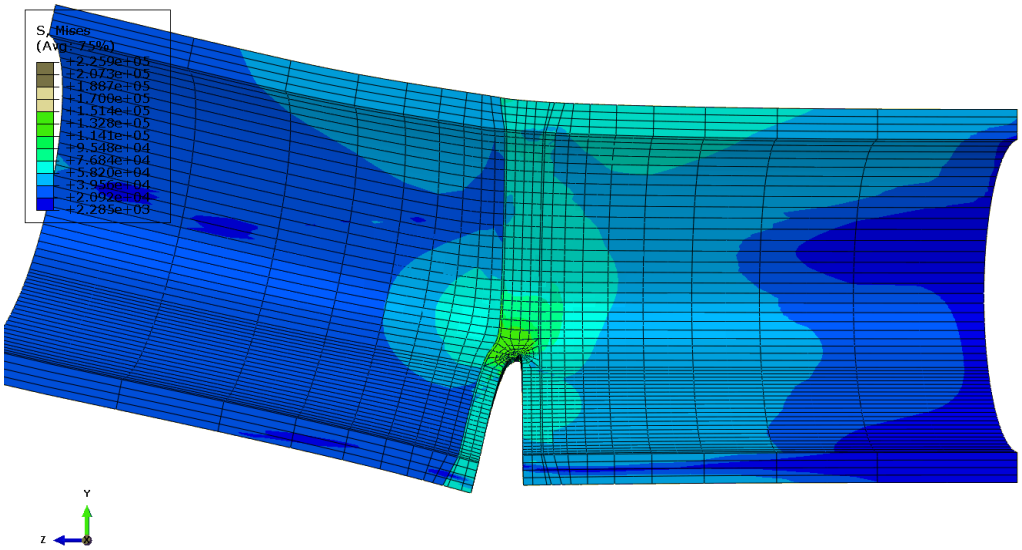


Figure 5.3. Side view (YZ) of DMW 2 5c modified TWCr model moment applied.

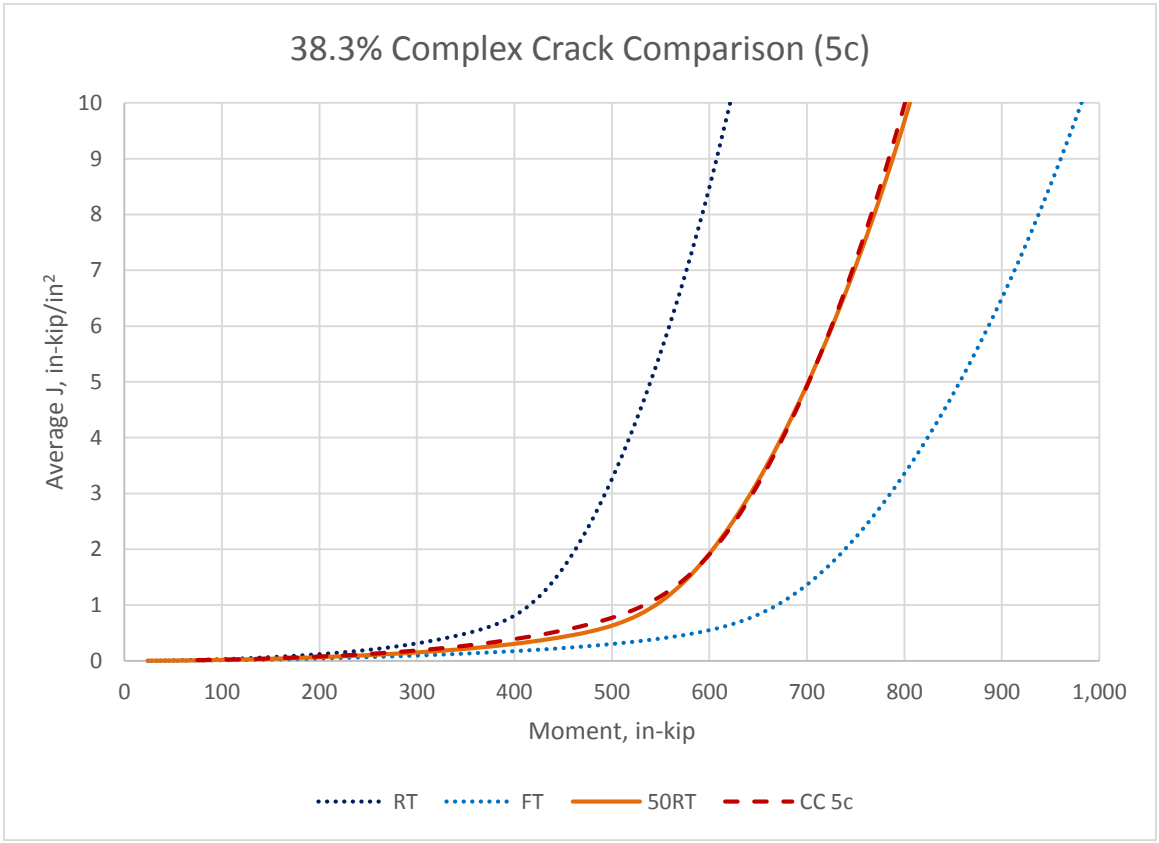


Figure 5.4. Illustration of the DMW2 (5c) FE models. Comparing the driving force for crack growth of the RT, FT, and MRT models to the CC FE model.

The data from the DMW 2 (5c) analysis combined with the previous two analyses (DMW1 and 3) yield Figure 5.5. DMW 2 is illustrated by a red "●". The MRTF is selected based on the SC size, and is only applicable for a TWC half crack length of 5 in. The MRTF has not been evaluated for different pipe sizes or different materials, thus it is only applicable for a nominal pipe diameter of 8.5 inches with a DMW weld specific to the materials of this research. The CC to TWC modification factor curve is bounded by lines for the RT and FT, as illustrated. The real benefit of the CC to TWC modification curve is for use in computation solutions like NRCpipe or xLPR. A mathematical equation can be generated from the curve which can be coded into a program, like xLPR, to simplify analysis of a CC. With additional experiments, more curves and subsequent equations can be generated to account for crack growth.

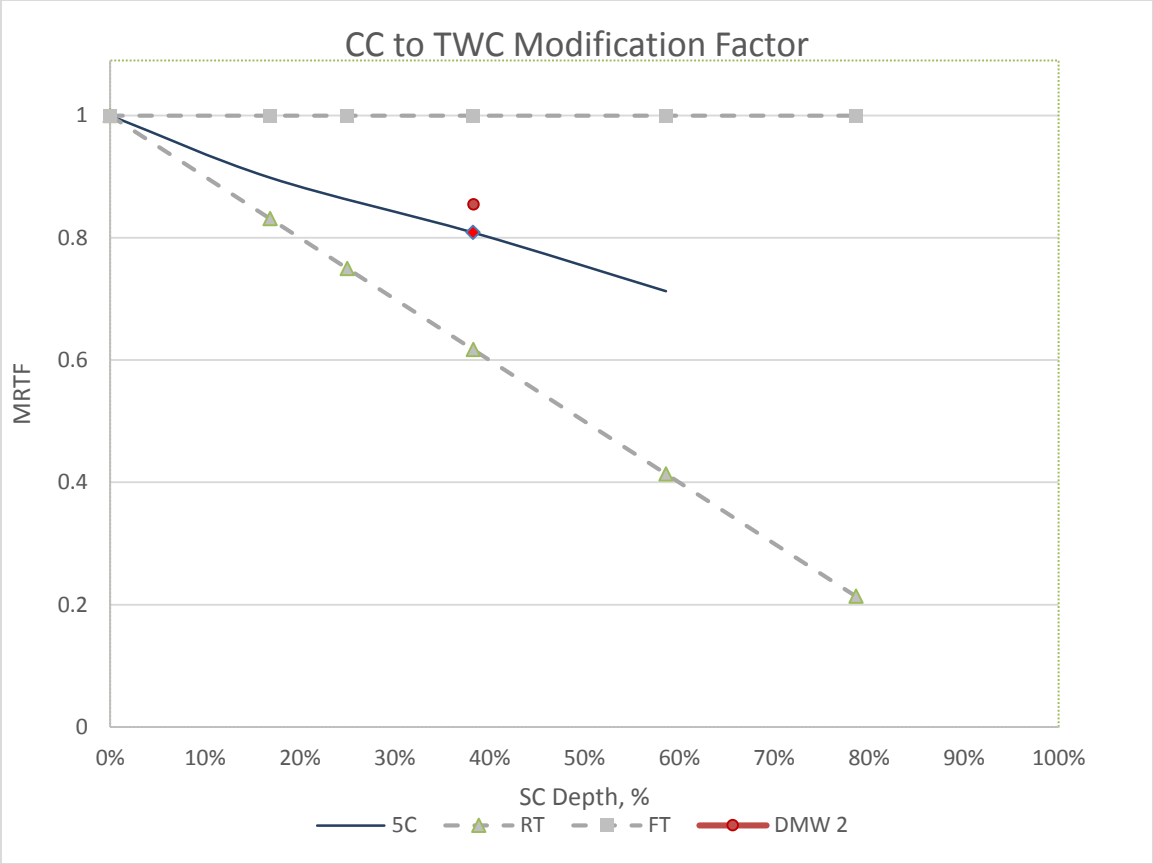


Figure 5.5. Graphical illustration of the correlation between the SC depth and the MRTF.

The J versus moment solutions for the modified TWCr are illustrated together n Figure 5.6. The models very slightly in outside diameter and very in thickness. To verify that the new TWCr are independent of model thickness and pipe diameter, the j versus moment solution needs to be normalized by thickness and pipe diameter. To do this, the moment can be normalized by the net-section-collapse moment [9], which is a function of the thickness and radius of the pipe. The net-section-collapse moment is the fully plastic solution for a pipe. Normalizing by the net-section-collapse moment removes the dependency of the solution on the diameter and the thickness of the pipe. The equation for the net-section-collapse moment is:

$$M_{NSC} = 2\sigma_f {R_m}^2 t \left(2\sin\beta - \frac{a}{t}\sin\theta\right)$$

Where beta, the stress inversion angle is given by:

$$\beta = \frac{\pi - \theta(\frac{a}{t})}{2} - \frac{\pi R_i^2 p}{4R_m \sigma_f t}$$

Θ = half crack angle
$M_{NSC}$ = NSC limit moment
$R_i$ = inner radius of pipe
$R_m$ = mean radius of pipe
p = internal pressure
t = pipe wall thickness
a = surface crack depth (1 for a TWC)
σ = flow stress (the average of the ultimate and yield stress)

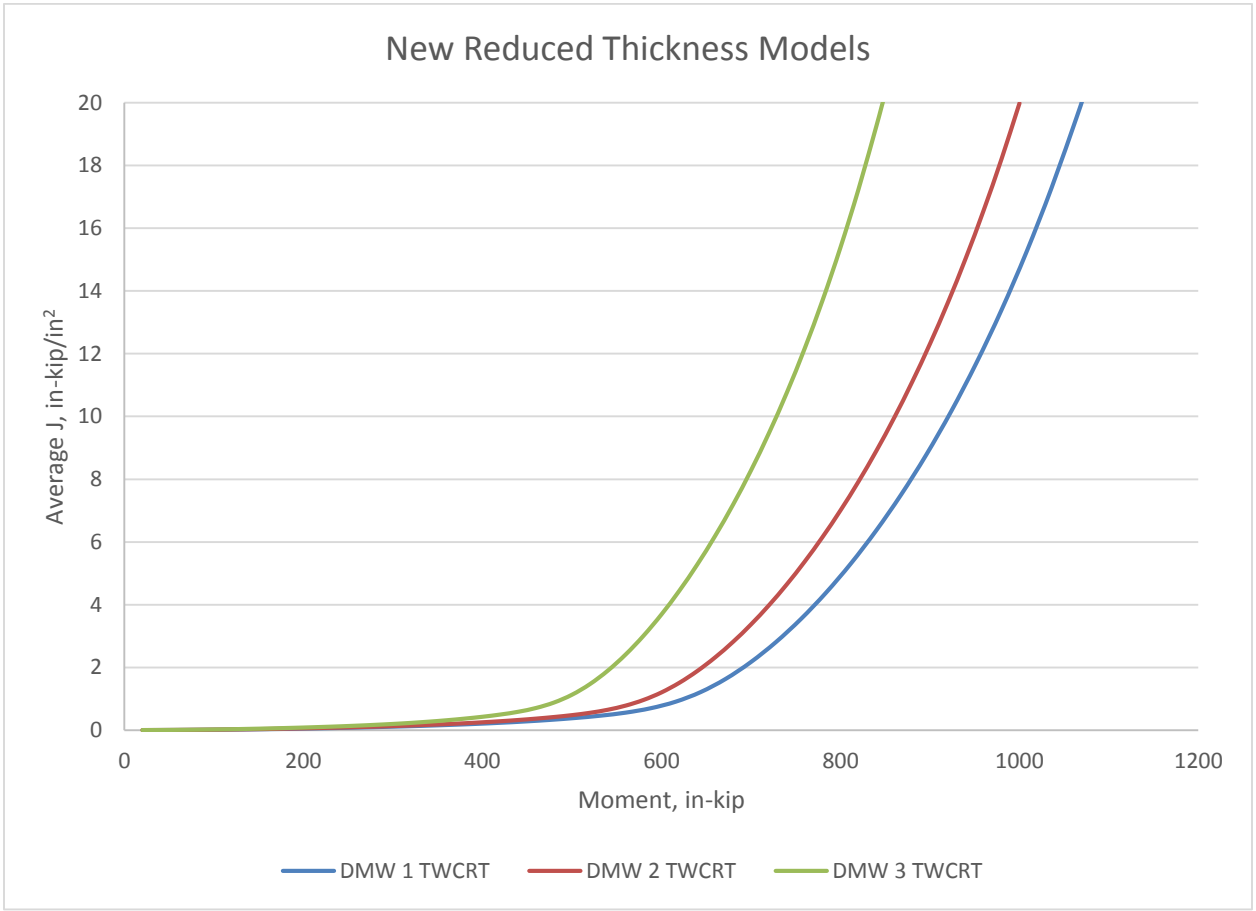


Figure 5.6. J versus moment curves for the new reduced thickness models

Since all three experiments are composed of the same materials with no pressure, the relations resolves down to a function of the mean radius and the thickness. The results for normalizing the J versus moment results are illustrated in Figure 5.7. The results indicate that the new reduced thickness solution is not dependent on the diameter or the thickness since, after normalizing by the net-section-collapse moment, the plots are approximately the same. Since the MRTF is based on J and moment, the MRTF can be used regardless of pipe diameter and pipe thickness.

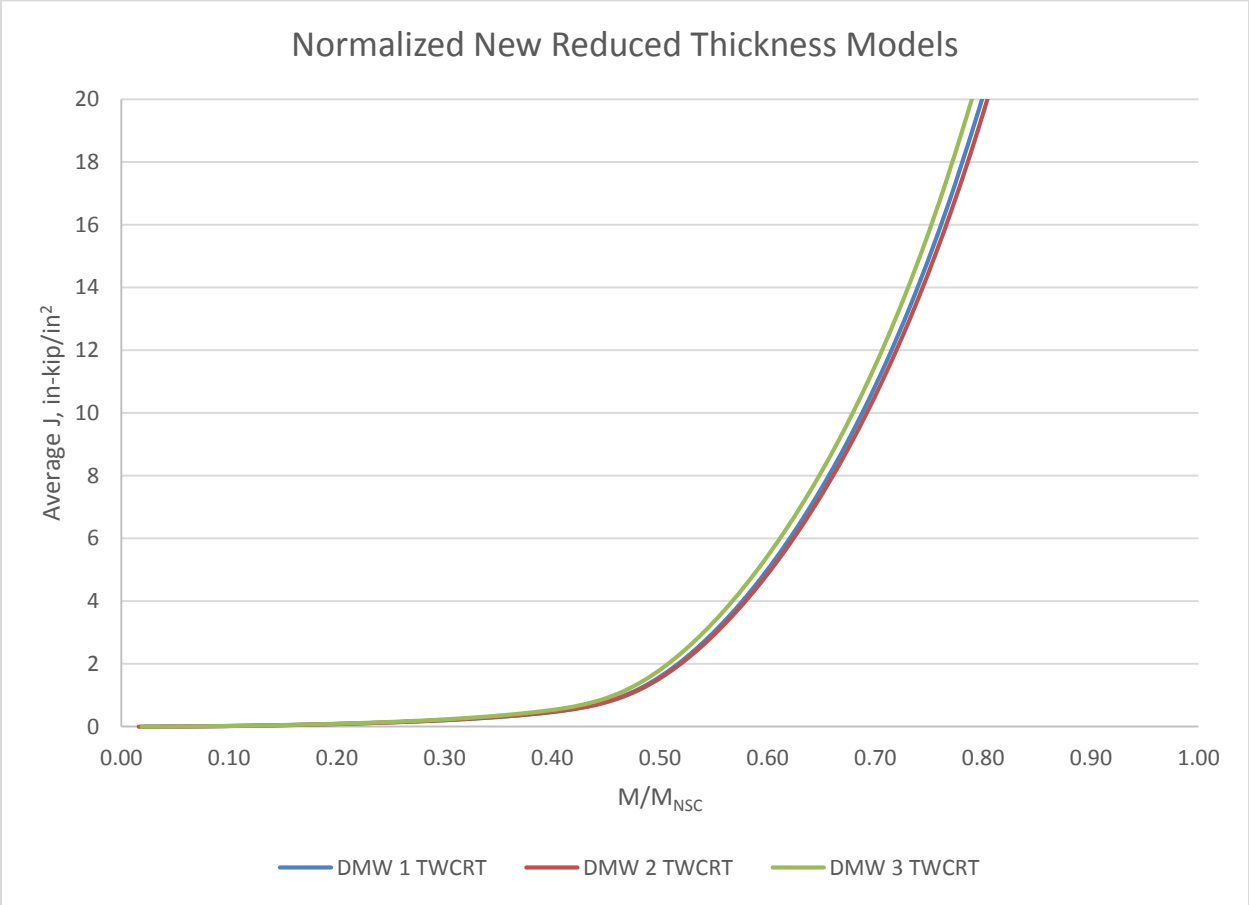


Figure 5.7. J versus moment solution with moment normalized by the net-section-collapse moment.

# CHAPTER 6

## FUTURE RESEARCH

The experiments conducted as a part of this research are prohibitively expensive, to the point that performing future large diameter pipe fracture experiments will be limited. However the experiments performed provide a significant improvement to the knowledge base as it pertains nuclear specific applications of concern. To fully address the knowledge gap in the DM weld fracture arena, a few additional experiments would completely encompass the bounds of the experiment. Some additional experiments that would provide additional insight to this research are:

- Larger and smaller TWC half lengths as part of the CC
- CC's with smaller SC's (1-15% SC depths), and with larger SC's (>90% SC depths)

Currently the TWC portion of the CC was limited to 37%, which limits the verified solutions to that starting crack size. This does not limit the solutions that can be obtained using the techniques outlined in this research, but it does limit the verification of this technique because of the lack of actual data. Additionally, the SC portion of the CC was limited to a range of 16.9 to 58.6%. It would be of great benefit to examine if the behavior of the load displacement curve changed at the SC extremes. Even just one additional experiment at the extreme cases would have allowed for a better representation of the CC to TWC correction factor curve and allowed for the development of a trend line

and resulting equation to represent the behavior. The resulting equation could be used in computer programs such as xLPR.

The previously outlined additional experiments would allow for greater accuracy in prediction for the case that is of interest to the nuclear arena. However, to get a better understanding of the general behavior, the outlined technique would greatly benefit from many more experiments. Some of the experiments that this research would benefit from include:

- Experiments of different size pipes with DM welds (4 and 16 inch pipes)
- Additional base metal experiments to supplement the DPP experiments
    - Different size base metal experiments
    - Different SC sizes for the CC
    - Different TWC for the CC

With these additional experiments, equations could be generated to cover a wide spectrum of fractures and pipe materials.

# CHAPTER 7

# CONCLUSIONS

The primary outcome of this research is the development of a new method to accurately predict the load displacement behavior for a pipe with a CC. The new method was developed based on observations made from the performance of complex crack experiments. The observation that led to the development of a new CC analysis method was that a CC only grows in the TWC direction. From this observation a correlation was developed that allowed for the creation of a TWC FEA model that would accurately represent the load displacement of a CC FEA model. This correlation was found to be independent of the diameter and thickness of the pipe when normalized to the net-section–collapse moment.

This result is a significant improvement over the existing fracture analysis methods for CC's in DM welds. This new method yields an accurate solution that is much less computationally complex than a FEA solution. Most importantly, the new method developed in this research will allow for the use of existing coded solutions, such as LBBeng, which yields an output that is easily input into PRA tools producing a more thorough analysis when analyzing CC's.

## REFERENCES


1 Generic Letter 97-01, "Degradation of Control Rod Drive Mechanism Nozzle and Other Vessel Closure Head Penetrations," April 1, 1997.

2 Bulletin 2001-01, "Circumferential Cracking of Reactor Pressure Vessel Head Penetration Nozzles," August 3, 2001. [ADAMS Accession No. ML012080284]

3 Rudland, D.L., Shim, D.-J., Xu, H., and Wilkowski, G.W., "Evaluation of Circumferential Indications in Pressurizer Nozzle Dissimilar Metal Welds at the Wolf Creek Power Plant," Summary report to the NRC, April 2007. ADAMS ML071560398

4 Harrington, C., Csontos, A., "Development of A Probabilistic Pipe Rupture Assessment Code," PVP2010- 26158, Proceedings of ASME-PVP 2010: 2010 ASME Pressure Vessels and Piping Division Conference, July 18-22, 2010, Bellevue, Washington, USA

5 D. Rudland, P. Scott, R. Orson, and A. Cox, "Complex Crack Stability in Dissimilar Metal Welds: Background and Test Plan," Proceedings of ASME-PVP 2010, paper PVP2010-57535, July 17-21, 2011

6 U.S. Nuclear Regulatory Commission, "Investigation and Evaluation of Stress Corrosion Cracking in Piping of Light Water Reactor Plants,"NUREG-0531, Feb. 1979.

7 Goldberg, A., Streit, R. D., and Scott, R. G., "Evaluation of Cracking in Feedwater Piping Adjacent to the Steam Generators in Nine Pressurized Water Reactor Plants" NUREG/CR-1603, October 1980.

8 ASME Boiler Pressure Vessel Code. Section XI, Appendices C and H. 1995 Edition (1995).

9 Rahman, S., Wilkowski, G. Net-section-collapse analysis of circumferentially cracked cylinders-part I: arbitrary shaped cracks and generalized equations. Engineering Fracture Mechanics 1998; 61(2):177-197.

10 Rice, J. R., "A Path Independent Integral and the Approximate Analysis of Strain Concentrations by Notches and Cracks," Journal of Applied Mechanics', Vol. 35, pp 379-386, 1968.

11 Wilkowski, G. M., and others, “Degraded Piping Program - Phase II, Summary of Technical Results and Their Significance to Leak-Before-Break and In-Service Flaw Acceptance Criteria,” March 1984-January 1989, NUREG/CR-4082, Vol. 8, March 1989.

12 Wilkowski, G., and others, “International Piping Integrity Research Group (IPIRG) Program, Final Report:’ NUREG/CR-6233 Vol. 4, June 1997.

13 Wilkowski, G., and others, “Short Cracks in Piping and Piping Welds,” Seventh Program Report, NUREG/CR-4599, Vol. 4, No. 1, April 1995.

14 Scott, P., Olson, R., and Wilkowski, G., "Development of Technical Basis for Leak- Before-Break Evaluation Procedures" NUREG/CR-6765, May 2002.

15 Hopper, A., and others, “The Second International Piping Integrity Research Group (IPIRG-2) Program”, NUREG/CR-6452, January 1997.

16 Wilkowski, G., and others, “The Battelle Integrity of Nuclear Piping (BINP) Program, Final Report” NUREG/CR-6837 Vol. 1, June 2005.

17 Takumi, K., “Results of the Japanese Carbon Steel Pipe Fracture Program,” NUREG/CP-0109, Leak-Before-Break: Further Development in Regulatory Policies and Supporting Research, Taipei, Taiwan, pp 13-31, February 1990.

18 Fujioka, T., Miura, N., Kashima, K., Kanno, S., Miyazaki, K., Ishiwata, M., and Gotoh, N., “A Fracture Strength Evaluation Method for Carbon Steel Pipes Subjected to Dynamic/Cyclic Loadings: Evaluation of Dynamic/Cyclic Pipe Fracture Tests at Elevated Temperature,” ASME PVP vol. 304, pp 191-197, 1995.

19 Olson, R., and others, “Validation of Analysis Methods for Assessing Flawed Piping Subjected to Dynamic Loading,” NUREG/CR-6234, August 1994.

20 Materials Reliability Program (MRP) Crack Growth Rates for Evaluating Primary Water Stress Corrosion Cracking (PWSCC) of Alloy 82, 182, and 132 Welds (MRP-115), EPRI, Palo Alto, CA: 2004. 1006696.

21 Materials Reliability Program: Advanced FEA Evaluation of Growth of Postulated Circumferential PWSCC Flaws in Pressurizer Nozzle Dissimilar Metal Welds (MRP-216, Rev. 1) EPRI, Palo Alto, CA: 2007. 1015383. MRP-216, Rev.1.

22 Rudland, D.L., Shim, D.-J., Zhang, T., and Wilkowski, G., “Implications of Wolf Creek Indications – Final Report,” Program final report to the NRC, August 2007. ADAMS ML072470394

23 52 Federal Register 41288, "10 CFR Part 50 Modification of General Design Criterion 4 Requirements for Protection Against Dynamic Effects of Postulated Pipe Ruptures." October 27, 1987.

24 Kumar, V., and others, "An Engineering Approach for Elastic-Plastic Fracture Analysis:' EPRI Report NP- 1931, July 1981.

25 Kumar, V., and others, "Advances in Elastic-Plastic Analysis; EPRI Report NP-3607, August1984.

26 Brust, F. W., and Gilles, P., "Approximate Methods for Fracture Analysis of Tubular Members Subjected to Combined Tensile and Bending Loads; ASME Journal ofOffshore Mechanics and Arctic Engineering, Vol. 116, pp 221-227, November 1994.

27 Gilles, P., and Brust, F., "Approximate Fracture Methods for Pipes - Part I: Theory,"Nuclear Engineering and Design, Vol. 127, pp 1-17, 1991.

28 Gilles, P., and others, "Approximate Fracture Methods for Pipes - Part II: Applications," Nuclear Engineering and Design, Vol. 127, pp 19-31, 1991.

29 Bmst, F. W., and others, "Assessment of Short Through-Wall Circumferential Cracks in Pipes," NUREG/CR-6235, April 1995.

30 Paris, P. C., and Tada, H., "Application of Fracture Proof Methods Using Tearing Instability Theory to Nuclear Piping Postulating Circumferential Through Wall Cracks, "NUREG/CR-3464, September 1983.

31 Klecker, R., and others, "NRC Leak-Before-Break (LBB.NRC) Analysis Method for Circumferentially Through-Wall Cracked Pipes Under Axial Plus Bending Loads:' NUREG/CR-4572, May 1986.

32 "Evaluation of Flaws in Austenitic Steel Piping," (Technical basis document for ASME IWB-3640 analysis procedure), prepared by Section XI Task Group for Piping Flaw Evaluation, EPRI Report NP-4690-SR, April 1986.

33 NUREG-1061, Volume 3, "Report of the U.S. Nuclear Regulatory Commission Piping Review Committee, Evaluation of Potential for Pipe Breaks," November 1984.

34 T. L. Anderson, *Fracture Mechanics*, Third Edition, CRC Press, Taylor & Francis Group, New York, 2005

35 G. Wilkowski, H. Xu, D.-J. Shim, and D. Rudland, "Determination of the Elastic-Plastic Fracture Mechanics Z-factor for Alloy 82/182 Weld Metal Flaws for Use in the ASME Section XI Appendix C Flaw Evaluation Procedures," Proceedings of ASME-PVP 2007, paper PVP2007- 26733, July 22-26, 2007.

36 Materials Reliability Program: Crack Growth Rates for Evaluating Primary Water Stress Corrosion Cracking (PWSCC) of Thick-Wall Alloy 600 Materials (MRP-55) Revision 1, EPRI, Palo Alto, CA:2002. 1006695

37 Wilkowski, G. M., Olson, R. J., and Scott, P. M., "Stateof- the-Art Report on Piping Fracture Mechanics," U.S. Nuclear Regulatory Commission report NUREG/CR- 6540, BMI-2196, February 1998.

38 Kanninen, M. F., Broek, D., Marschall, C. W., Rybicki, E. F., Sampath, S. G., Simonen, F. A., and Wilkowski, G. M., "Mechanical Fracture Predictions for Sensitized Stainless Steel Piping with Circumferential Cracks," EPRI Report NP-192, September 1976.

39 Wilkowski G, Ahmad J, Brust F, Guerrieri D, Kramer G, Kulhowvick G, Landow M, Marshall C, Nakagaki M, Papaspyropoulos V, Scott P., "Analysis of experiments on stainless steel flux welds". U.S. NRC Report. NUREG/CR-4878, BMI-2151; 1987.

40 Landes, J. D., "Extrapolation of the J-R Curve for Predicting Reactor Vessel Integrity," NUREG/CR-5650, January 1992.

41 US NRC, Standard Review Plan, 3.6.3 Leak-Before- Break Evaluation Procedures, NUREG-800, Revision 1, March 2007.

42 Kurihara, R., and others, "Estimation of the Ductile Unstable Fracture of Pipe with a Circumferential Surface Crack Subjected to Bending," Nuclear Engineering and Design, Vol. 106, pp 265-273, 1988.

## APPENDIX A - DATA FROM DM WELD EXPERIMENTS

The data in this appendix was recorded during the experiment. The data has been reduced from 30000 plus entries to less than 1000 entries. The purpose of this reduction was to put the data into an easily useable table that can be used by other researchers. The reduced data set maintains the shape of the load displacement curve.

Table A.1. DMW1 CC - SC 16.9% 37% TWC

| North Ram Load (klbf) | South Ram Load (klbf) | North Ram Displacement (in) | South Ram Displacement (in) | North Total Moment (in-kips) | South Total Moment (in-kips) | North Crack Rotation (deg) | South Crack Rotation (deg) | Total Crack Rotation (deg) |
|---|---|---|---|---|---|---|---|---|
| 0.8322 | 0.8906 | 0.0035 | 0.0025 | 2.5744 | 3.6160 | -0.0012 | -0.0006 | 0.0018 |
| 0.8170 | 0.7746 | -0.0062 | 0.0036 | -0.6097 | -0.7646 | 0.0015 | -0.0015 | 0.0000 |
| 0.8108 | 0.7593 | 0.0000 | 0.0009 | -1.8833 | -0.3664 | 0.0036 | 0.0071 | -0.0107 |
| 0.8170 | 0.8540 | 0.0026 | 0.0034 | 1.5395 | 6.2435 | 0.0060 | 0.0070 | -0.0130 |
| 0.8047 | 0.8143 | 0.0048 | 0.0039 | 0.1864 | 3.2174 | -0.0020 | -0.0005 | 0.0025 |
| 0.8566 | 0.7013 | 0.0035 | -0.0004 | -3.5551 | -3.3932 | -0.0020 | 0.0027 | -0.0007 |
| 0.7986 | 0.7258 | 0.0026 | 0.0021 | -0.8484 | -1.1629 | -0.0006 | -0.0027 | 0.0033 |
| 0.8322 | 0.9211 | 0.0024 | 0.0034 | 3.5296 | 7.1202 | 0.0021 | 0.0062 | -0.0082 |
| 0.7773 | 0.7899 | 0.0035 | 0.0045 | -0.5298 | 1.4654 | 0.0057 | 0.0051 | -0.0108 |
| 2.2696 | 2.1481 | 0.0491 | 0.0438 | 60.1321 | 61.0480 | -0.0154 | -0.0125 | 0.0279 |
| 5.6449 | 5.5912 | 0.1536 | 0.1491 | 218.8502 | 219.2751 | -0.0620 | -0.0613 | 0.1234 |
| 8.6327 | 8.5336 | 0.2685 | 0.2595 | 353.8855 | 352.7365 | -0.1152 | -0.1191 | 0.2342 |
| 11.0040 | 11.0396 | 0.3772 | 0.3786 | 466.0566 | 463.4473 | -0.1799 | -0.1824 | 0.3623 |
| 12.6458 | 12.6512 | 0.4835 | 0.4831 | 542.8378 | 537.4666 | -0.2642 | -0.2698 | 0.5340 |
| 13.8788 | 13.8294 | 0.5977 | 0.5911 | 595.5291 | 591.3837 | -0.3738 | -0.3777 | 0.7515 |
| 14.7913 | 14.8275 | 0.7105 | 0.7150 | 638.4576 | 635.2903 | -0.4903 | -0.4893 | 0.9796 |
| 15.5603 | 15.4777 | 0.8232 | 0.8247 | 670.7072 | 662.1610 | -0.6049 | -0.6007 | 1.2057 |
| 15.9876 | 16.0729 | 0.9326 | 0.9369 | 693.7686 | 688.3675 | -0.7142 | -0.7100 | 1.4242 |
| 16.5919 | 16.6162 | 1.0782 | 1.0889 | 721.2018 | 716.3775 | -0.8844 | -0.8786 | 1.7630 |
| 17.0496 | 17.0985 | 1.1970 | 1.2003 | 742.8283 | 740.5883 | -1.0131 | -1.0038 | 2.0169 |
| 17.4769 | 17.4495 | 1.3063 | 1.3118 | 760.6893 | 751.8312 | -1.1364 | -1.1293 | 2.2657 |
| 17.4464 | 17.6265 | 1.4146 | 1.4220 | 764.4778 | 758.2052 | -1.2668 | -1.2483 | 2.5151 |
| 17.8706 | 17.8707 | 1.5676 | 1.5771 | 780.9884 | 773.7030 | -1.4332 | -1.4134 | 2.8466 |
| 18.0750 | 18.0447 | 1.7538 | 1.7661 | 790.5822 | 774.0879 | -1.6654 | -1.6414 | 3.3068 |
| 17.9102 | 18.1088 | 1.8674 | 1.8832 | 786.5539 | 780.3179 | -1.8099 | -1.7807 | 3.5906 |
| 17.9041 | 17.8676 | 2.0531 | 2.0684 | 781.3148 | 768.1670 | -2.0281 | -1.9951 | 4.0232 |
| 17.6203 | 17.6967 | 2.2411 | 2.2588 | 770.4244 | 765.4273 | -2.2720 | -2.2410 | 4.5129 |
| 17.4311 | 17.3671 | 2.4269 | 2.4457 | 759.1945 | 751.7959 | -2.5101 | -2.4783 | 4.9884 |
| 16.7200 | 16.9062 | 2.6515 | 2.6755 | 732.2786 | 727.8198 | -2.7977 | -2.7583 | 5.5560 |
| 16.2684 | 16.3018 | 2.7985 | 2.8285 | 707.3430 | 713.2186 | -2.9946 | -2.9586 | 5.9531 |
| 15.7465 | 15.7707 | 2.9504 | 2.9789 | 684.5359 | 689.6342 | -3.1957 | -3.1714 | 6.3672 |
| 15.2704 | 15.3159 | 3.0629 | 3.0863 | 661.5800 | 667.2991 | -3.3600 | -3.3151 | 6.6751 |
| 14.7913 | 14.8153 | 3.1808 | 3.2054 | 641.0414 | 646.4841 | -3.5067 | -3.4767 | 6.9835 |
| 14.1260 | 14.0950 | 3.2891 | 3.3236 | 609.4689 | 612.6499 | -3.6617 | -3.6350 | 7.2968 |
| 13.4149 | 13.3990 | 3.4388 | 3.4740 | 578.4179 | 581.1361 | -3.8693 | -3.8427 | 7.7120 |
| 12.7527 | 12.7916 | 3.5576 | 3.5832 | 546.3120 | 550.3381 | -4.0218 | -3.9992 | 8.0211 |
| 11.9073 | 11.9309 | 3.6489 | 3.6735 | 507.8738 | 513.3617 | -4.1510 | -4.1288 | 8.2799 |
| 11.3336 | 11.3021 | 3.7610 | 3.7857 | 481.7983 | 485.2923 | -4.3110 | -4.2942 | 8.6052 |
| 10.6530 | 10.5695 | 3.9123 | 3.9343 | 449.2159 | 452.4972 | -4.5162 | -4.5015 | 9.0176 |
| 10.1250 | 10.0201 | 4.0227 | 4.0556 | 424.8111 | 428.1177 | -4.6678 | -4.6561 | 9.3240 |
| 9.6276 | 9.4859 | 4.0950 | 4.1181 | 400.2396 | 403.8816 | -4.7625 | -4.7381 | 9.5005 |
| 9.0294 | 9.1593 | 4.2127 | 4.2421 | 380.7639 | 385.2670 | -4.9266 | -4.9009 | 9.8275 |

Table A.2. DMW 2 CC- SC 38.3% 37% TWC

| North Ram Load (klbf) | South Ram Load (klbf) | North Ram Displacement (in) | South Ram Displacement (in) | North Total Moment (in-kips) | South Total Moment (in-kips) | North Crack Rotation (deg) | South Crack Rotation (deg) | Total Crack Rotation (deg) |
|---|---|---|---|---|---|---|---|---|
| 1.0825 | 1.0279 | 0.0127 | 0.0124 | 22.5241 | 15.4256 | -0.0048 | -0.0057 | 0.0105 |
| 1.0184 | 0.9913 | 0.0142 | 0.0159 | 17.9729 | 20.9371 | -0.0048 | -0.0040 | 0.0088 |
| 6.1485 | 5.9391 | 0.1757 | 0.1690 | 249.2429 | 248.0416 | -0.0579 | -0.0671 | 0.1250 |
| 9.5635 | 9.4310 | 0.3153 | 0.3066 | 406.6553 | 405.9430 | -0.1439 | -0.1415 | 0.2854 |
| 12.0263 | 11.9828 | 0.4771 | 0.4744 | 523.7433 | 519.8888 | -0.2675 | -0.2732 | 0.5407 |
| 14.3701 | 14.1041 | 0.7786 | 0.7692 | 625.2612 | 621.4240 | -0.5606 | -0.5761 | 1.1367 |
| 15.1026 | 15.0290 | 0.9492 | 0.9434 | 663.5641 | 658.4514 | -0.7473 | -0.7584 | 1.5057 |
| 15.3650 | 15.1785 | 1.0757 | 1.0746 | 672.0944 | 668.9785 | -0.8943 | -0.9107 | 1.8049 |
| 15.6244 | 15.7310 | 1.2338 | 1.2413 | 688.1998 | 685.9887 | -1.0803 | -1.0946 | 2.1749 |
| 15.7496 | 15.7982 | 1.3985 | 1.4017 | 694.8524 | 694.1483 | -1.2718 | -1.2909 | 2.5627 |
| 15.5390 | 15.8195 | 1.5350 | 1.5331 | 691.2574 | 686.5793 | -1.4379 | -1.4598 | 2.8978 |
| 14.4800 | 14.9618 | 1.8229 | 1.8298 | 645.9225 | 644.6952 | -1.8159 | -1.8352 | 3.6511 |
| 13.3111 | 13.4937 | 2.0574 | 2.0612 | 587.1411 | 591.8141 | -2.1348 | -2.1613 | 4.2960 |
| 11.9989 | 11.9278 | 2.2184 | 2.2230 | 520.6879 | 522.6284 | -2.3756 | -2.4019 | 4.7774 |
| 10.1617 | 10.3009 | 2.4887 | 2.4900 | 441.4613 | 443.1093 | -2.7529 | -2.7860 | 5.5388 |
| 10.1281 | 10.1727 | 2.4990 | 2.5027 | 436.8657 | 437.3366 | -2.7703 | -2.7966 | 5.5670 |
| 9.2003 | 8.8236 | 2.6534 | 2.6426 | 386.8817 | 388.3876 | -2.9772 | -3.0136 | 5.9908 |

Table A.3. DMW3 CC – SC 58.6%, 37% TWC

| North Ram Load (klbf) | South Ram Load (klbf) | North Ram Displacement (in) | South Ram Displacement (in) | North Total Moment (in-kips) | South Total Moment (in-kips) | North Crack Rotation (deg) | South Crack Rotation (deg) | Total Crack Rotation (deg) |
|---|---|---|---|---|---|---|---|---|
| 0.5637 | 0.3625 | 0.0007 | 0.0016 | -0.1696 | 2.4895 | 0.0001 | -0.0008 | 0.0008 |
| 0.5026 | 0.6037 | 0.0009 | 0.0056 | 1.4287 | 3.8375 | -0.0003 | 0.0007 | -0.0004 |
| 0.5484 | 0.5365 | 0.0029 | 0.0058 | 0.2299 | 3.6801 | -0.0005 | -0.0001 | 0.0006 |
| 1.9583 | 1.9620 | 0.0472 | 0.0492 | 64.0731 | 64.2190 | -0.0186 | -0.0196 | 0.0383 |
| 3.7742 | 3.7537 | 0.1131 | 0.1135 | 145.5577 | 146.8150 | -0.0470 | -0.0479 | 0.0950 |
| 5.4283 | 5.5027 | 0.1875 | 0.1866 | 224.4254 | 221.7974 | -0.0867 | -0.0901 | 0.1767 |
| 6.9328 | 6.7022 | 0.2560 | 0.2518 | 286.9021 | 287.8594 | -0.1306 | -0.1357 | 0.2662 |
| 8.0040 | 8.3291 | 0.3257 | 0.3196 | 347.7531 | 344.9771 | -0.1841 | -0.1841 | 0.3682 |
| 8.9440 | 9.4829 | 0.3975 | 0.4009 | 396.6766 | 393.9185 | -0.2459 | -0.2449 | 0.4908 |
| 9.9755 | 10.3284 | 0.4725 | 0.4733 | 440.1601 | 438.7660 | -0.3156 | -0.3115 | 0.6271 |
| 10.8697 | 10.2246 | 0.5424 | 0.5231 | 457.1077 | 455.4808 | -0.3684 | -0.3818 | 0.7502 |
| 11.7944 | 11.0854 | 0.6790 | 0.6561 | 497.0909 | 494.4359 | -0.5132 | -0.5170 | 1.0302 |
| 12.1087 | 11.5066 | 0.7453 | 0.7325 | 513.0719 | 514.8235 | -0.5857 | -0.5927 | 1.1784 |
| 12.0813 | 11.8607 | 0.8823 | 0.8730 | 521.2231 | 519.3122 | -0.7551 | -0.7623 | 1.5174 |
| 11.8341 | 12.4986 | 0.9598 | 0.9677 | 527.9600 | 524.7639 | -0.8648 | -0.8498 | 1.7145 |
| 10.9002 | 11.6287 | 1.1085 | 1.1025 | 489.3729 | 485.3884 | -1.0596 | -1.0511 | 2.1107 |
| 10.5187 | 10.3925 | 1.1544 | 1.1433 | 453.7526 | 450.3054 | -1.1298 | -1.1289 | 2.2587 |
| 9.6581 | 10.0262 | 1.2262 | 1.2253 | 425.7954 | 414.3414 | -1.2472 | -1.2405 | 2.4877 |
| 8.8463 | 8.2650 | 1.3003 | 1.2754 | 364.7778 | 363.4126 | -1.3489 | -1.3572 | 2.7061 |
| 5.1719 | 5.1028 | 1.6089 | 1.5954 | 211.7472 | 209.2070 | -1.8311 | -1.8309 | 3.6620 |
| 4.4273 | 4.8372 | 1.6881 | 1.6820 | 188.8840 | 182.2453 | -1.9530 | -1.9489 | 3.9019 |

## APPENDIX B - MATERIAL PROPERTY DATA USED IN FEA MODEL DEVELOPMENT

Data in this appendix is segregated by material. These are the material properties used in the FE analysis and is listed as elastic and plastic properties for each material at experimental temperature. Data is listed as "stress, strain" in English standard units (psi, in/in)

Table B.1. Carbon Steel

MATERIAL NAME=SA508
ELASTIC
0.27022000E+08, 0.30000
PLASTIC
42201, 0.000000
43471, 0.000255
45836, 0.000342
48041, 0.000563
49081, 0.000750
50148, 0.001044
51232, 0.001464
52982, 0.002396
54378, 0.003373
55554, 0.004354
56535, 0.005342
57383, 0.006292
58255, 0.007331
59009, 0.008281
65246, 0.018177
70667, 0.027991
74832, 0.037928
78037, 0.047867
80677, 0.057877
82759, 0.067901

84401, 0.077870
85708, 0.087891
86648, 0.097870
86939, 0.107917
86494, 0.118050
85296, 0.128091
83283, 0.138145
80308, 0.148224
76065, 0.158331

Table B.2. Inconel 182/82

MATERIAL, NAME=IN182
ELASTIC
0.29500000E+08, 0.30000
PLASTIC
55474.98187,0
57645.52773, 0.004648478
61043.18324, 0.010635868
63489.3657, 0.01665551
65119.08254, 0.02270283
66844.903, 0.028746892
68438.35712, 0.03479544
69763.3925, 0.040853088
71379.02881, 0.046900885
73021.91284, 0.052947758
74251.54429, 0.05900864
75327.32112, 0.065074737
76893.95426, 0.071124195
78187.7572, 0.077182901
79944.36531, 0.083225919
80875.88959, 0.089296906
82485.4819, 0.095344908
83589.64683, 0.101410042
84565.78947, 0.107479517
86033.08444, 0.113532342
87577.2463, 0.119582562
88751.72377, 0.125645313
90151.63004, 0.131700423
91496.66667, 0.137757392

92422.58159, 0.14382857
94301.68165, 0.149867435
96097.40583, 0.155909127
97644.36813, 0.161959252
99106.7202, 0.168012245
100661.0728, 0.174062119
102578.2827, 0.180099693
104295.757, 0.186144038
105713.4421, 0.192198545
107679.6177, 0.198234459
109604.5013, 0.204271773
110986.9136, 0.210327475
112535.1898, 0.216377555
114265.8261, 0.222421454
115866.3199, 0.228469764
117935.7143, 0.234502179

Table B.3. Stainless Steel

MATERIAL, NAME=SS304
ELASTIC
0.24937000E+08, 0.30000
PLASTIC
23250, 0
37350, 0.0508
53350, 0.1135
64600, 0.2493

## APPENDIX C – DETAILED J VERSUS MOMENT PLOTS

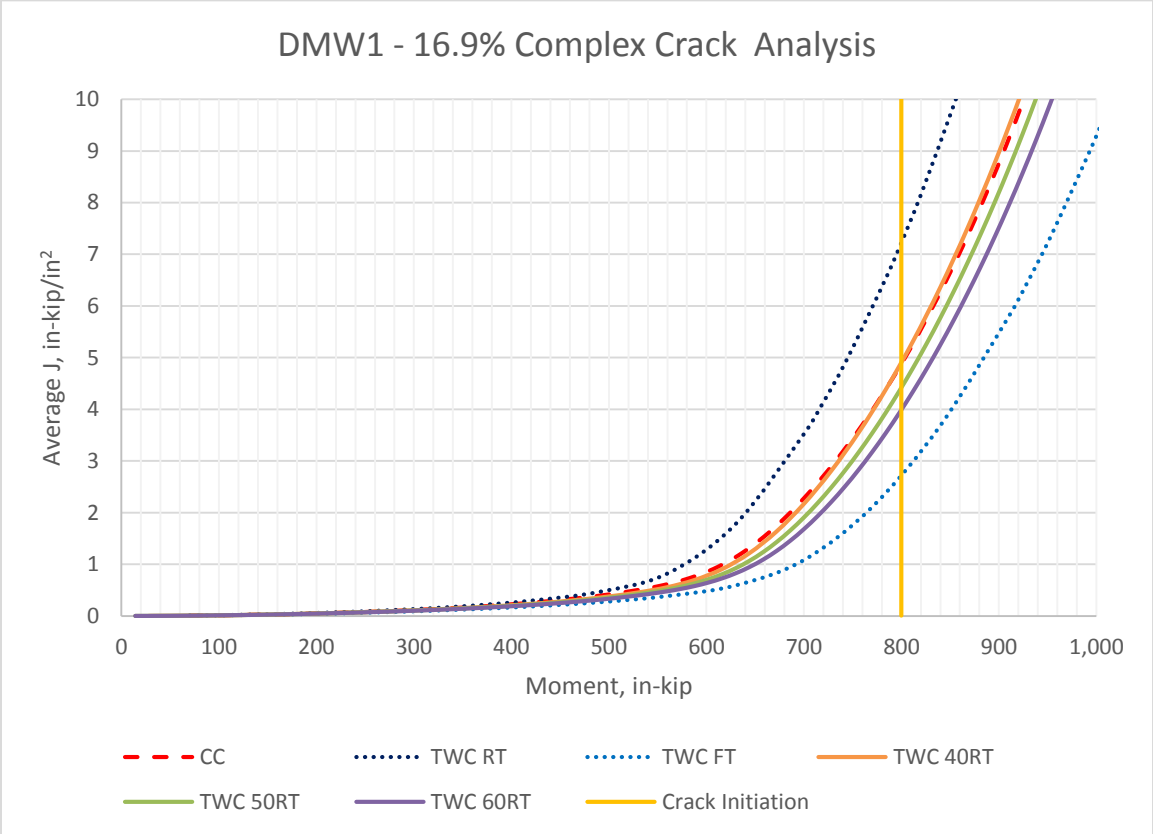


Figure C.1. Illustration of the DMW 2 FE models. Comparing the driving force for crack growth of all the performed TWC models to the CC FE model.

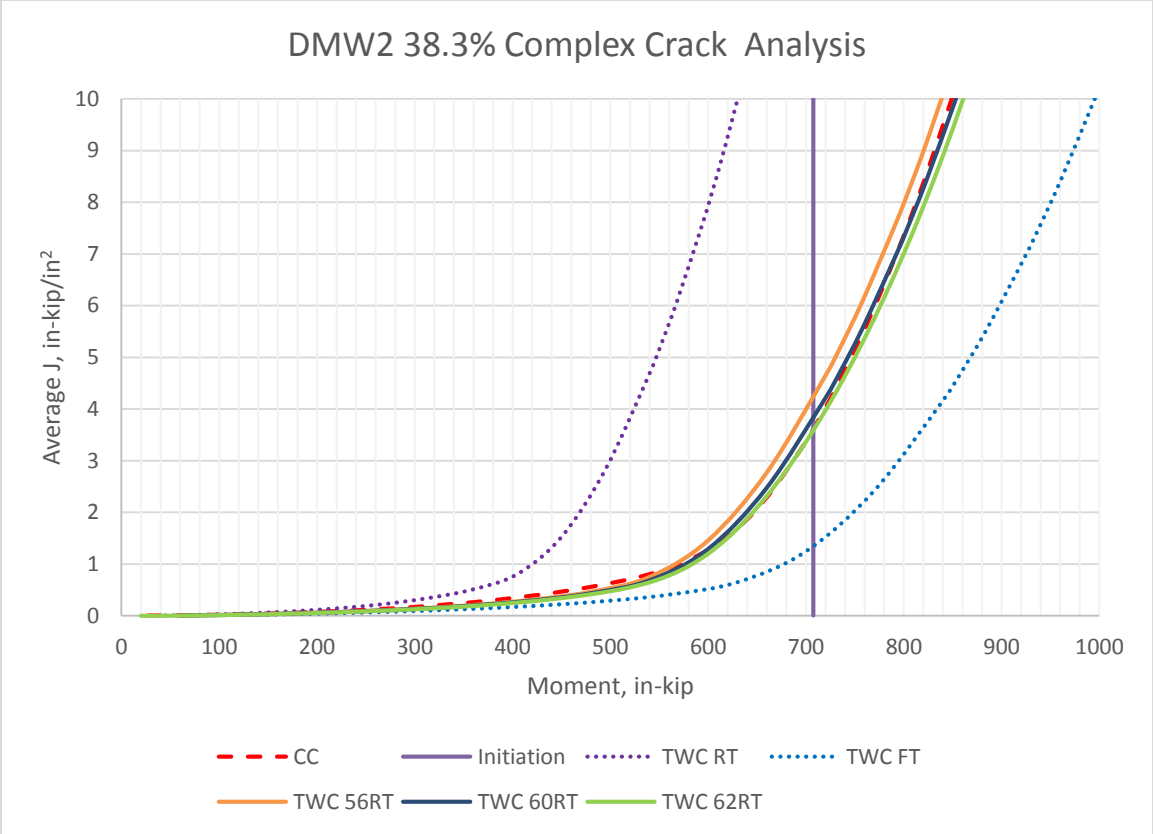


Figure C.2. Illustration of the DMW 2 FE models. Comparing the driving force for crack growth of all the performed TWC models to the CC FE model.

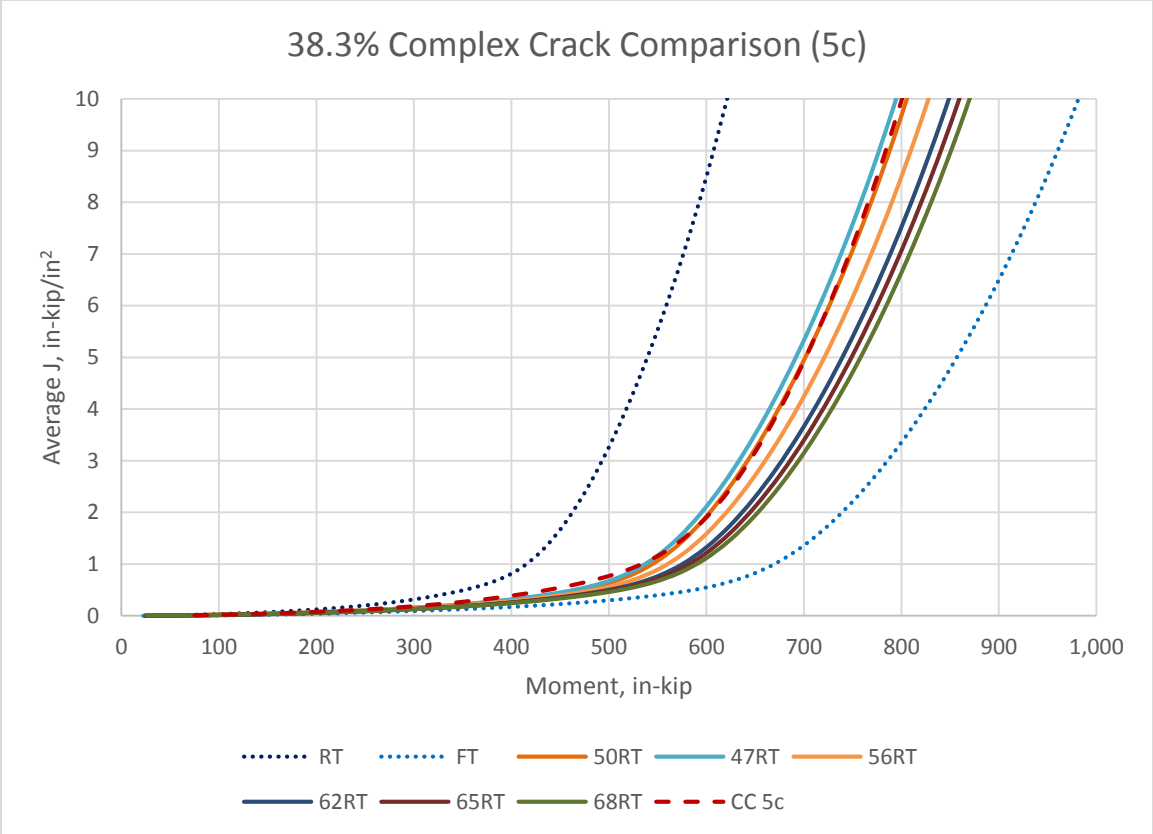


Figure C.3. Illustration of the DMW 2 (5c) FE models. Comparing the driving force for crack growth of all the performed TWC models to the CC FE model.

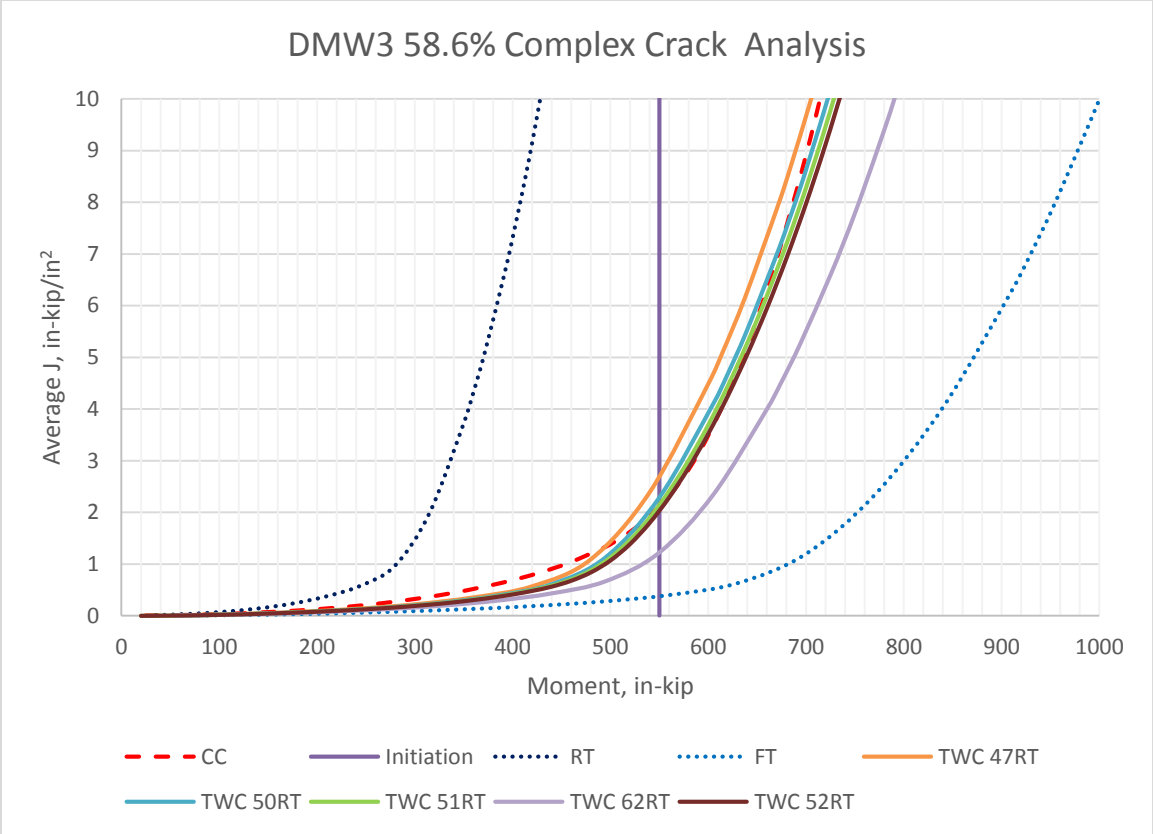


Figure C.4. Illustration of the DMW 3 FE models. Comparing the driving force for crack growth of all the performed TWC models to the CC FE model.

## APPENDIX D – EXPERIMENT TEST FRAME